THE EQUILIBRIUM AND STABILITY

OF THE MULTIPOLE

by

MICHAEL WALLACE PHILLIPS

A thesis submitted in partial fulfillment of the
requirements for the degree of

DOCTOR OF PHILOSOPHY
(Physics)

at the

UNIVERSITY OF WISCONSIN--MADISON

1982

To the loving memory

of my father, Fred Eugene Phillips,

and my brother, Emmet Charles Phillips.

ACKNOWLEDGEMENTS

I would like to thank my adviser, K. R. Symon, for many valuable discussions and suggestions during the course of my studies at the Univ. of Wisconsin. I am grateful to S. Prager for his help in understanding the MHD aspects of this work and for his interest in the numerical results. I thank J. Callen for his helpful tips and suggestions concerning the kinetic aspects of this work. I'm also grateful to my colleague C. Kieras for the insight gleaned from many debates and discussions on physics problems. Special thanks to my mother, Lois Phillips, for her love and encouragement during my graduate studies.

THE EQUILIBRIUM AND STABILITY OF THE MULTIPOLE

Michael Wallace Phillips

Under the supervision of Professor Keith R. Symon

The equilibrium and linear ballooning mode stability of a plasma in an axisymmetric closed field line device such as the multipole is investigated. Two models of the plasma are used, a kinetic model and an ideal MHD model, and the results are compared. Numerical calculations are made of the equilibrium and of ballooning mode stability criteria in the Wisconsin Levitated Octupole device.

The ballooning stability is analyzed using a high toroidal mode number expansion of the linearized ideal MHD equations. The most unstable mode has infinite toroidal mode number, n, even symmetry and is localized on a flux surface. The critical beta, β_c, for the onset of this mode is calculated. For $\beta > \beta_c$ there is a critical mode number, n_c. Only modes with $n > n_c$ are unstable. The full mode structure of the instability is calculated.

A general set of kinetic equations governing low frequency, $\omega < \Omega_c$, modes in a closed field line geometry are derived for two classes of modes: lower frequency modes with $\omega \ll \omega_{bi} \ll \omega_{be}$, where ω_b is the bounce frequency, and intermediate frequency modes with $\omega_{bi} \ll \omega \ll \omega_{be}$. The equations include finite ion Larmor radius effects, trapped and untrapped particle effects and drift particle resonances.

The lower frequency equations are used to investigate the effect of parallel particle dynamics on the ballooning mode. In the hydrodynamic limit $\omega^*/\omega \to 0$, $\omega_D/\omega \to 0$, $\rho_i \to 0$, the equations are combined to form the Kruskal-Oberman energy principle. A Kruskal-Oberman analysis of the ballooning mode shows a modest increase in the critical beta over that calculated from MHD. Also, the odd mode is the most unstable mode.

The effect of finite ion Larmor radius on the ballooning mode is investigated using the intermediate frequency equations. These equations are expanded in high n to obtain a single partial differential equation for high n modes. Finite ion Larmor radius has a large stabilizing effect on the ballooning mode due to the conversion of the mode into a drift type oscillation with $Re(\omega) \sim \omega_i^*$.

TABLE OF CONTENTS

CHAPTER 1

Introduction

In proposed magnetic confinement fusion reactor designs a thermonuclear plasma is contained by a strong magnetic field. For a given magnetic field one would generally like to confine as much plasma pressure as possible. One very significant reason is that large magnets cost a good deal of money and it pays to use them as efficiently as possible. A measure of the efficiency of a confined plasma is the ratio of plasma pressure to magnetic pressure or beta, $\beta = 2\mu_0 p/B^2$, where p is the plasma pressure and B is the magnetic field strength. Another important reason for wanting beta as large as possible is that it cuts the energy loss due to synchroton radiation. Synchroton radiation will be one of the major energy loss mechanisms in a magnetically confined thermonuclear plasma. In a high beta plasma the plasma displaces the magnetic field decreasing the field strength inside the core of the plasma and thereby decreasing the synchroton radiation loss of the particles.

A major obstacle in attaining high beta is the ballooning instability. The ballooning instability is a pressure driven instability which is predicted to occur above a certain threshold in beta. The beta limit the ballooning mode imposes on a plasma device is a severe threat to the economic viability of the magnetically confined fusion reactor concept. Because of this the ballooning mode

and the question of the beta limit it sets on a device has been under intense investigation both theoretically and experimentally.

In this thesis the ballooning mode stability of axisymmetric closed field line systems such as multipoles is investigated theoretically. First the linear stability of the ballooning mode is studied using ideal magnetohydrodynamic (MHD) theory. Then a theory of low-frequency drift type instabilities in a nonuniform collisionless plasma is developed for the multipole field configuration. This theory includes trapped and untrapped particle effects, finite Larmor radius effects and drift and bounce particle resonances. The result is a set of three coupled partial differential equations governing low frequency modes in the plasma. These equations are used to study the effect of finite Larmor radius and parallel particle dynamics on the ballooning mode. Part of this thesis is a specific application of this theory to the calculation of the ballooning mode beta limit of the Wisconsin Levitated Octupole experiment. However, the theory and computer codes developed to study this problem are general and can be applied to any multipole configuration.

Some encouraging results have come out of the experimental research of high beta plasmas. They seem to indicate that the beta limit predicted by MHD theory is overly pessimistic. The general strategy of these experiments has been to push the plasma beta as high as possible and see what happens. What is significant is that so far nothing has happened. In the ISX-B experiment peak beta values of

8-10% have been achieved through neutral beam heating of the plasma[1]. This is close to beta limit predicted by MHD theory for this device. No evidence of a beta limit caused by a ballooning or other type of instability was observed. In the UCLA dodecapole experiment, a multipole device, betas in the bridge of 8% have been measured for large gyroradius plasmas[2]. The MHD beta limit of this device has been predicted to be 7%[3]. The equilibrium appeared stable with a decay time in excess of 400 Alfvèn times. Ideal MHD activity usually occurs on a time scale less then the Alfvèn time. In the Wisconsin Levitated Octupole[4] betas up to 35% for large Larmor radius highly collisonal plasmas have been observed with decay times on the order of 1000 Alfvèn times. This is 8 times larger than predicted by ideal MHD theory[5]. Betas of 8% have been measured for less collisional small Larmor radius plasmas. These conditions conform more to the ideal single fluid plasma model yet the beta is still 2 times larger then that predicted by MHD. These plasmas were also observed to have equilibrium properties similar to those predicted by ideal MHD theory. These experiments indicate the need for a more complete analysis of the ballooning mode.

A. The Interchange Instability

The ballooning mode is closely related to the MHD interchange instability. This instability is characterized by a long constant flux perturbation along the magnetic field. The term "interchange"

comes from a simple energy principle analysis[6] found in most elementary plasma physics textbooks. In the energy principle analysis two thin adjacent flux tubes in the plasma are interchanged and the change in the stored energy, δW, in the plasma is calculated. If δW is negative the system is unstable. If δW is positive the system is stable. It is found that δW can be made negative for this type of perturbation only if $\delta p \delta V' < 0$, where δp is the change in the plasma pressure and $\delta V'$ is the change in volume associated with the flux tube interchange. This means a necessary condition for stability of the interchange mode in a magnetic field without shear is $p'V'' > 0$, where the prime denotes the derivative with respect to the flux surface label ψ.

In a closed field line system $V' = \oint \frac{d\ell}{B}$ where the integral is around an entire field line. If the flux surfaces are labeled by ψ, increasing outwards from the plasma, near the edge of the plasma $p' < 0$ and V'' must be negative for the stabilization of the interchange mode. This is refered to as the negative V'' condition. This led to the concept of minimum-average B stabilization of the plasma. The inverse of the integral for V' is in effect an average of the magnetic field. When V' decreases outward the magnetic field average V'^{-1} increases. In a minimum-average B device the plasma is confined by an effective magnetic well. The quantity V'' is related to the inverse curvature of a field line, $\vec{\kappa} = \hat{B} \cdot \nabla \hat{B}$, by the relation

$$V'' = \oint d\ell \, \frac{D}{B} \qquad (1.1)$$

where $D = -\frac{2}{rB}\hat{\psi}\cdot\vec{\kappa}$. From this expression for V'' it can be seen that regions along a field line where the pressure gradient and magnetic field gradient are in opposite directions contribute to making the integral V'' negative. These regions are stabilizing and are called good curvature regions. Regions where the pressure gradient and magnetic field gradient are in the same direction make a positive contribution to the integral V''. These regions are destabilizing and are called bad curvature regions.

The multipole is a minimum-average B device. The pressure peaks on the separatrix and decreases inwards toward the rings and outwards toward the walls. Inside the separatrix, in the common flux region, field lines have good curvature all the way around. Outside the separatrix field lines have regions of both good and bad curvature. Starting at the separatrix V' decreases outward. Since the pressure gradient is in the same direction as that of V' these flux surfaces are interchange stable. However, a point is reached where V'' equals zero. This flux surface is called the critical flux surface. At this point the interchange mode is marginally stable. Assuming the pressure continues to decrease outward the remaining flux surfaces outside the critical flux surface are interchange unstable.

B. Early MHD Ballooning Mode Work

The interchange mode is just one way of perturbing the plasma. Although the interchange mode is stable inside the critical flux surface, the plasma can still be unstable to other types of perturbations. A general form for the change in stored energy, δW, due to a small displacement, $\vec{\xi}$, of a perfectly conducting plasma was first derived by Bernstein et al.[7]. This is the magnetohydrodynamic or MHD energy principle,

$$\delta W = \frac{1}{2}\int d\tau \left[\frac{1}{\mu_0}\vec{B}_1^2 - \vec{j}_0\cdot\vec{B}_1\times\vec{\xi} + (\vec{\xi}\cdot\nabla p)(\nabla\cdot\vec{\xi}) + \gamma p(\nabla\cdot\vec{\xi})^2\right] . \qquad (1.2)$$

where $\vec{B}_1 = \nabla\times(\vec{\xi}\times\vec{B}_0)$ is the perturbed magnetic field, $\mu_0\vec{j}_0 = \nabla\times\vec{B}_0$ is the equilibrium current density and $d\tau$ is the volume element. The contribution of the various terms in the MHD energy integral to the stability of a system is more apparent when Eq. (1.2) is written in the form,

$$\delta W = \frac{1}{2}\int d\tau \left\{\frac{1}{\mu_0}\vec{B}_{1\perp}^2 + \mu_0\left[\frac{1}{\mu_0}\vec{B}_{1\parallel} - \frac{\vec{B}_0}{B_0^2}\vec{\xi}\cdot\nabla p\right]^2 + \gamma p(\nabla\cdot\vec{\xi})^2 + \frac{\vec{j}_0\cdot\vec{B}_0}{B_0^2}\vec{B}_0\times\vec{\xi}\cdot\vec{B}_1 - 2\vec{\xi}\cdot\nabla p\,\vec{\xi}\cdot\vec{\kappa}\right\} , \qquad (1.3)$$

where $\vec{B}_{1\parallel} = \hat{B}\cdot\vec{B}_1$ is the parallel component of $\vec{B}_1$ and $\vec{B}_{1\perp} = \vec{B}_1 - \vec{B}_{1\parallel}$ is the perpendicular component of $\vec{B}_1$. The equilibrium equation

$\vec{j}_0 \times \vec{b}_0 = \nabla p$ was used to arrive at the above expression for δW. This form of δW is due to Greene and Johnson[8]. The first term represents the change in energy due to the field line bending in the perpendicular direction. This term is responsible for the shear Alfvèn wave. The second term is the potential energy of the magnetoacoustic wave. The third term is the source of sound waves in the plasma. The fourth term can be negative and causes the kink instability. In closed field line systems $\vec{j}_0 \cdot \vec{b}_0 = 0$ so this term is not present. In a closed field line system the only term that can be negative is the last term called the interchange or ballooning term. For a constant perturbation in flux it can be seen directly from Eq. (1.3) that δW can be made negative if $p'V''$ is negative. For field lines that are stable to interchange type perturbations an instability can still occur if there are bad curvature regions along a field line. Bending the field lines causes a positive contribution to δW but if the perturbation is localized in the bad curvature region and p' is large enough δW can still be made negative. This is the ballooning instability, so called because the flux tube perturbation balloons out in the bad curvature region something like the bulge on an old inner tube.

In the paper by Bernstein et al.[7] the MHD energy principle was applied to the problem of a shearless axisymmetric plasma. It was found that a mode with infinite toroidal mode number, $n \to \infty$, was the most unstable mode. This is because the shorter the perpendicular wavelength of the mode, the less the field lines are bent in the

toroidal direction. An eigenmode equation for the most unstable mode was derived and from this a slightly more general form of the interchange stability criterion was found. Ohkawa and Kerst[9] looked specifically at the MHD stability of the multipole configuration. As a trial function to the energy principle they constructed what they called the "worst mode", one in which the perturbation was large in the bad curvature region and small in the good curvature region. This is essentially the shape of the ballooning mode perturbation. They also derived a beta limit for this perturbation. The condition for stability was estimated to be $\beta < \pi^2 \frac{L_n L_B}{L_c}$, where L_n is the density scale length, $L_n^{-1} = \nabla p/p$, L_B is the magnetic scale length, $L_B^{-1} = \nabla B/B$, and L_c is the connection length along the field line between the good and bad curvature regions. This formula gives a pretty good back of the envelope estimate of the ballooning mode beta limit. The eigenmode equation governing infinite toroidal mode number modes was again looked at by Johnson, Kulsrud and Weimer[10] who found that for marginal stability an incompressible mode is the most unstable mode in closed field line geometries. Their equation has since been solved numerically to determine the beta limit in multipole geometries[3,5].

C. Review of Kinetic Work

Early kinetic work on low frequency electromagnetic instabilities include the Kruskal-Oberman or collisionless energy principle derived by Kruskal and Oberman[11] and Rosenbluth and Rostoker[12]. This energy principle is similar in many respects to the MHD energy principle but with ideal adiabatic terms replaced with kinetic terms that include the effect of collisionless adiabatic compression of the plasma and the Fermi acceleration of the particles that occurs when the magnetic field lines are perturbed. This energy principle is studied in Chapter 5 of this thesis.

A huge amount of work has been done with linear kinetic theory treating plasmas in simplified geometries. For a geometry with at least 2 ignorable coordinates, a generalized framework has been developed by Lewis and Symon[13] for analyzing collisionless Vlasov plasmas. Using the numerical procedure they developed the linear stability of these geometries can be treated to almost any degree of accuracy needed. However, most plasma experiments have only 1 or no ignorable coordinate. So far explicit solutions for these geometries that can in any sense be called exact have not been developed.

Many important results have been discovered using simplified geometries. One result in particular should be mentioned because of implications it has concerning the finite Larmor radius stabilization of the ballooning mode. Rosenbluth, Krall and Rostoker[14] showed that finite Larmor radius effects can considerably influence the interchange or flute instability in slab and cylindrical geometries. The instability they considered is similar to the MHD interchange

instability discussed above with the difference that the force of the magnetic field gradient is replaced by a gravitational force, mg. The dispersion relation for this stability from a hydromagnetic analysis is $\omega^2 - g\frac{p'}{p} = 0$ where p' is the pressure gradient. If the pressure gradient is opposite to the direction of the gravitational field the growth rate of the flute instability is given by $\gamma = \left(-g\frac{p'}{p}\right)^{1/2}$. Rosenbluth et al. showed when the lowest order finite Larmor radius effects are included in the analysis the dispersion relation becomes $\omega^2 - \omega\omega^* - g\frac{p'}{p} = 0$ where $\omega^* = -k\frac{T}{qB}\frac{p'}{p}$ is the diamagnetic drift frequency. Here k is the wave number of the mode and T is the ion temperature. From this dispersion relation the system is now stable if $(k\rho_i)(\rho_i\frac{p'}{p}) > \frac{4\gamma}{\Omega_i}$ where Ω_i is the ion cyclotron frequency and ρ_i is the average ion Larmor radius, $\rho_i = \sqrt{\frac{2T}{m_i}}\frac{1}{\Omega_i}$. This criterion shows that the flute instability is stabilized for large enough ion Larmor radius.

The physical picture of the flute instability is that when the magnetic field is perturbed the gravitational drift of the ions causes a pile up of space charge along the instability flutes. This causes an electric field and associated with it an $\vec{E} \times \vec{B}$ velocity drift, $\vec{v}_E = \frac{\vec{E} \times \vec{B}}{B^2}$, which reinforces the perturbation. When finite Larmor radius effects are included the $\vec{E} \times \vec{B}$ velocity drift of the ions is modified by an extra term $\vec{v}_E = \left(1 + \frac{1}{2}\rho_i^2\nabla_\perp^2\right)\frac{\vec{E} \times \vec{B}}{B^2}$. This extra term is not present in the electron $\vec{E} \times \vec{B}$ drift due to the disparity in the size of the Larmor radius. The new term causes a charge separation out of phase with the original charge separation in such a way as to

stabilize the mode. This coupling of hydromagnetic perturbations to drift type oscillations also has an important effect on the ballooning mode.

The usual approach to the linear kinetic analysis of plasmas in complex geometries has been to expand in some sort of small parameter. For low frequency modes of the type considered here the frequency of the mode is much less then the cyclotron frequency, Ω. The quantity ω/Ω can be used as an expansion parameter. For low betas and strong magnetic fields ρ/L_n and ρ/L_B can also be used as expansion parameters in most situations. Here ρ is the Larmor radius of a particle. In the limits $\omega/\Omega \ll 1$, $\rho/L_n \ll 1$, $\rho/L_B \ll 1$ the particle motion is described by the guiding-center approximation. In a guiding-center plasma low frequency modes are characterized by long wavelengths parallel to the magnetic field and short wavelengths perpendicular to the magnetic field. This is because along field lines particles, particularly electrons, can move rapidly to prevent electric field perturbations with short parallel wavelengths. Also, any bending of the field lines is stabilizing. Because of their gyromotion around field lines particles move perpendicular to field lines on a much longer time scale. In addition, small perpendicular wavelengths minimize the stabilizing contribution due to field line bending. The perpendicular wavelength is limited by the size of the Larmor radius, generally, $k_\perp \rho < 1$.

The low frequency small Larmor radius short perpendicular wavelength expansion of the linear Vlasov equation was originally developed by Rutherford and Frieman[15] and Taylor and Hastie[16] for electrostatic perturbations in an inhomogeneous plasma. These treatments dealt with closed field line systems and specific applications were made to the multipole[17,18]. In this thesis expansion techniques similar to that of Rutherford and Frieman are employed to treat electromagnetic perturbations as well as electrostatic perturbations. The problem of electrostatic oscillations in axisymmetric mirror machines was treated by Horton, Callen and Rosenbluth[19] using a different but to lowest order equivalent technique. In their analysis the single-particle gyro-orbits were first calculated. These were then used to evaluate the time history integral for the perturbed distribution function due to electrostatic perturbations in a manner reminiscent of the method of integration over unperturbed orbits.

One of the first attempts at a general kinetic formalism for the ballooning mode in tokamaks was made by Chu et al.[20]. Their treatment is similar to the analyis by Rosenbluth and Sloan[21] of the electromagnetic trapped particle instability but includes inertial terms. In a report by Liewer and Liu[22] an instructive application of the drift kinetic equation is made to the ballooning mode problem. High mode number pertubation analysis of the tokamak is hindered by the ergodic and sheared nature of the magnetic field. This problem was remedied by the invention of the ballooning mode formalism[23,24]

which correctly handles the doubly periodic nature of the perturbation in tokamak geometry. A big demand for the correct kinetic treatment of ballooning modes sparked a flurry of papers from a number of sources incorporating the ballooning mode formalism. Among these Van Dam[25] includes in his analysis collisional effects. Antonsen and Lane[26] developed a set of low frequency kinetic equations and used them to construct a variational principle. Frieman et al.[27] include in their analysis a calculation of the radial structure of the ballooning mode in a tokamak. Other similar kinetic analyses have been done by Connor, Hastie and Taylor[28] and by Tang, Connor and Hastie[29] who show explicitly that in the hydromagnetic limit the kinetic equations reduce to familiar MHD forms.

D. The Levitated Octupole

The Levitated Octupole has four internal rings carrying current in the same direction inside a conducting vacuum vessel. A picture of the poloidal cross section of the Levitated Octupole is shown in Fig. (1.1). This figure shows the dimensions of the device used for the calculations presented in this thesis. Also shown in Fig. (1.1) are the contours of poloidal magnetic flux for an MHD equilibrium with $\beta = 4.33\%$. The length of discharge is short enough that the rings and walls of the vacuum vessel can be considered to lowest order perfectly conducting. The vacuum vessel is modeled as a toroidal vessel with a rectangular cross section. In each corner of the rectangle are

gussets which serve the purpose of lessening the severity of the bad curvature behind the rings. Another feature are two trapezoidal wedges pointing into the machine, one on the inside of the torus and one on the outside. These are known as the noses. The main purpose served by the noses is to lower the inductance of the machine so that for a given stored energy in the capacitor banks the magnitude of the magnetic field is larger. However, this also shortens the pulse length of the discharge. It was also thought the noses would have a stabilizing effect on ballooning modes. At high beta the flux surfaces are distorted in a manner that decreases the amount of good curvature. It was hoped that the noses would help lessen the amount of distortion. To some extent they do this. However, the noses also have the effect of wrapping the flux surfaces around the rings thereby creating a larger bad curvature region. The MHD beta limit for the same Levitated Octupole configuration with the noses removed is actually about 2% higher then with the noses in. An estimate of the beta limit of the Levitated Octupole can be found by using the Ohkawa-Kerst formula $\beta_c = \pi^2 \frac{L_n L_B}{L_c}$. Taking $L_n = 3$ cm., $L_B = 15$ cm. and $L_c = 70$ cm the beta limit is predicted to be about 6%. The actual ideal MHD ballooning mode beta limit is 4.33%.

E. Organization of this Thesis

In Chapter 2 the MHD equilibrium of multipole configurations is treated. In an axisymmetric geometry the problem of finding MHD equilibrium is reduced to solving the Grad-Shafranov equation. A numerical procedure for solving this equation in multipole geometry is given. Results of the calculation for the Levitated Octupole geometry are presented and the effects of beta on the equilibrium are discussed. The equilibrium distribution function for a collisionless plasma is derived by a small Larmor radius expansion of the equilibrium Vlasov equation. To lowest order the kinetic equilibrium satisfies the MHD equilibrium equation. Once the MHD equilibrium has been calculated the lowest order distribution function can be evaluated locally in the plasma.

Any stability analysis require first an equilibrium. Equilibria for the Levitated Octupole were calculated for betas ranging up to 17% in increments of 1% or less. For each case equilibrium quantites were mapped out in flux coordinates and stored in a library on the computer for future use in the stability calculations.

Chapter 3 deals with the linear high mode number MHD stability of multipoles. A single partial differential equation governing the ballooning mode is derived by a high toroidal mode number expansion of the MHD energy principle. This equation is solved by a perturbation expansion using the inverse toroidal mode number as the smallness parameter. This reduces the problem to solving two ordinary differential equations, one determining the structure of the mode along field lines and the other determining the structure of the mode

perpendicular to the field lines. Numerical solution to these equations for the Levitated Octupole configuration are given.

In Chapter 4 the kinetic equations for studying low frequency electromagnetic modes in an axisymmetric collisionless plasma with no toroidal magnetic field are derived. The derivation consists of a small frequency $\omega/\Omega \ll 1$, small Larmor radius, $\rho/L_n \ll 1$, $\rho/L_B \ll 1$ expansion of the linear Vlasov equation. The perturbed distribution function due to small electromagnetic and electrostatic perturbations is obtained. Moments of the perturbed distribution function are calculated and used in the quasi-neutrality condition and the force balance equations to obtain a complete set of equations governing the modes. Two frequency limits relative to the ion and electron bounce frequencies are considered, a low frequency limit where $\omega \ll \omega_{bi} \ll \omega_{be}$ and an intermediate frequency limit where $\omega_{bi} \ll \omega \ll \omega_{be}$. Here ω_b is the bounce frequency of a particle defined by $\omega_b^{-1} = 2\pi \oint \frac{d\ell}{|v_\chi|}$ where the integral is taken along a field line between the turning points of the particle.

Chapter 5 deals with the effect of parallel particle dynamics on the ballooning mode. A collisionless variational principle is constructed from the complete set of equations governing low frequency modes that were derived in Chapter 4. In the hydrodynamic limit $\omega^*/\omega \to 0$, $\omega_b/\omega \to 0$, $\rho \to 0$ this variational principle reduces to the Kruskal-Oberman energy principle. This energy principle is minimized in the same manner as the MHD energy principle resulting in an integro-differential equation for the marginally stable ballooning

mode. This equation contains a stabilizing kinetic term that takes into account the collisionless adiabatic compression of the plasma and the Fermi acceleration of the particles. The equation is solved for the Levitated Octupole configuration and compared with the MHD results.

In Chapter 6 finite Larmor radius effects on the ballooning mode are investigated. The set of three equations for the intermediate frequency regime $\omega_{bi} << \omega << \omega_{be}$ that were derived in Chapter 4 are used. Using a high toroidal mode number expansion these equations can be combined into a single partial differential equation. Ballooning mode stability criteria are found by solving this equation for the marginally stable mode with the largest temperature. The stability criteria for different plasma beta and Larmor radii are calculated for the Levitated Octupole.

A summary of the main results can be found in Chapter 7. In addition, some suggestions for future work are given.

The flux coordinates and velocity coordinates used in the derivations throughout this thesis are summarized in Appendix A. The representation of the perturbed magnetic and electric fields used in the kinetic analysis plus many useful identities are given in Appendix B. In Appendix C a table of Bessel function identities and integral relations helpful in the derivation of the kinetic equations can be found. Moments of the perturbed distribution function used in the derivation of the complete set of kinetic equations for low-frequency modes are summarized in Appendix D. The moments for two frequency

regimes are given: $\omega << \omega_b$ and $\omega_b << \omega$. Some of the data from the computer calculations of the stability criteria can be found in Appendix E. These cases are for the marginally stable mode with the largest temperature for a given plasma beta. The computer codes used for the equilibrium and stability calculations in this thesis are located on the National MFE computers. Appendix F gives details of the availability of these codes and where to find documentation.

Fig. (1.1) The Levitated Octupole Configuration

This picture shows the poloidal cross section of the Levitated Octupole. The dimensions in this diagram are used for all calculations presented in this thesis. All dimensions are in centimeters. This plot shows contours of poloidal magnetic flux for the Levitated Octupole with $\beta = 4.33\%$. $\psi_{s1} = 0.5318$, $\psi_{s2} = 0.5258$, $\psi_c = 0.8245$.

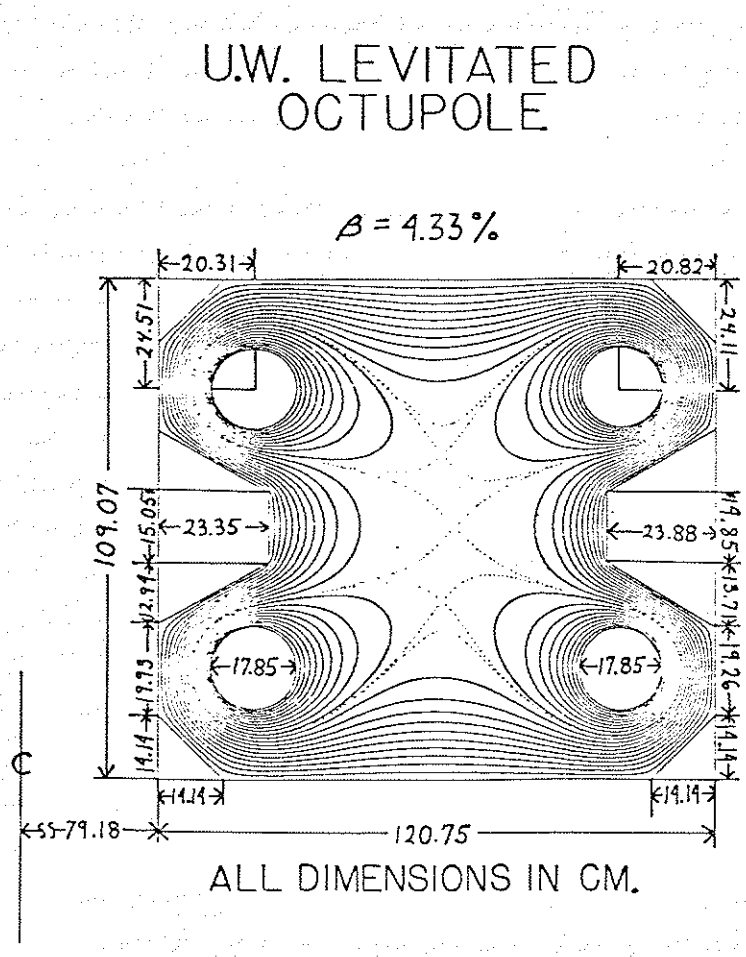

Fig. (1.1)

CHAPTER 2

Equilibrium

The starting place for any linear stability calculation is with equilibrium. This is a description of the steady state magnetic field configuration and the shape of the plasma. The critical beta for the occurrence of the ballooning mode is sensitive to the shape of the pressure profile and details of the magnetic field. Since one of the goals of this thesis is to calculate stability criteria that can be compared with experimental measurements, the stability calculation must be done in "real geometry", i.e., some reasonable facsimile of the actual device. This chapter deals with MHD and kinetic equilibrium in multipole devices.

In the multipole the vacuum magnetic field without any plasma gives a good approximation the magnetic field with plasma. By the vacuum magnetic field we mean the field generated by the currents in the rigid conductors. The reason why the plasma does not have a large effect on the equilibrium fields is that there are no large currents in the plasma. Since there is no inductively driven current in the plasma only the diamagnetic current due to the pressure gradient is present. This current is proportional to beta which is often small. One might wonder whether it is really necessary to calculate MHD equilibrium in a multipole. There are two reasons for solving the full equilibrium equations. The first reason is that the plasma beta is significant enough where it should be taken into account. Betas up to 35% have

been measured experimentally. For a plasma beta of 20% the diamagnetic effects of the plasma can change the stability criteria relative to a vacuum calculation by 20-30%. Another reason is that both the diamagnetic current and the relative change in the magnetic field can be measured. This means the applicability of the model can be checked directly.

In section A of this chapter the MHD equilibrium equations are introduced. In an axisymmetric geometry the MHD equilibrium is found by solving the Grad-Shafranov equation. Section B deals with collisionless kinetic equilibrium. The equilibrium distribution function is derived using a small Larmor radius expansion. It turns out the coefficients of the lowest order distribution function can be evaluated from an MHD equilibrium. In section C numerical procedures for solving the Grad-Shafranov equation in multipole geometry are discussed. Emphasis is on the OCTEC MHD equilibrium code. This code solves for MHD equilibrium in up-down symmetric multipoles with up to eight internal rings in an arbitrary polygon shaped vacuum vessel. Results of the calculation for the Levitated Octupole geometry are presented and the effect of beta on the equilibrium is discussed.

The stability calculations that will be presented in future chapters will be done self-consistently. This means plasma parameters such as beta, the currents and the pressure used in the stability calculation are in equilibrium. As a basis on which to do the stability calculations a series of MHD equilibria for the Levitated Octupole configuration were calculated and stored in a library on the

computer. This library consists of equilibria with beta ranging to 17% in the bridge region in increments of 1% or less. For these equilibria the field lines are mapped out and various equilibrium quantities needed for the stability calculations are computed.

A. MHD Equilibrium

The basic magnetohydrodynamic equations governing a steady state plasma are.

$$\vec{j}_0 \times \vec{B}_0 = \nabla p \tag{2.1}$$

$$\nabla \times \vec{B}_0 = \mu_0 \vec{j}_0 \tag{2.2}$$

$$\nabla \cdot \vec{B}_0 = 0 \ , \tag{2.3}$$

where $\vec{j}_0$ is the equilibrium current density, $\vec{B}_0$ is the equilibrum magnetic field and p is the scalar plasma pressure. These equations assume the absence of gravitation and a zero fluid velocity. For an axisymmetric configuration the cylindrical coordinates r, θ, z can be used. The magnetic field can be written in terms of the flux function ψ and the function I,

$$\vec{B}_0 = \frac{1}{r}\hat{\theta} \times \nabla\psi + \frac{I}{r}\hat{\theta} \ . \tag{2.4}$$

Here $I = rB_\theta$ and $\psi = \frac{1}{2\pi}\int \vec{B}_0 \cdot d\vec{S}$ where the surface integral is over the toroidal strip between a reference point and the point of interest.

The quantitiy ψ is related to the poloidal magnetic flux, ψ_p, by $\psi = \psi_p/2\pi$ and to the θ conponent of the magnetic vector potential by $\psi = rA_\theta$.

From Eq. (2.1) it follows that $\vec{B}_0 \cdot \nabla p = 0$ implying p is a function of ψ only, i.e. $p = p(\psi)$. Similarly $\vec{j}_0 \cdot \nabla p = 0$ and using Eq. (2.2) it is easy to show $rB_{0\theta} = I(\psi)$ is also a function of ψ only. Using the representation Eq. (2.4) for $\vec{B}_0$ in Eq. (2.1) and Eq. (2.2) one finds the equilibrium must satisfy the equation,

$$L\psi = \frac{\partial^2\psi}{\partial r^2} - \frac{1}{r}\frac{\partial\psi}{\partial r} + \frac{\partial^2\psi}{\partial z^2} = \mu_0 j_{0\theta} r \tag{2.5}$$

$$= -\mu_0 r^2 p'(\psi) - II'(\psi)$$

where the prime denotes the derivative with respect to ψ. Eq. (2.5) is commonly known as the Grad-Shafranov equation. The functions $p(\psi)$ and $I(\psi)$ are arbitrary functions of ψ. MHD theory does not give a clue to what the functions $p(\psi)$ and $I(\psi)$ are and they must be defined using outside considerations. If $p(\psi)$ and $I^2(\psi)$ are anything other then a linear or quadratic functions of ψ then Eq. (2.5) is a nonlinear equation.

The equilibrium current is given by,

$$\vec{j}_0 = \frac{1}{r}\hat{\theta} \times \nabla I(\psi) + j_{0\theta}\hat{\theta} \ . \tag{2.6}$$

where $j_{0\theta} = -rp'(\psi) - \frac{1}{r}II'(\psi)$. For the multipole there is no

toroidal magnetic field so $I(\psi) = 0$. This means there is no current parallel to the field lines. The only current is the diamagnetic current from $p'(\psi)$ and it is in the toroidal direction.

B. Kinetic Equilibrium

For the kinetic linear stability analysis the equilibrium distribution functions of the particle species are needed. The equilibrium distribution function for a collisionless plasma is found by solving the equilibrium Vlasov equation:

$$\vec{v}\cdot\nabla f_0 + \frac{q}{m}\left[\vec{E}_0 + \vec{v}\times\vec{B}_0\right]\cdot\nabla_v f_0 = 0 \ , \qquad (2.7)$$

where $\vec{E}_0$ and $\vec{B}_0$ are the equilibrium electric field and magnetic field respectively and f_0 is the equilibrium distribution function. Eq. (2.7) is solved self-consistently with Ampere's law and Poisson's equation.

In the absence of collisions and for static fields the energy of the individual particles is conserved. This means $\varepsilon = \frac{1}{2}v^2 + \frac{q}{m}\phi$ is a constant where $\vec{E}_0 = -\nabla\phi_0$ and ε is the energy per unit mass of a particle. In addition for axisymmetric configurations the canonical momentum cojugate to the ignorable coordinate θ is conserved. This means $p_\theta = mrv_\theta - q(\psi - \psi_0)$ is a constant of motion of the particle. Any function, $f_0(\varepsilon, p_\theta)$, that is a function of ε and p_θ only, satisfies

the equilibrium Vlasov equation. This means there are many solutions to Eq. (2.7).

A somewhat simplified case will be considered here. It will be assumed that the equilibrium varies over a scale length much larger then the Larmor radius of a particle i.e. $\rho/L_n \ll 1$ and $\rho/L_B \ll 1$ where ρ is the Larmor radius, L_n is the density scale length and L_B is the magnetic field scale length. The temperature will be assumed to be constant across the plasma. Using ρ/L_n and ρ/L_B as expansion parameters an approximate solution to Eq. (2.7) can be found by perturbation expansion. A derivation for the general case where there is an equilibrium electric field and the particle pressure is allowed to vary along field lines can be found in the paper by Rutherford and Frieman[15]. For the particular case where the system is axisymmetric and the pressure is scalar along a field line with no electric field the equilibrium satisfies the Grad-Shafranov equation[25]. A brief summary for the case of interest here where the toroidal magnetic field is zero is included below.

The orthogonal flux coordinates ψ, χ, θ will be used in this derivation and throughout the paper. The coordinate ψ is the flux function defined in Eq. (2.4). The unit vector $\hat{\psi}$ points perpendicular to a field line and lies in a constant θ plane. The coordinate χ measures along field lines and $\hat{\chi}$ is parallel to the field line. The coordinate θ is the toroidal coordinate. The Jacobian will be denoted by $\mathcal{J}$ and is given by $\mathcal{J}^{-1} = (\nabla\psi\times\nabla\chi)\cdot\nabla\theta$. Refer to Appendix A for a summary of the vector identities and differential operators for this

coordinate system. In this coordinate system $\vec{v} = v_\psi\hat{\psi} + v_\chi\hat{\chi} + v_\theta\hat{\theta}$. However, it is often convenient to use the velocity coordinates v_χ, $v_\perp$, ζ where $v_\perp^2 = v_\psi^2 + v_\theta^2$ is the perpendicular velocity and $\tan\zeta = -v_\psi/v_\theta$ is the gyrophase angle.

If we assume $\rho/L_n \ll 1$, $\rho/L_B \ll 1$ the first term in Eq. (2.7) is much smaller then the second term. To lowest order then, $\vec{v}\times\hat{\chi}\cdot\nabla_v f_0^0 = \partial f_0^0/\partial\zeta = 0$. This means f_0^0 does not depend on the gyrophase angle ζ so $f_0^0 = f_0^0(v_\chi, v_\perp, \vec{x})$. To first order

$$\vec{v}\cdot\nabla f_0^0 + \frac{q}{m} B_0 \frac{\partial f_0^1}{\partial\zeta} = 0 \ . \qquad (2.8)$$

Integrating over the coordinate ζ in Eq. (2.8) from 0 to 2π gives the additional condition $\hat{\chi}\cdot\nabla f_0^0 = 0$ which means f_0^0 is independent of the coordinate χ. As a consequence of axisymmetery f_0^0 is also independent of θ, hence, $f_0^0 = f_0^0(v_\chi, v_\perp, \psi)$. Solving Eq. (2.8) for f_0^1 gives

$$f_0^1 = -\frac{v_\perp}{\Omega}\cos\zeta\ \hat{\psi}\cdot\nabla f_0^0 = -mv_\perp\frac{r}{q}\cos\zeta\frac{\partial f_0^0}{\partial\psi} \ , \qquad (2.9)$$

where Ω is the gyrofrequency, $\Omega = \frac{qB}{m}$.

The selection of one particular particle distribution from the many possible solutions to Eq. (2.7) must be made from outside considerations. It is reasonable to assume that the plasma at one time in the past was collisional and the distribution function is mainly Maxwellian with a simple density gradient across the field. To lowest

order then we will assume $f_0^0 = f_m\left[1 + (\psi - \psi_0)\frac{1}{n_0}\frac{\partial n_0}{\partial\psi}\right]$ where f_m is the Maxwellian distribution function $f_m = n_0\left(\frac{m}{2\pi T}\right)^{3/2}\exp\left(-\frac{m\varepsilon}{T}\right)$. Here ε is the energy per unit mass of a particle, $\varepsilon = \frac{1}{2}v_\chi^2 + \frac{1}{2}v_\perp^2$, and the quantity n_0 is the particle density on the flux surface ψ_0. To lowest order in Larmor radius we then have as our equilibrium distribution function,

$$f_0 = f_0^0 + f_0^1 = f_m\left[1 + (\psi - \psi_0)\frac{1}{n_0}\frac{\partial n_0}{\partial\psi} - mv_\perp\frac{r}{q}\cos\zeta\frac{1}{n_0}\frac{\partial n_0}{\partial\psi}\right]$$

$$= f_m\left[1 + (\psi - \psi_0)\frac{1}{n_0}\frac{\partial n_0}{\partial\psi} + \frac{mv_\theta v^*}{T}\right] \ , \qquad (2.10)$$

where $v^* = -\frac{T}{q}\frac{r}{n_0}\frac{\partial n_0}{\partial\psi}$ is the diamagnetic drift velocity. Note that $f_0 = f_0(\varepsilon, p_\theta)$ and so Eq. (2.10) satisfies the equilibrium Vlasov equation exactly for $\vec{E}_0 = 0$. However, for some values of ψ and v_θ Eq. (2.10) for f_0 is negative and so the requirement $\rho/L_n \ll 1$ is still necessary for this distribution function to make sense physically.

One of the properties of Eq. (2.10) for f_0 is that the particle species has a net fluid velocity $\vec{v}_0 = \int f_0\vec{v}\, d^3v = v^*\hat{\theta}$. There is no equilibrium electric field and $\vec{j}_0 = -r\frac{\partial p}{\partial\psi}\hat{\theta}$ where $p = \sum n_0 T$ with the sum over all the particle species. For this form of the current density the equilibrium satisfies the Grad-Shafranov equation with $I(\psi) = 0$. The equilibrium quantities from the solution of the Grad-Shafranov equation can be used to evaluate the coefficients of f_0

in Eq. (2.10). Hence, knowing the MHD equilibrium the distribution function to lowest order in Larmor radius can be determined locally.

C. Numerical Method and Results

In most cases MHD equilibrium must be solved numerically. Not many analytic solutions conform to real situations. Much work has been done on the problem of numerically solving the MHD equations in axisymmetric geometry particularly in tokamaks. The tokamak liturature on this topic is relavant to the problem of solving for MHD equilibrium in multipoles as well since the two problems have many simularities. In fact, the multipole equilibrium code, OCTEC, used for the study here was adapted from the tokamak equilibrium code TOPEC used to study equilibrium in the Tokapole device[30].

No attempt will be made to review the vast amount of liturature dealing with the solution of the Grad-Shafranov equation. A few papers the author found particularly helpful for certain problems are worth mentioning. For a review of the problem and techniques for numerically solving MHD equilibrium Lackner[31] and Johnson et. al.[32] are good starting places. Specific iteration techniques are dicused by Chu et.al.[33] and Marder and Weitzner[34]. The paper by Chu et.al. also looks at a wide variety of plasma shapes. The paper by Marder and Weitzner gives a three-level iteration scheme which allows for the possibility of more then one solution depending on the initialization of the problem. Callen and Dory[35] numerically investigate the

effects of different pressure and current profiles including high beta plasmas. Suzuki[36] discusses the problem of solving free-boundary tokamak equilibrium.

The nonlinearity of the Grad-Shafranov equation for a general pressure profile requires the use of an iteration scheme for finding the solution. For low beta, the simple Picard iteration scheme can be used,

$$L\psi^{n+1} = \mu_0 j_{0\theta}(r,\psi^n)r = -\mu_0 r^2 p'(\psi^n) \ .$$

Here n is the number of the nth iteration. For configurations like the multipole where the equilibrium is similar to the vacuum field the iteration procedure can be started off by taking ψ_0 as the vacuum field flux function. The toroidal current $j_{0\theta}(r,\psi^n)$ is then evaluated resulting in an inhomogeneous equation that can be solved by conventional means for the new values of ψ. For the calculations presented here the operator L is inverted using a finite difference scheme. This procedure is then repeated until the difference between ψ^{n+1} and ψ^n is small.

For higher beta's the Picard iteration converges very slowly. Then the following iteration scheme is used,

$$L\psi^{n+1/3} = \mu_0 j_{0\theta}(r,\psi^n)r$$

$$L\psi^{n+2/3} = \mu_0 j_{0\theta}(r,\psi^{n+1/3})r$$

$$\psi^{n+1} = \alpha\psi^{n+1/3} + (1-\alpha)\psi^{n+2/3} \ ,$$

where α is chosen by trial and error until a good convergence rate is achieved. It is not known exactly why for higher betas the solution converges very slowly. A high beta equilibrium and a vacuum flux plot look very much the same. One possible answer is the existence of several solutions for the same boundary conditions, beta and pressure profile prescription. Something like this has been observed analytically in a straight multipole configuration by Spencer[37] for the case of $\beta = 1$ sharp boundary equilibria. Spencer found sometimes 2 and 3 separate solutions for the same boundary conditions. In most cases the solutions were very similar to each other.

In order to solve Eq. (2.5), a pressure profile is needed. One requirement is that the pressure gradient be zero on a separatrix. This is a numerical requirement as well as a stability requirement. Since the change in the flux tube volume near the separatrix is large a pressure gradient would create a large current near the field null. This causes numerical instabilities since small changes in the current causes large changes in the surrounding fields. It is also known from resistive MHD theory that a pressure gradient across an x-point is not a stable situation. For an arbitrary multipole configuration there are $m - 1$ null points possible for m current carrying conductors. Some of these nulls might be degenerate but in general the pressure gradient must go to zero on each separatrix. The interchange stability criterion $p'V'' > 0$ must also be satisfied. Since V'' changes sign at the critical flux surface p' must change sign also. This means p' must equal zero at the point where V'' equals zero. This occurs at the

critical flux surface, ψ_c. Another condition is that the pressure go to zero at the wall. For the flux surfaces to be interchange stable between ψ_c and the wall and still meet this condition, p must equal zero in this entire region. For an octupole configuration with one null on the midplane and two symmetric nulls above and below the midplane a suitable function for the pressure is,

$$
\begin{aligned}
p &= 0 && \psi_w < \psi < \psi_c \\
p &= p_0 \sin^2\left[\frac{\pi}{2}\left(\frac{\psi - \psi_c}{\psi_{s1} - \psi_c}\right)^{\nu 1}\right] && \psi_c < \psi < \psi_{s1} \\
p &= p_0 && \psi_{s1} < \psi < \psi_{s2} \\
p &= p_0 \sin^2\left[\frac{\pi}{2}\left(\frac{\psi - \psi_r}{\psi_{s2} - \psi_r}\right)^{\nu 2}\right] && \psi_{s2} < \psi < \psi_r
\end{aligned}
\qquad (2.11)
$$

where ψ_w is the value of the flux at the vacuum vessel wall, ψ_c is the flux at the critical flux surface, ψ_{s1} is the flux at the separatrix, ψ_{s2} is the flux at the second separatrix, and ψ_r is the flux at the ring. The quantities $\nu 1$ and $\nu 2$ are parameters used to shape the pressure profile. The peak pressure p_0 is usually chosen to give a specific beta. This pressure profile peaks on the separatrices and goes to zero at the wall and the critical flux surface. It has zero pressure gradient at the wall, at ψ_c and at the separatrices.

The Levitated Octupole has four copper rings inside a conducting vacuum vessel. For the calculation here, the rings and walls are assumed to be perfectly conducting. The function ψ is constant on the

surfaces of these conductors and they serve as the boundaries for solving Eq. (2.5). The flux function can be divided into two parts $\psi = \psi_{vac} + \psi_{plas}$, where ψ_{vac} is the flux function of the vacuum magnetic field due to the currents in the rings and their image currents in the walls and ψ_{plas} is the contribution to the flux function of the diamagnetic current of the plasma and its image currents in the rings and walls.

The vacuum field is calculated by solving the problem consisting of Eq. (2.5) with the right hand side set equal to zero along with the boundary conditions that ψ be constant on the rings and walls such that the difference $2\pi(\psi_w - \psi_r)$ is equal to the total amount of flux in the machine. The operator L is finite differenced using a 5-point difference scheme and the values of ψ are solved on a discete 125 × 57 grid. The dimensions of the grid were chosen for convenience since their ratio closely approximates the ratio of the width of the Levitated Octupole to half its height and also allows enough points to represent the solution in the bridge region between the rings and wall. Wall boundary conditions can be imposed on up to 20 discrete line segments inside the grid. The placement of the line segments is arbitrary so a wide variety of polygon shaped vacuum vessels can be simulated. The bridge region will be used as a reference point for most of these calculations. It is a convenient place for comparisons of the theory and experiments. The bridge region is defined here as the chord running from the center of the outside ring radially to the outside wall.

The finite difference equations are solved by the method of successive line over relaxation. The procedure involves finding an entire row of ψ values explicitly holding adjacent rows fixed. Successive rows are solved using the latest values of ψ. This process is carried out across the entire mesh and repeated until the solution converges. In addition a relaxation parameter is used to speed convergence. This procedure is described in more detail in reference[38]. Generally the solution converges to a relative error of less then 10^{-6} between successive iterations in about 140 sweeps over the entire mesh. On the MFE Cray 1 computer the vacuum field calculation takes less then 1 second of computer time.

Flux is assumed conserved with the addition of the plasma so the boundary conditions for solving the inhomogeneous problem is that ψ_{plas} equal zero on the rings and walls. The problem is a free boundary problem because the boundary of the plasma ψ_c, is solved as a part of the problem. During each iteration ψ_c, ψ_{s1}, and ψ_{s2} are recalculated and the latest values are used in evaluating $\partial p/\partial\psi$. For most of the calculations here the beta in the bridge region on the separatrix is prescribed and the peak pressure, p_0, is calculated each iteration from the formula $p_0 = \beta_{bridge}(B_0^2/2\mu_0)$.

Fig.(2.1) shows the contours of the flux function ψ for the vacuum field of the Levitated Octupole configuration. One particular feature is that there are three null points, one lying on the midplane and two more above and below the midplane. The Levitated Octupole is an minimum average B device. This is illustrated in Fig. (2.2). Here is

plotted $V' = \oint \frac{dl}{B}$ versus ψ for the field lines outside of the separatrix. Stable confinement requires that $p'V'' > 0$ and from this plot it can be seen that the slope of V' and p have the same sign between the separatix an ψ_c. Near ψ_c the slope of V' is zero and the interchange mode is marginally stable at this point. Outside ψ_c the curve of V' again rises slowly.

Fig. (2.3) shows the flux function contours for an equilibrium with $\beta = 10\%$. The boundary conditions for this calculation were $\psi_r = 0.0$ and $\psi_w = 1.0$. For this equilibrium $\psi_{s2} = 0.4922$, $\psi_{s1} = 0.4966$ and $\psi_c = 0.7845$. The shaping parameters were $\nu_1 = 1.4$ and $\nu_2 = 1.0$ giving the pressure profile shown in Fig. (2.4). Here the pressure is plotted as a function of r in the bridge region. This pressure profile is plotted as a function of ψ in Fig. (2.5). This pressure profile is similar to that observed experimentally for this β. The main difference between the vacuum field equilibrium and higher beta equilibrium is that the field lines are pushed away from the separatrix in the common flux region and toward the separatrix in the private flux region. The diamagnetic current of the plasma in the common flux region is in the same direction as the ring current. This causes the flux in the common flux region to increase with the addition of plasma. The diamagnetic current of the plasma in the private flux region is in the direction opposite that of the ring current. This causes the flux in the private flux region to decrease with the addition of plasma. One consequence of the field lines being displaced by plasma is that near the separatrix the volume of a flux tube, V', increases. This can

be seen in Fig. (2.6). Here V' is plotted for the vacuum field case and for the case $\beta = 15\%$. For this plot the coordinate ψ is normalized relative to $\psi_c - \psi_{s1}$ for each case. The flux tube volume is greater near the separatrix for the $\beta = 15\%$ case. Also, the slope of the curve is everywhere greater or equal to the slope or the curve for the vacuum field case. This is taking in to account the fact that $\psi_c - \psi_{s1}$ is smaller for $\beta = 15\%$ then for a vacuum. Fig. (2.6) is evidence that the plasma digs its own well. The minimum average B magnetic well gets deeper as the plasma beta is raised. This has a stabilizing effect on the ballooning instability. However, in the case of the multipole this effect is rather small.

Another effect of beta on the equilibrium is to make the critical flux surface move inwards. As the field lines outside the separatrix are pushed outwards the radius of curvature of the field lines in the good curvature region increases. This makes the point where the average good curvature is zero move closer to the separatrix. This means for a given amount of flux in the machine $\psi_c - \psi_{s1}$ decreases as β increases. Fig. (2.7) illustrates this effect. Here $\psi_c - \psi_{s1}$ versus β is plotted. This has a detrimental effect on the stability of the plasma because the pressure scale length decreases with increasing beta. The effect is small but noticeable.

The next few plots illustrate some of the characteristics of an equilibrium in the Levitated Octupole. Fig. (2.8) shows the magnitude of the magnetic field line for the vacuum field as a function of relative distance along the field line for one half of the field line.

This particular field line lies on the flux surface with $\psi = 0.7003$ which is half way between ψ_c and ψ_{sl}. Basically the magnetic field is like that of a straight multipole with a 1/r dependence superimposed. In addition there are several local magnetic wells caused by the corners of the vacuum vessel. However, if the magnetic field were allowed to soak into the outside walls as is the case in the actual experiment one would expect these little local magnetic wells to be smoothed out. With this magnetic field configuration there are basically three classes of particles: those trapped in the multipole magnetic wells, particles trapped in the toroidally induced well and circulating particles. Fig. (2.9) shows a plot of the magnitude of the magnetic filed as a function of relative distance along the field line and ψ for the flux surfaces between ψ_c and ψ_{sl}. The main thing to note from this plot is that the magnetic field scale length is quite a bit larger then the pressure scale length. Also the small local magnetic wells disappear near ψ_{sl}. Fig. (2.10) shows the function $2/rB^2R_c$ as a function of relative distance along the field line for the field line with $\psi = 0.7003$ of a vacuum field. Here R_c is the radius of curvature of a field line. The function $2/rB^2R_c$ is a measure of how good the curvature is. Integrating along a field line $\int d\ell \frac{2}{rB^2R_c} = -V''$. This plot shows the good and bad curvature regions along a typical field line. The ballooning mode is generally localized in the bad curvature region having the smallest magnitude of the magnetic field. This occurs in the region between the outside ring and the nose and wall.

In summary, the MHD equilibrium for the Levitated Octupole was calculated using a numerical scheme which solves the Grad-Shafranov equation in this geometry. The plasma beta affects the equilibrum by increasing the depth of the minimum average B well. This has a stabilizing effect on on ballooning instabilities. However, as beta is raised the difference $\psi_c - \psi_{sl}$ decreases steepening the pressure gradient. This has a destabilizing effect on ballooning instabilities. The lowest order distribution function was calculated by a small Larmor radius expansion of the equilibrium Vlasov equation. This distribution function can be evaluated locally using an MHD equilibrium.

Using the procedures discussed in this chapter the MHD equilibrium for the Levitated Octupole configuration was calculated for a sequence of betas ranging up to 17% in increments of 1% or less. The field lines were mapped out in the coordinate ψ and as a function of the relative length along the field line. In the multipole mapping out the fields in terms of the relative length along field line is more convenient then mapping them out as a function of χ. By relative length along field line we mean that for each ψ the field line is divided an equal number of steps. The step size is a function of ψ. This method of mapping out the field lines represents the fields well and also allows the derivative to be numerically evaluated using a fairly simple procedure both along field lines and across field lines. The coordinate χ was not used along field lines because the region near the field null is represented with too few points for calculation purposes. For each equilibrium calculated for the Levitated Octupole

equilibrium quantities needed for the stability analysis were calculated as functions of ψ and relative length along a field line. The equilibrium quantities that are needed are the magnetic field strength, the inverse curvature, the radial coordinate r plus several functions of ψ only such as pressure, p′ and step size.

Fig. (2.1) Vacuum Flux Contours for Levitated Octupole

Contours of the poloidal flux function ψ for the Levitated Octupole for a vacuum magnetic field. $\psi_r = 0.0$, $\psi_{s2} = 0.5522$, $\psi_{s1} = 0.5592$, $\psi_c = 0.8483$, $\psi_w = 1.0$.

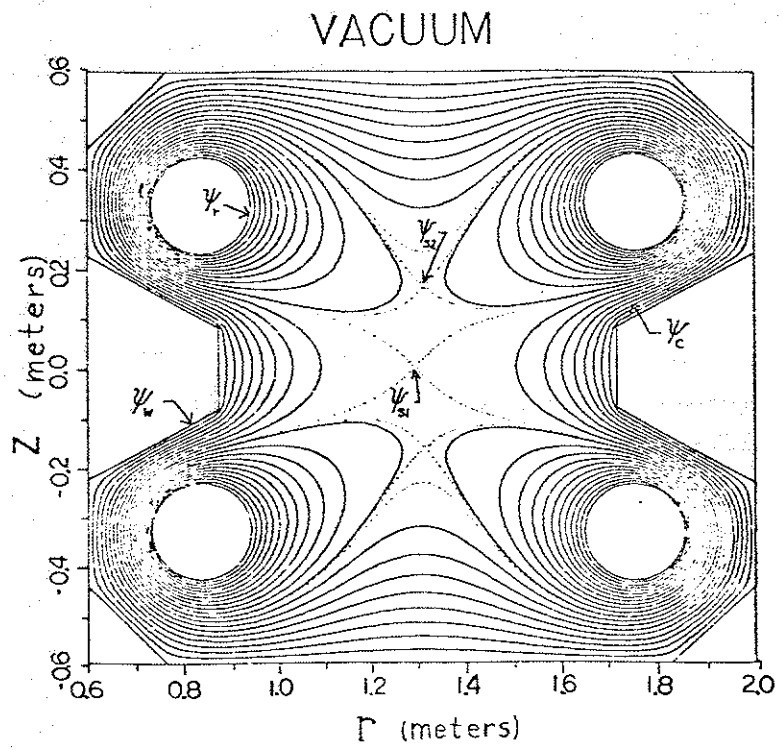

Fig. (2.1)

Fig. (2.2) V' vs ψ for Levitated Octupole Vacuum Field

Plot of $V' = \oint \frac{d\ell}{B}$ versus ψ for the vacuum magnetic field in the Levitated Octupole. The range of ψ is from the separatrix, $\psi_{s_1} = 0.5592$, to the critical flux surface, $\psi_c = 0.8483$. At ψ_c $\partial V'/\partial\psi = 0$.

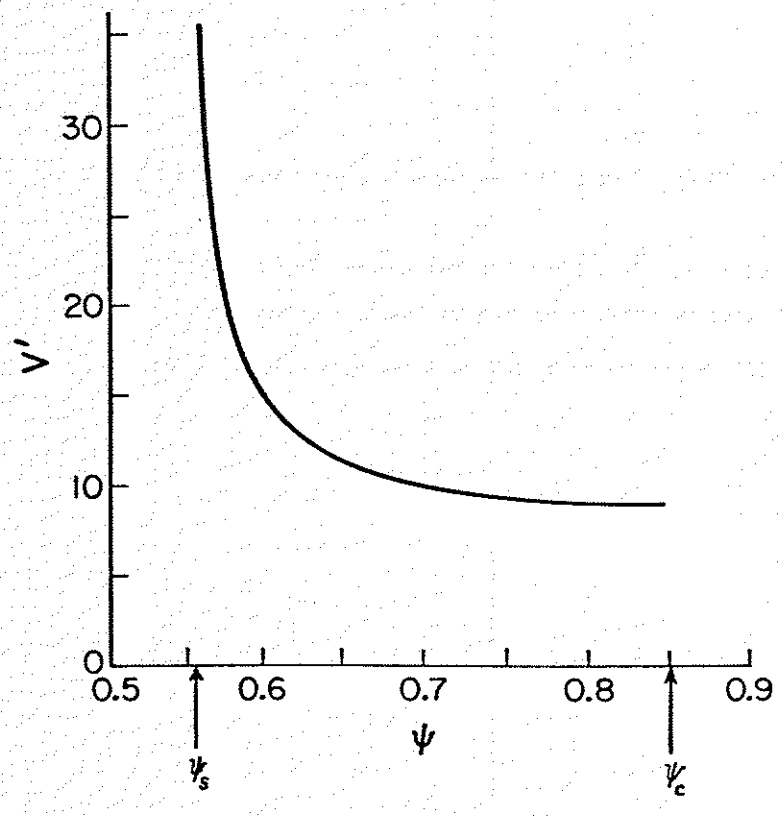

Fig. (2.2)

Fig. (2.3) Equilibrium Flux Contours for β = 10%

Contours of the flux function ψ for the Levitated Octupole for an MHD equilibrium with β = 10%. $\psi_r = 0.0$, $\psi_{s2} = 0.4922$ $\psi_{s1} = 0.4966$, $\psi_c = 0.7845$, $\psi_w = 1.0$.

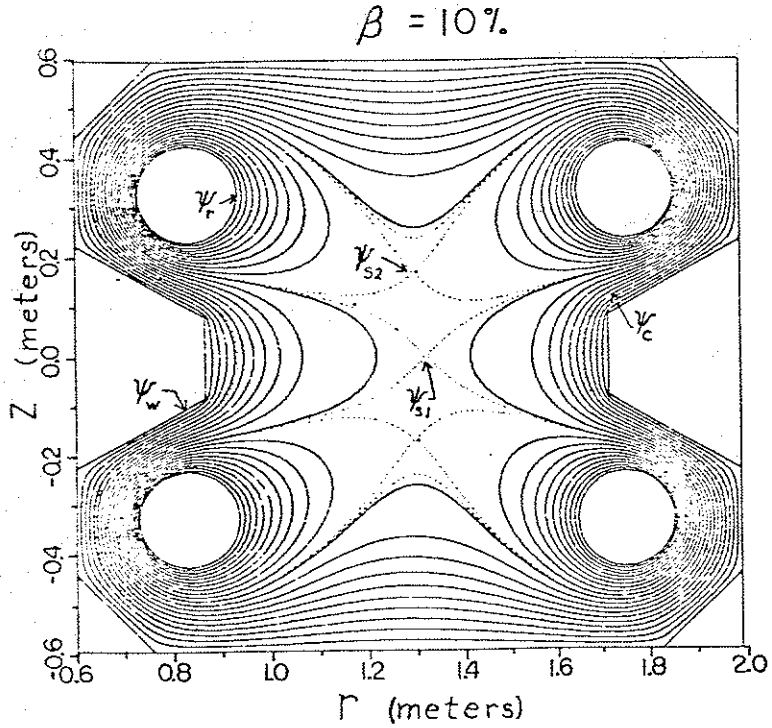

Fig. (2.3)

Fig. (2.4) Pressure vs r Bridge Region

The equilibrium pressure for β = 10% versus r in the bridge region of the Levitated Octupole. $p_0 = 1.784 \times 10^4$ nt/m^2, $\nu_1 = 1.4$, $\nu_2 = 1.0$.

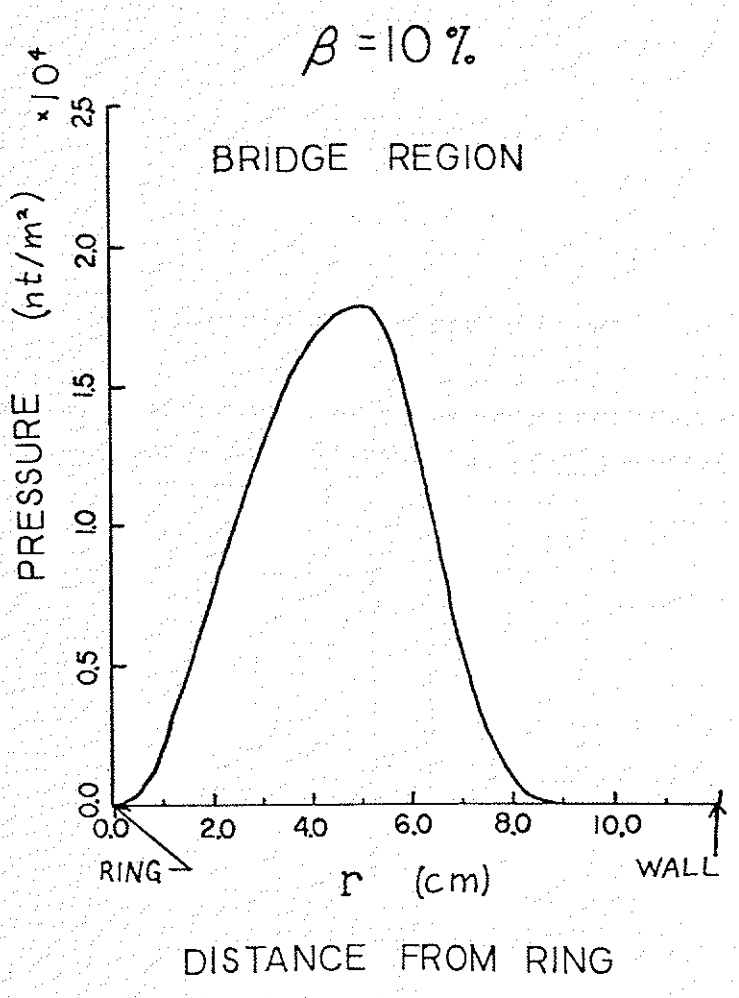

Fig. (2.4)

Fig. (2.5) Pressure vs ψ for β = 10%

The equilibrium pressure profile vs ψ for an equilibrium with β = 10%. $p_0 = 1.784 \times 10^4$ nt/m^2, $\nu_1 = 1.4$, $\nu_2 = 1.0$.

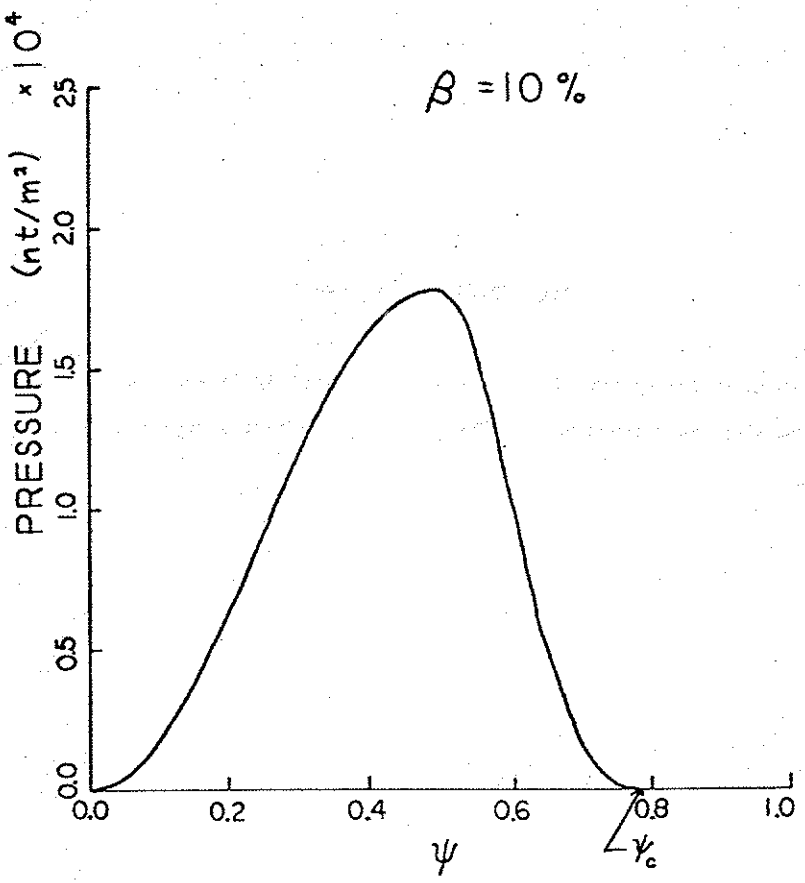

Fig. (2.5)

Fig. (2.6) V' vs ψ for Vacuum and β = 15%

Plot of $V' = \oint \frac{dl}{B}$ for the vacuum field case and the β = 15% case. V' is plotted relative to $\psi - \psi_{s1}$. For the vacuum case $\psi_c - \psi_{s1}$ = 0.2961. For the β = 15% equilibrium $\psi_c - \psi_{s1}$ = 0.2834.

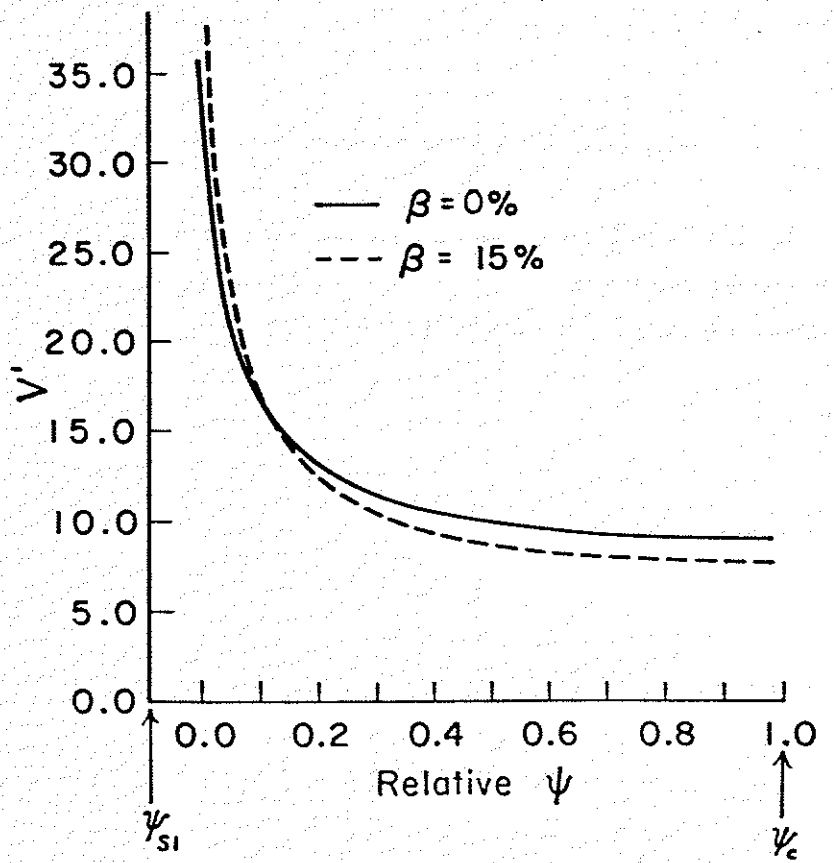

Fig. (2.6)

Fig. (2.7) $\psi - \psi_{s1}$ vs β

Plot of the amount of flux between the separatrix and the critical flux surface as a function β. The pressure gradient steepens as β is raised.

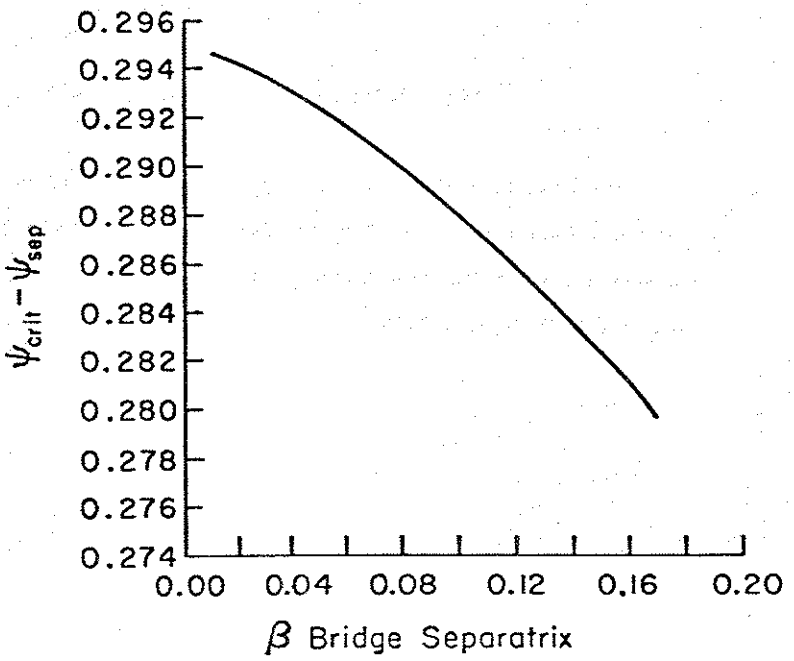

Fig. (2.7)

Fig. (2.8) |B| vs ℓ

The magnitude of the vacuum magnetic field as a function of the relative distance along a field line for the flux surface $\psi = 0.7003$. Plot shows half of the field line starting ot the inside midplane moving along the field line to the outside midplane.

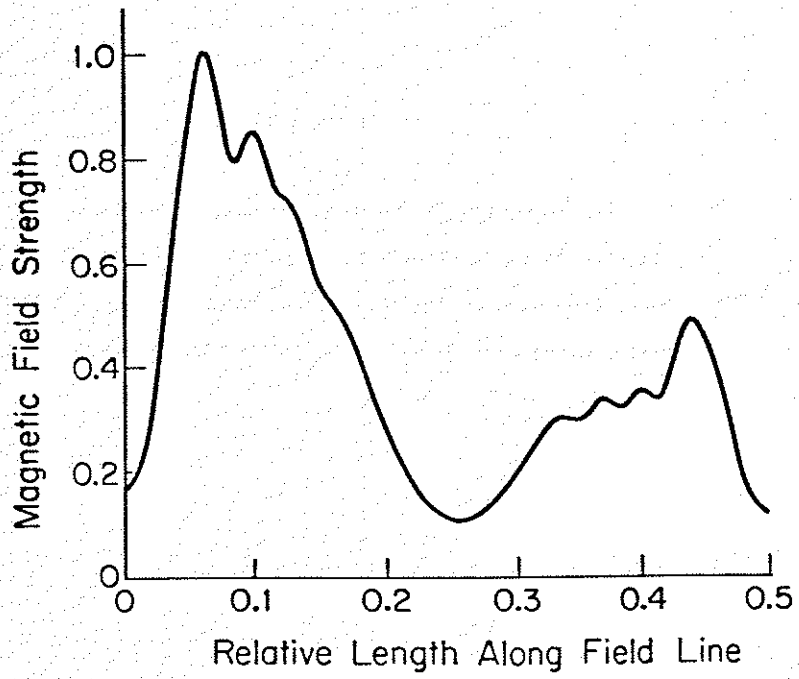

Fig. (2.8)

Fig. (2.9) |B| for Levitated Octupole

The magnitude of the vacuum magnetic field plotted as a function of the relative distance along the field line and ψ for the flux surfaces between the separatrix and the critical flux surface. $\psi_{sl} = 0.5592$, $\psi_c = 0.8483$.

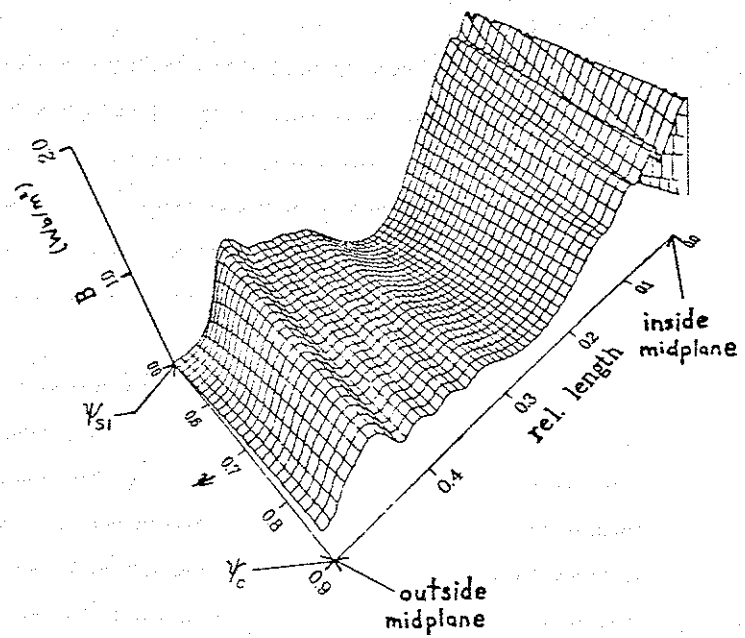

Fig. (2.9)

Fig. (2.10) $\frac{2}{rB^2R_c}$ vs ℓ

The function $\frac{2}{rB^2R_c}$ as a function of the relative distance along the field line with $\psi = 0.7003$ for the vacuum field. The function $2/rB^2R_c$ is a measure of how good the curvature is: $\oint \frac{2}{rB^2R_c} = -V''$. Plot shows half the field line starting at the inside midplane moving along the field line to the outside midplane.

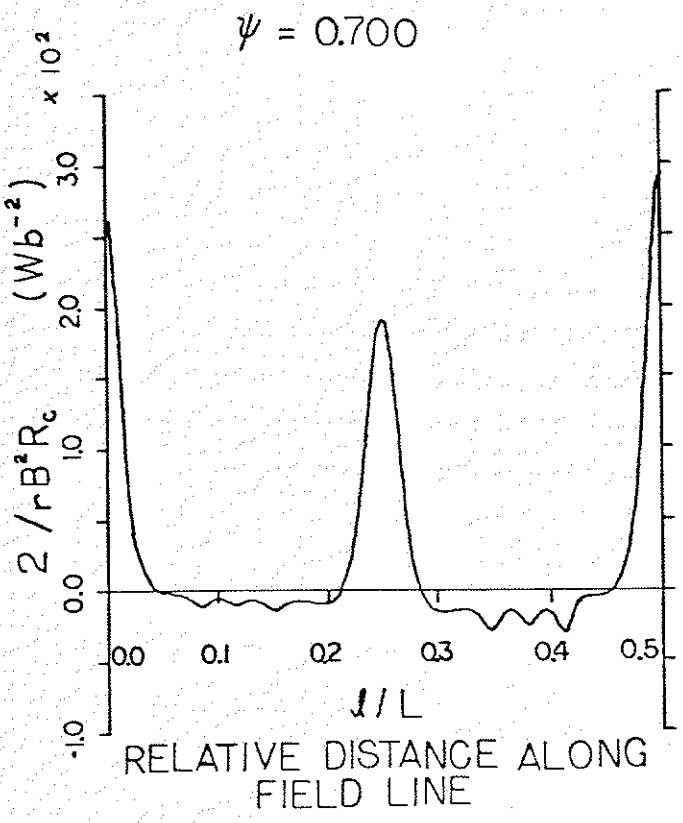

Fig. (2.10)

CHAPTER 3

High Mode Number MHD Stability of Toroidal Multipoles

The ballooning mode is basically a magnetohydrodynamic (MHD) instability. The main structure of the ballooning mode is determined by the MHD equations. MHD theory also gives a prediction of the critical beta. Since MHD is also the simplest model of a plasma for which ballooning modes are possible it is the logical starting place for our analysis. This chapter deals with the MHD stability of axisymmetric closed field line systems.

The linear MHD stability of a shearless axisymmetric plasma was first analyzed by Bernstein et al.[7] who found a mode with infinite toroidal mode number, $n = \infty$, is the most unstable mode. This is because the shorter the toroidal wavelength the less the field lines are bent in the toroidal direction. The MHD stability of the multipole was first worked out analytically for a straight multipole by Ohkawa and Kerst[9]. In the limit $n \to \infty$ the question of stability can be reduced to solving a second order ordinary differential equation on each field line. The eigenvalue of this equation gives a critical pressure gradient above which the system is unstable[10]. This equation has been solved numerically for several configurations modeling experiments[3,5,39]. The results generally predict a low beta limit for the multipole. For the case of the Levitated Octupole

the infinite n beta limit is 4.33%. Experiments in this device have observed betas up to 35%[4].

It is well known that low frequency modes with short wavelengths are stabilized by finite Larmor radius effects. Thus, the actual beta limit may be set by lower n number modes. In this chapter the MHD stability is analyzed for large but not infinite toroidal mode number in an axisymmetric closed field line system. Previous work on high n MHD stability has been done in tokamak geometries by Conner, Hastie and Taylor[23]. In their study shear plays an important role in the high n expansion which makes their analysis not applicable to closed field line systems. Other analyses contemporary to the work presented here have been done by Adler and Lee[40] and Dobrott and Moore[41].

In section A the partial differential eigenvalue equation governing high n modes is derived. In section B a method for finding approximate solutions to this equation is developed. The method involves a perturbation expansion around the $n = \infty$ solutions. The problem is reduced to solving two ordinary differential equations, one determining the structure of the mode along field lines and the other determining the structure perpendicular to the field lines. From the solution of these equations the full 3-dimensional structure of the mode is determined. Numerical solutions to these equations for a Levitated Octupole configuration are given in section C. The results give stability criteria for high n modes at various betas.

A. MHD Large n Expansion

The large n expansion of the linearized MHD equations is obtained by minimizing the energy integral and retaining terms of order n^{-2}. The orthogonal flux coordinate system (ψ, χ, θ). The coordinate ψ is related to the poloidal magnetic flux by $\psi = \psi_p/2$ and is in the direction perpendicular to a field line in a constant θ plane, χ is in the direction parallel to a field line and in MKS units has dimensions webers/m, and θ is the toroidal angle. The Jacobian is given by $\mathcal{J}^{-1} = (\nabla\psi \times \nabla\chi)\cdot\nabla\theta$. Refer it Appendix A for a summary of these coordinates. The MHD energy integral for a small displacement $\vec{\xi}$ is,

$$\delta W = \frac{1}{2}\int d\tau \left[\frac{1}{\mu_0}\vec{B}_1^2 - \vec{j}_0\cdot\vec{B}_1\times\vec{\xi} + (\vec{\xi}\cdot\nabla p)(\nabla\cdot\vec{\xi}) + \gamma p(\nabla\cdot\vec{\xi})^2\right] , \tag{3.1}$$

where $\vec{B}_1 = \nabla\times(\vec{\xi}\times\vec{B}_0)$ is the perturbed magnetic field, $\mu_0\vec{j}_0 = \nabla\times\vec{B}_0$ is the equilibrium current density and $d\tau$ is the volume element, $d\tau = \mathcal{J}\, d\psi\, d\chi\, d\theta$.

The θ dependence of the perturbation $\vec{\xi}$ can be represented by a Fourier series. For an axisymmetric system it is sufficient to look at one Fourier component at a time since the Fourier components are uncoupled. It is convenient to express $\vec{\xi}$ in the following form,

$$\xi_\psi = \frac{1}{rB} X(\psi,\chi)\exp(-in\theta) , \tag{3.2.1}$$

$$\xi_\chi = BZ(\psi,\chi)\exp(-in\theta) , \tag{3.2.2}$$

$$\xi_\theta = i \frac{r}{n} Y(\psi,\chi) \exp(-in\theta) , \qquad (3.2.3)$$

where X is the pertubation in units of the flux function ψ, Y is in units of an angular displacement in the toroidal direction, and Z is in units of $\vartheta\chi$. Carrying out the integration over θ and expressing $\vec{\xi}$ in terms of X, Y, Z the equation for δW becomes

$$\delta W = \pi \int d\psi\, d\chi\, \mathcal{J} \Big\{ \frac{1}{\mu_0} \frac{1}{\mathcal{J} r^2 B^2} \Big(\frac{\partial X}{\partial \chi}\Big)^2 + \frac{1}{\mu_0} \frac{1}{n^2} \frac{r^2}{\mathcal{J}^2} \Big(\frac{\partial Y}{\partial \chi}\Big)^2$$

$$+ p' D X^2 + \frac{B^2}{\mu_0} \Big[Y + \frac{\partial X}{\partial \psi} + \frac{\mu_0 p'}{B^2} X \Big]^2$$

$$+ \gamma p \Big[Y + \frac{\partial X}{\partial \psi} + DX + \frac{\mu_0 p'}{B^2} X + \frac{1}{\mathcal{J}} \frac{\partial Z}{\partial \chi} \Big]^2 \Big\} . \qquad (3.3)$$

where the prime denotes the derivative with respect to ψ. The quantity D is related to the inverse of the radius of curvature, $\vec{\kappa}$, of the field lines.

$$D = \frac{1}{\mathcal{J}} \frac{\partial \mathcal{J}}{\partial \psi} - \frac{\mu_0 p'}{B^2} = - \frac{2\mu_0}{B^2} \frac{\partial}{\partial \psi} \Big(p + \frac{B^2}{2\mu_0} \Big) = - \frac{2}{rB} |\vec{\kappa}| . \qquad (3.4)$$

where $\vec{\kappa} = \hat{\chi} \cdot \nabla \hat{\chi}$.

Two things are immediately obvious from this form of δW. The only term that can make δW negative is the term involving D, and the mode with $n = \infty$ is the most unstable since it minimizes the

stabilizing contribution due to stretching the field lines in the θ direction by the perturbation Y.

As the normalizing condition we choose to hold fixed the perpendicular kinetic energy,

$$\delta K_\perp = \frac{1}{2} \int d\tau\, \rho_m \vec{\xi}_\perp^* \cdot \vec{\xi}_\perp \qquad (3.5)$$

$$= \pi \int d\psi\, d\chi\, \rho_m \mathcal{J} \Big\{ \frac{X^2}{r^2 B^2} + \frac{r^2}{n^2} Y^2 \Big\} ,$$

where ρ_m is the mass density. The main reason for neglecting Z in the kinetic energy is that it makes subsequent analysis difficult. Also in calculating the stability criteria we are principally interested in finding the point at which the mode is marginally stable. At this point ω^2 equals zero and the normalizing condition is not important. Furthermore, it can be shown that the contribution of Z to the kinetic energy is smaller than $\delta K_\perp$. This means that the quantity ω^2 calculated by minimizing the expression $\omega^2 = \delta W / \delta K_\perp$ is close to the true MHD frequency of the mode. Minimizing $\omega^2 = \delta W / \delta K_\perp$ with respect to Y yields an expression identical with the θ component of the equation of motion.

$$\frac{1}{\mu_0} \frac{1}{n^2} \frac{\partial}{\partial \chi} \Big(\frac{r^2}{\mathcal{J}} \frac{\partial Y}{\partial \chi} \Big) = - \frac{1}{n^2} \rho_m \omega^2 \mathcal{J} r^2 Y \qquad (3.6)$$

$$+ \mathcal{J} \frac{B^2}{\mu_0} \Big(Y + \frac{\partial X}{\partial \psi} + \frac{\mu_0 p'}{B^2} X \Big) + \mathcal{J} \gamma p \Big[Y + \frac{\partial X}{\partial \psi} + \frac{\mu_0 p'}{B^2} X + DX + \frac{1}{\mathcal{J}} \frac{\partial Z}{\partial \chi} \Big] .$$

For large n^2 a perturbation expansion in orders of n^{-2} of Eq. (3.6) yields to lowest order

$$Y = -\frac{\partial X}{\partial \psi} - \frac{1}{B^2/\mu_0 + \gamma p}\left\{\left[p' + \gamma p\left(D + \frac{\mu_0 p'}{B^2}\right)\right]X + \frac{\gamma p}{\mathcal{J}}\frac{\partial Z}{\partial \chi}\right\} . \tag{3.7}$$

In addition to considering $1/n^2 \sim O(\varepsilon)$ where ε is the smallness parameter low beta will also be assumed so that $\beta \sim O(\varepsilon)$. Also generally with low beta plasmas it is also the case that the pressure scale length is smaller than the magnetic scale length. This implies $p' >> pD$ so that $pD/p' \sim O(\varepsilon)$. Substituting Eq. (3.7) for Y into Eq. (3.3) for δW and retaining terms to $O(\varepsilon)$ gives,

$$\delta W = \pi \int d\psi\, d\chi \left\{\frac{1}{\mu_0}\frac{1}{\mathcal{J} r^2 B^2}\left(\frac{\partial X}{\partial \chi}\right)^2 + \frac{1}{\mu_0}\frac{1}{n^2}\frac{r^2}{\mathcal{J}}\left[\frac{\partial}{\partial \chi}\left(\frac{\partial X}{\partial \psi} + \frac{\mu_0 p'}{B^2}X\right)\right]^2\right.$$

$$\left. + \mathcal{J}p'DX^2 + \frac{\mathcal{J}}{\mu_0/B^2 + 1/\gamma p}\left(DX + \frac{1}{\mathcal{J}}\frac{\partial Z}{\partial \chi}\right)^2\right\} . \tag{3.8}$$

Here it was assumed that the term involving $\partial Z/\partial \chi$ in the expression for Y, Eq. (3.7), is of order ε. Substituting Eq. (3.7) into Eq. (3.5) for $\delta K_\perp$ gives the high n expression for the perpendicular kinetic energy,

$$\delta K_\perp = \pi \int d\psi\, d\chi\, \rho_m \mathcal{J}\left\{\frac{X^2}{r^2 B^2} + \frac{r^2}{n^2}\left(\frac{\partial X}{\partial \psi} + \frac{\mu_0 p'}{B^2}X\right)^2\right\} . \tag{3.9}$$

Minimizing $\omega^2 = \delta W/\delta K_\perp$ with respect to Z yields

$$\frac{\partial}{\partial \chi}\left[\frac{1}{\mu_0/B^2 + 1/\gamma p}\left(DX + \frac{1}{\mathcal{J}}\frac{\partial Z}{\partial \chi}\right)\right] = 0 . \tag{3.10}$$

Integrating with respect to χ around a field line gives

$$\frac{\partial Z}{\partial \chi} = \left(\frac{\mu_0}{B^2} + \frac{1}{\gamma p}\right)\mathcal{J}f(\psi) - \mathcal{J}DX . \tag{3.11}$$

Here $f(\psi)$ is a constant of integration found by requiring $\partial Z/\partial \chi$ to be single valued on the closed field lines.

$$f(\psi) = \frac{1}{\mu_0 L' + V'/\gamma p}\int d\chi\, \mathcal{J}DX , \tag{3.12}$$

where $L' = \int d\chi \frac{\mathcal{J}}{B^2}$ and $V' = \int d\chi\, \mathcal{J}$. Using Eq. (3.11) in Eq. (3.7) for Y one can verify that the term involving $\partial Z/\partial \chi$ is indeed $O(\varepsilon)$. Substituting Eq. (3.11) for $\partial Z/\partial \chi$ into Eq. (3.8) gives an expression for δW in terms of the perturbation X,

$$\delta W = \pi \int d\psi\, d\chi \left\{\frac{1}{\mu_0}\frac{1}{\mathcal{J} r^2 B^2}\left(\frac{\partial X}{\partial \chi}\right)^2 + \frac{1}{\mu_0}\frac{1}{n^2}\frac{r^2}{\mathcal{J}}\left[\frac{\partial}{\partial \chi}\left(\frac{\partial X}{\partial \psi} + \frac{\mu_0 p'}{B^2}X\right)\right]^2\right.$$

$$\left. + \mathcal{J}p'DX^2 + \mathcal{J}\left(\frac{\mu_0}{B^2} + \frac{1}{\gamma p}\right)f^2(\psi)\right\} . \tag{3.13}$$

Minimizing $\omega^2 = \delta W/\delta K_1$ with respect to X results in the Euler equation for X,

$$\frac{\partial}{\partial X}\left(\frac{1}{\mathcal{J}r^2B^2}\frac{\partial X}{\partial X}\right) - \frac{1}{n^2}\frac{\partial}{\partial\psi}\frac{\partial}{\partial X}\left[\frac{r^2}{\mathcal{J}}\frac{\partial}{\partial X}\left(\frac{\partial X}{\partial\psi} + \frac{\mu_0 p'}{B^2}X\right)\right]$$

$$+ \frac{1}{n^2}\frac{\mu_0 p'}{B^2}\frac{\partial}{\partial X}\left[\frac{r^2}{\mathcal{J}}\frac{\partial}{\partial X}\left(\frac{\partial X}{\partial\psi} + \frac{\mu_0 p'}{B^2}X\right)\right] - \mathcal{J}\mu_0 p' DX$$

$$= -\mu_0\rho_m\omega^2\left\{\frac{\mathcal{J}X}{r^2B^2} - \frac{1}{n^2}\frac{\partial}{\partial\psi}\left[\mathcal{J}r^2\left(\frac{\partial X}{\partial\psi} + \frac{\mu_0 p'}{B^2}X\right)\right]\right.$$

$$\left. + \frac{1}{n^2}\frac{\mu_0 p'}{B^2}\mathcal{J}r^2\left(\frac{\partial X}{\partial\psi} + \frac{\mu_0 p'}{B^2}X\right) + \mathcal{J}\mu_0 Df\right. . \qquad (3.14)$$

This is an integro-partial differential eigenvalue equation governing high n MHD modes. Either ω^2 or n^2 can be specified with the other solved for as the eigenvalue. The boundary condition is X = 0 on conducting surfaces. A difficulty arises if there is a vacuum region outside the plasma because Eq. (3.14) does not apply to the vacuum. One remedy that has been suggested is to replace the vacuum with a zero pressure plasma. However, there is still another problem in the case of the multipole. For calculating stability criteria we are interested in finding the point at which the ballooning mode is marginally stable. In Chapter 2 the MHD equilibria of multipoles was calculated with the pressure gradient set equal to zero at the critical flux surface so that the equilibria would be stable to interchange modes. This makes the interchange mode marginally stable. For marginal stability the interchange mode will always be present.

In the numerical calculation below this causes difficulties since the interchange mode tends to dominate the picture. The interchange mode does not limit beta since the pressure is zero out at the critical flux surface. Furthermore, if one considers slightly growing modes the ballooning mode is present but the interchange is not. For these reasons we will ignore the interchange mode and concentrate our attention on the ballooning mode. This will be done by considering internal modes only. For internal modes the boundary condition is X = 0 at the critical flux surface.

B. Approximate Solution

In this section a method of finding an approximate solution to Eq. (3.14) is developed. The method is based on a perturbation expansion about the $n = \infty$ solution. There is an another method used by Adler and Lee[40] of solving Eq. (3.14). They adopted the procedure used by Spies[42] of expanding the solution in terms of a complete set of eigenfunctions along a field line. The equation for the high n stability then becomes an infinite set of coupled differential equations. Generally only the lowest order equation is kept. The method used below is different and is more similar to a straight forward perturbation expansion. Using the method presented here it is easier to obtain an explicit solution to the problem including the ψ dependence of the mode. This has not been done in

previous analyses for multipoles. In operator notation Eq. (3.14) can be written in the form,

$$L_0X + \frac{1}{n^2} L_1X - \mathcal{J}\mu_0 p' DX$$

$$= -\mu_0\rho_m\omega^2 M_0X - \mu_0\rho_m\omega^2 \frac{1}{n^2} M_1X , \qquad (3.15)$$

where $L_0X = \frac{\partial}{\partial\chi}\left(\frac{1}{r^2 B^2 \mathcal{J}} \frac{\partial X}{\partial\chi}\right) - \mathcal{J}\mu_0 Df$,

$$L_1X = -\frac{\partial}{\partial\psi}\frac{\partial}{\partial\chi}\left[\frac{r^2}{\mathcal{J}}\frac{\partial}{\partial\chi}\left(\frac{\partial X}{\partial\psi} + \frac{\mu_0 p'}{B^2} X\right)\right]$$

$$+ \frac{\mu_0 p'}{B^2}\frac{\partial}{\partial\chi}\left[\frac{r^2}{\mathcal{J}}\frac{\partial}{\partial\chi}\left(\frac{\partial X}{\partial\psi} + \frac{\mu_0 p'}{B^2} X\right)\right] ,$$

$$M_0X = \mathcal{J}\frac{X}{r^2 B^2} ,$$

$$M_1X = -\frac{\partial}{\partial\psi}\left[\mathcal{J}r^2\left(\frac{\partial X}{\partial\psi} + \frac{\mu_0 p'}{B^2} X\right)\right]$$

$$+ \frac{\mu_0 p'}{B^2}\mathcal{J}r^2\left(\frac{\partial X}{\partial\psi} + \frac{\mu_0 p'}{B^2} X\right) .$$

Treating n^{-2} as the perturbing parameter in Eq. (3.15) the lowest order equation is

$$L_0X_0 - \mathcal{J}\mu_0 p_0' DX_0 = -\mu_0\rho_m\omega_0^2 M_0X_0 . \qquad (3.16)$$

This is the $n = \infty$ MHD equation. It is a Sturm-Liouville type equation and is solved using periodic boundary conditions. In devices with up-down symmetry the solutions of Eq. (3.16) have either even or odd symmetry with respect to reflection across the midplane. Solutions with even symmetry have the boundary condition $\partial X/\partial\chi = 0$ on the midplane and solutions with odd symmetry have the boundary condition $X_0 = 0$ on the midplane. Either p_0' or ω_0^2 is specified with the other solved for as an eigenvalue.

Setting $\omega_0^2 = 0$ in Eq. (3.16) and solving for p_0' gives the critical pressure gradient at which the $n = \infty$ mode is marginally stable. For a field line with average good curvature the solution corresponding to the p_0' with the smallest magnitude and with the same sign as $V'' = \oint \frac{D}{B}\, d\ell$ determines the critical pressure gradient. This is the solution with even symmetry, no nodes, which peaks in the region having bad curvature and the smallest magnitude of the magnetic field. If the equilibrium pressure gradient is greater then p_0' on any of the flux surfaces the system is unstable to ballooning modes. For the case $\omega_0^2 = 0$ in order for the mode to be continuous around a field line the condition $\oint \mathcal{J} DX_0 = 0$ must be satisfied. This means $f(\psi) = 0$ and since $\nabla\cdot\vec{\xi} = f(\psi)/\gamma p$ the marginally stable $n = \infty$ mode is incompresssible.

Another way of solving Eq. (3.16) is to set p_0' equal to the equilibrium pressure gradient and solve for ω_0^2. For p' greater then the critical pressure gradient $\mathrm{Im}(\omega_0)$ gives the growth rate of the $n = \infty$ mode. Generally the mode with the largest growth rate occurs on a flux surface nearest the flux suface with the steepest pressure gradient. This is the point where p' is likely to be farthest above the critical pressure gradient. There are also an infinite number of discrete eigenvalues, ω_0^2, that are positive. These correspond to stable oscillating modes. If p' is less then the critical pressure gradient then there are no negative ω_0^2 eigenvalues.

The solution X_0 of Eq. (3.16) is defined only up to an arbitrary multiplicative constant. We'll write X_0 in terms of two functions $X_0 = R_0(\psi)U_0(\psi,\chi)$ where $U_0(\psi,\chi)$ is a solution to Eq. (3.16) and also satisfies a normalizing condition which fully determines $U_0(\psi,\chi)$. The normalizing condition is completely arbitrary as long it is the same on all the flux surfaces. The final solution for X_0 will not not depend on it. The equation for $R_0(\psi)$ is found by going to the next highest order in $1/n^2$. To first order in $1/n^2$ Eq. (3.15) gives,

$$L_0X_1 + \frac{1}{n^2} L_1 R_0(\psi)U_0 - \mathcal{J}\mu_0 p_0' DX_1 - \mathcal{J}\mu_0 p_1' DR_0(\psi)U_0$$

$$= -\mu_0\rho_m\omega_0^2 M_0 X_1 - \mu_0\rho_m\omega_1^2 M_0 R_0(\psi)U_0 - \mu_0\rho_m\omega^2 \frac{1}{n^2} M_1 R_0(\psi)U_0 \,. \tag{3.17}$$

where $p_1' = p' - p_0'$, $\omega_1^2 = \omega^2 - \omega_0^2$. Here p' is the equilibrium pressure gradient, and $R_0(\psi)$ is is the correction in the ψ direction

to the zeroth order solution, X_0. For the perturbation expansion to be valid it is necessary to choose either p_0' or ω_0^2 in Eq. (3.16) in such a way that will make p_1' and ω_1^2 small in Eq. (3.17). For the calculations here $p_0' = (p' + p_c')/2$ is normally chosen, where p_c' is the critical pressure gradient. Multiplying Eq. (3.17) by U_0 and integrating over χ gives a constraint equation that determines $R_0(\psi)$,

$$\frac{1}{n^2}\oint U_0 L_1 R_0(\psi)U_0 \, d\chi - \mu_0 p_1' \oint \mathcal{J} D R_0(\psi) U_0^2 \, d\chi$$

$$= -\mu_0\rho_m\omega_1^2 \oint U_0 M_0 R_0(\psi)U_0 \, d\chi - \mu_0\rho_m\omega^2 \frac{1}{n^2}\oint U_0 M_1 R_0(\psi)U_0 \, d\chi \,. \tag{3.18}$$

where use was made of the self adjoint property of L_0 to eliminate terms involving X_1. Eq. (3.18) is a second order ordinary differential equation in ψ with either n^2 or ω^2 determined as the eigenvalue. This is more apparent when the operators in Eq. (3.18) are written out explicitly:

$$\frac{d}{d\psi}\Big[\Big(\oint \frac{\partial U_0}{\partial\chi}\frac{r^2}{\mathcal{J}}\frac{\partial U_0}{\partial\chi}\, d\chi - \mu_0\rho_m\omega^2 \oint U_0^2 \mathcal{J} r^2 \, d\chi\Big)\frac{dR_0(\psi)}{d\psi}\Big]$$

$$+ \Big\{\frac{d}{d\psi}\Big[\oint \frac{\partial U_0}{\partial\chi}\frac{r^2}{\mathcal{J}}\frac{\partial}{\partial\chi}\Big(\frac{\partial U_0}{\partial\psi} + \frac{\mu_0 p'}{B^2} U_0\Big)\, d\chi\Big]$$

$$- \oint \frac{r^2}{\mathcal{J}}\Big[\frac{\partial}{\partial\chi}\Big(\frac{\partial U_0}{\partial\psi} + \frac{\mu_0 p'}{B^2} U_0\Big)\Big]^2 \, d\chi$$

$$- \mu_0\rho_m\omega^2 \frac{d}{d\psi}\Big[\oint U_0 \mathcal{J} r^2 \Big(\frac{\partial U_0}{\partial\psi} + \frac{\mu_0 p'}{B^2} U_0\Big)\, d\chi\Big]$$

$$+ \mu_0 \rho_m \omega^2 \oint \mathcal{J} r^2 \left[\frac{\partial U_0}{\partial \psi} + \frac{\mu_0 p'}{B^2} U_0\right]^2 d\chi \Big] R_0(\psi) \qquad (3.19)$$

$$= n^2 \Big[\mu_0 \rho_m (\omega_0^2 - \omega^2) \oint \mathcal{J} \frac{U_0^2}{r^2 B^2} d\chi + \mu_0 (p' - p_0') \oint \mathcal{J} D U_0^2 \, d\chi\Big] R_0(\psi).$$

The boundary conditions are that $R_0(\psi)$ go to zero on conducting surfaces and at the plasma-vacuum interface. The procedure for finding the lowest order solution to Eq. (3.14) has been reduced to solving two ordinary differential equations: Eq. (3.16) along field lines and Eq. (3.19) perpendicular to the field lines.

For cases where the ψ extent of the mode is expected to be limited a good approximation to the lowest eigenvalue n_c of Eq. (3.19) for a marginally stable mode can be found by WKB analysis. Using the WKB turning point formula,

$$n_c = \frac{\pi}{2 \int_{\psi_a}^{\psi_b} \sqrt{-Q(\psi)}\, d\psi},$$

where $$Q(\psi) = \frac{\mu_0 (p' - p_0') \oint \mathcal{J} D U_0^2 \, d\chi}{\oint \frac{r^2}{\mathcal{J}} \left(\frac{\partial U_0}{\partial \chi}\right)^2 d\chi},$$

and ψ_a and ψ_b are the points where $p' = p_0'$ with $|p'| > |p_0'|$ for $\psi_a < \psi < \psi_b$. Here p_0' is the critical pressure gradient. Also from WKB theory the radial width of the mode is predicted to be proportional to $1/\sqrt{n_c}$.

C. Numerical Results

We are interested in calculating the stability criteria of a multipole. For this the boundary between stable modes and unstable ones must be determined. To find points on this boundary Eq. (3.16) and Eq. (3.19) are solved using a sequence of equilibria with different betas for the marginally stable mode. First the beta limit must be determined. This means finding the beta at which the $n = \infty$ mode is marginally stable. For a given beta above the critical beta there is only one marginally stable mode with a specific toroidal mode number, n_c, the critical toroidal mode number. For this beta all modes with $n > n_c$ are ballooning unstable and all modes with $n < n_c$ are stable within the limitations of the large n expansion. The quantity n_c is found by first solving Eq. (3.17) for U_0 and ω_0^2 for some choice of p_0'. Here $p_0' = (p' + p_c')/2$ was chosen, where p_c' is the critical pressure gradient. Then Eq. (3.19) is solved with $\omega^2 = 0$ for the radial structure and n_c, the eigenvalue. For Eq. (3.19) the boundary conditions were that R_0 be zero at the plasma vacuum interface and also go to zero at the separatrix. Inside the separatrix the critical pressure gradient jumps by greater then a factor of ten. From this the mode would be expected to die out rapidly inside the separatrix. For this reason and also for numerical expediency the mode is taken to be zero at the separatrix.

We now apply the high n MHD analysis to the specific case of the Levitated Octupole. The equilibria were calculated using an MHD equilibrium code. Details of the equilibria can be found in Chapter 2. The term $\omega_0 Df$ in the expression for L_0X will be neglected. This is not a serious omission since this term is $O(\varepsilon)$ smaller then the other terms in Eq. (3.16) by virtue of $p' >> pD$. In addition since $f = 0$ for the $n = \infty$ marginally stable mode one would expect f to be small for high n modes as well. Taking $f = 0$ also simplifies the problem of finding the solution to Eq. (3.16).

The only region where the plasma may be unstable to ballooning modes is in the region between the separatrix and the critical flux surface where bad curvature exists. For $n = \infty$ modes the stability of each flux surface must be considered. Fig. (3.1) shows the critical pressure gradient for $n = \infty$ modes for two cases, the even mode and the odd mode, plotted with the marginally stable equilibrium pressure gradient. The plasma is marginally stable when the equilibrium pressure gradient is equal to but not greater than the critical pressure gradient at one or more points. In the Levitated Octupole this occurs at $\beta = 4.33\%$. Here β is defined as the local beta on the separatrix in the bridge region where the bridge region is the chord between the outside ring and outside wall. The even mode is the most unstable because the magnitude of its critical pressure gradient is everywhere less than or equal to the magnitude of the critial pressure gradient corresponding to the odd mode. At the separatrix the even and odd modes are degenerate. There the boundary

conditions $X = 0$ and $\partial X/\partial \chi = 0$ on the midplane are satisfied simultaneously. This minimizes the effect of the inverse curvature going to infinity at the field null. Several examples of the eigenfunction for the $n = \infty$ case are shown in Fig. (3.2). The eigenfunction is greatest in the outside bad curvature region as is typical of a ballooning mode. The eigenfunctions on surfaces close to the critical flux surface are more flute like in character and become constant at the critical flux surface. Toward the separatrix the modes become more strongly ballooning in character.

For equilibria with betas greater than the critical beta of 4.33% unstable $n = \infty$ modes exist. Fig. (3.3) shows the minimum ω^2 versus ψ for various betas. For $\omega^2 < 0$, ω is imaginary and the modes are unstable. Another way of solving the $n = \infty$ equation, Eq. (3.16), is to set ω_0^2 to some negative value and solve for p_0'. This value of p_0' gives a critical value of the pressure gradient for $n = \infty$ modes with a growth rate $\gamma = \sqrt{-\omega_0^2}$. If the equilibrium pressure gradient is greater than this value of p_0' then the $n = \infty$ mode has a growth rate greater than $\gamma = \sqrt{-\omega_0^2}$. If the equilibrium pressure gradient is smaller than p_0' then the $n = \infty$ mode has a growth rate less than γ. An example of solving the $n = \infty$ equation in this manner is shown in Fig. (3.4) for an equilibrium with $\beta = 6\%$. Here the critical pressure gradients of the marginally stable mode, a mode with $\mu_0 \rho_m \omega^2 = -1.0$ and a mode with $\mu_0 \rho_m \omega^2 = -2.0$ are shown. In particular Fig. (3.4) shows that for betas above the critical beta the ballooning mode is a growing mode but the interchange mode is not.

Above the critical beta there exists a critical toroidal mode number, n_c. Modes with $n > n_c$ are unstable and modes with $n < n_c$ are stable. The quantity n_c was found by solving Eq. (3.17) and Eq. (3.19) in the Levitated Octupole configuration. The results are shown in Fig. (3.5) where β versus $1/n_c$ is plotted. Note there is an almost linear relationship between β and $1/n_c$. For betas greater than the critical beta the marginally stable modes are no longer localized in the ψ direction but take up the whole region between the separatrix and the critical flux surface. The full reconstructed X_0 eigenfunction for $\beta = 5.0\%$ is shown in Fig. (3.6). Fig. (3.6) shows half of the X_0 eigenfunction plotted versus ψ and the relative length along a field line starting at the inside midplane and moving along a field line to the outside midplane. X_0 peaks around the outside bridge region where the curvature is the most unfavorable near the flux surface with the steepest pressure gradient. In Fig. (3.7) are plotted the projection of several X_0 eigenfunctions with various toroidal mode numbers into a constant χ surface. As n becomes larger the radial extent of the mode becomes narrower until at $n = \infty$ the radial part of the eigenfunction is a delta function located at the flux surface with the largest growth rate. The width of the marginally stable mode is proportional to $\sqrt{\beta - \beta_c}$, where β_c is the critical beta. It was mentioned earlier that the quantitiy $\beta - \beta_c$ is proportional to $1/n_c$. This implies $\lambda_\psi \sim \sqrt{\lambda_\theta}$ where λ_ψ and λ_θ are the wavelengths of the mode in the ψ and θ directions respectively. This means $k_\theta \sim k_\psi^2$ where k_ψ and k_θ are the wave numbers of the mode in the

ψ and θ direction. For a small increase in β over the critical β the modes initially spread out rapidly in the ψ direction but for further increases in β the mode does not change much.

In summary, the MHD energy integral was expanded in powers of n^{-2}. From this Eq. (3.14) governing high n modes in an axisymmetric closed field line system was derived. A straight forward perturbation expansion using n^{-2} as the smallness parameter provides an approximate solution to Eq. (3.14). This expansion is valid if equilibrium quantities vary slowly enough in the ψ-direction over the region of interest. The lowest order equation gives the structure of the modes along the field lines. The first order equation and the condition that the solution be continuous around field lines provide an equation which determines the toroidal mode number and its structure in the ψ-direction.

High n MHD does not predict a higher beta limit than infinite n MHD. The $n = \infty$ mode is still the most unstable mode. Some additional factor limiting n such as finite Larmor radius has to be introduced to get a change in the critical beta. This will be the subject matter of the next chapters.

One way of roughly estimating what the effect of finite Larmor radius is to assume the MHD mode excites drift type waves in the same manner as the flute mode excites drift type waves. Similar to the analysis of the flute mode discussed in the introduction the dispersion relation changes from $\omega^2 = \omega^2_{MHD}$ to $\omega(\omega - \omega^*_i) = \omega^2_{MHD}$, where ω^2_{MHD} is the MHD frequency of the mode and ω^*_i is the ion diamagnetic

drift frequency, $\omega_i^* = -\frac{nT}{e}\frac{p'}{p}$. Solving this quadratic equation for ω it is easy to see that the mode is stablized if $\omega_i^{*2} > 4\omega_{MHD}^2$. It can be shown that to lowest order the minimum MHD frequeny ω_{MHD}^2 has a 1/n dependence. This is apparent in Eq. (3.19) where if p_0' is chosen equal to p' the largest term involving ω^2 appears in the form $n^2(\omega_0^2 - \omega^2)$. To lowest order then $\omega_{MHD}^2 = -\gamma^2\left(1 - \frac{n_c}{n}\right)$ where for a given beta γ is the growth rate of the most unstable mode $\gamma = \sqrt{-\omega_{MHD\ min}^2}$ and n_c is the critical mode number for marginally stability. Multiplying the stability condition by the mass density gives,

$$n^2\rho_i^2\left(\frac{1}{rL_n}\right)^2 > 8\rho_m\gamma^2\left(1 - \frac{n_c}{n}\right) ,$$

where $\rho_i = \sqrt{\frac{T}{m_i}}\frac{1}{\Omega_i}$ and L_n is the density scale length. For marginal stability the largest value of ρ_i/rL_n occurs at $n = \frac{3}{2}n_c$. This gives a critical value of ρ_i/rL_n,

$$\left(\frac{\rho_i}{rL_n}\right)_c^2 = \frac{32}{27}\frac{\rho_m\gamma^2}{n_c^2}\frac{1}{p} .$$

For $\rho_i/rL_n > (\rho_i/rL_n)_c$ all modes are stable. For $\rho_i/rL_n < (\rho_i/rL_n)_c$ unstable modes exist. For $\rho_i/L_n = 0.2$ in the bridge region of the Levitated Octupole the beta limit predicted by this stability criterion is 8%.

Fig. (3.1) MHD Critical Pressure Gradient vs Ψ

Plot of the equilibrium pressure gradient and the MHD critical pressure gradient for the even and odd modes for $\beta = 4.33\%$. The even mode is marginally stable. $\Psi_{sep} = 0.5318$, $\Psi_{crit} = 0.8245$.

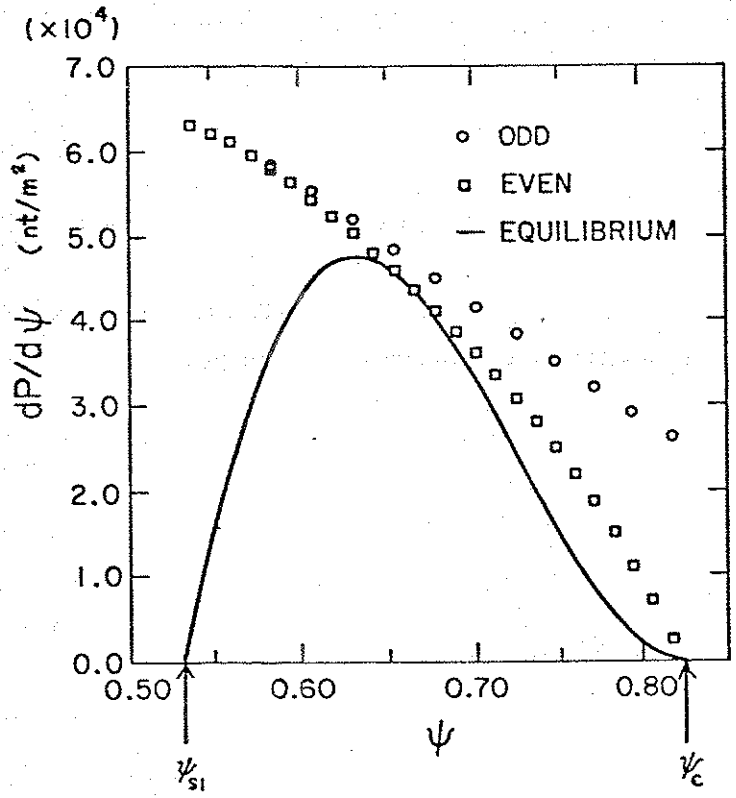

Fig. (3.1)

Fig. (3.2) X Eigenfunctions for MHD n = ∞ Modes

The X_0 eigenfunctions plotted relative to the distance along a field line for $\psi = 0.8011$, $\psi = 0.7426$, $\psi = 0.6840$. The eigenfunction is a delta function in the variable ψ. Near the critical flux surface the eigenfunction is flute like. Closer to the separatrix there is more ballooning in the bad curvature region.

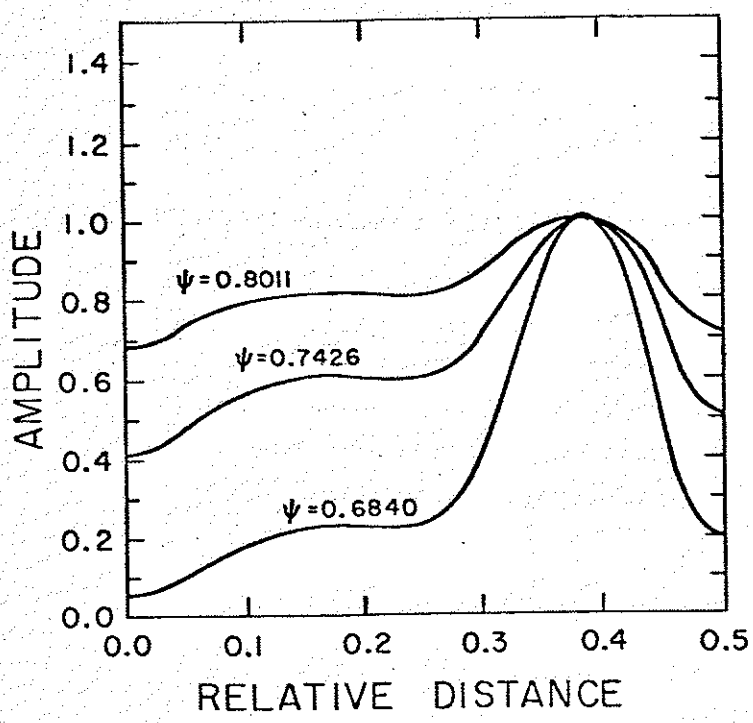

Fig. (3.2)

Fig. (3.3) $\mu_0 \rho_m \omega^2$ vs ψ for $n = \infty$ Ballooning Mode.

Plot of $\mu_0 \rho_m \omega^2$ vs ψ for β = 4.0%, 5.0%, 6.0%, 7.0%, 8.0%. Above β_c = 4.33% the mode is unstable. ω^2 is proportional to $\beta - \beta_c$.

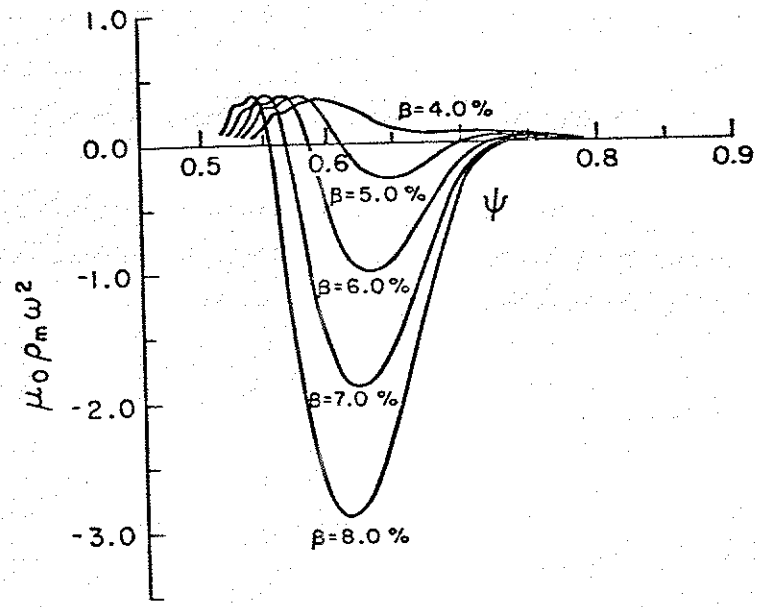

Fig. (3.3)

Fig. (3.4) Critical P′ for Various Growth Rates

This is a plot of the critical pressure gradients of the marginally stable mode, a mode with $\mu_0 \rho_m \omega^2 = -1.0$, and a mode with $\mu_0 \rho_m \omega^2 = -2.0$. These modes all have $n = \infty$ and the equilibrium beta is 6%.

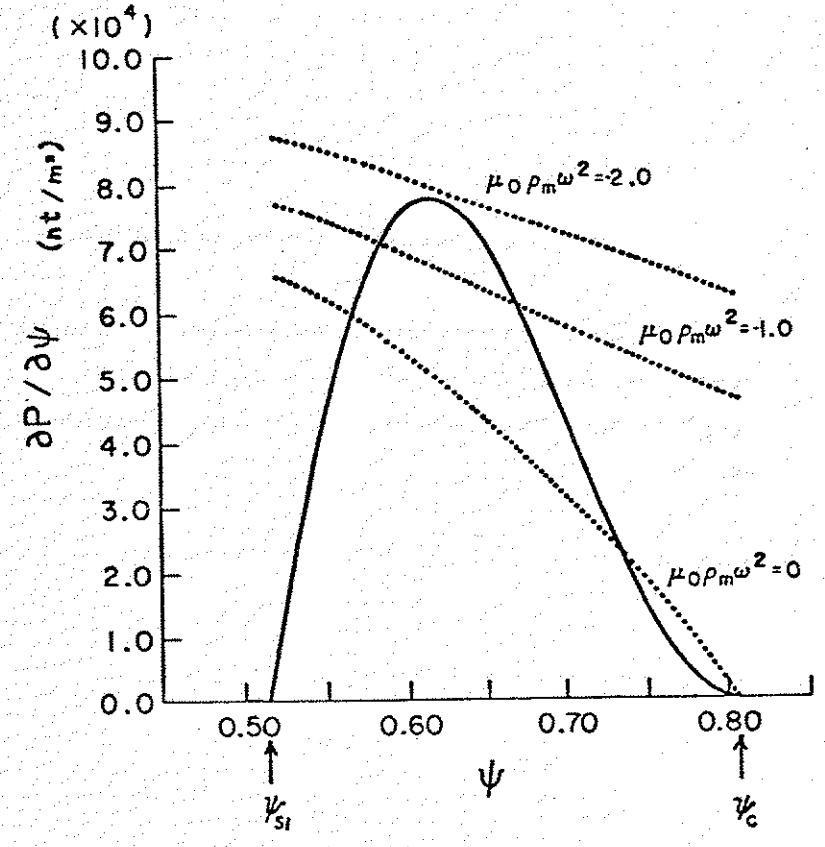

Fig. (3.4)

Fig. (3.5) Critical β vs $1/n_c$ Stability Criteria

Plot of the critical beta vs the inverse of the toroidal mode number of the marginally stable mode, $1/n_c$. For a given β modes with $n > n_c$ are unstable and modes with $n < n_c$ are stable.

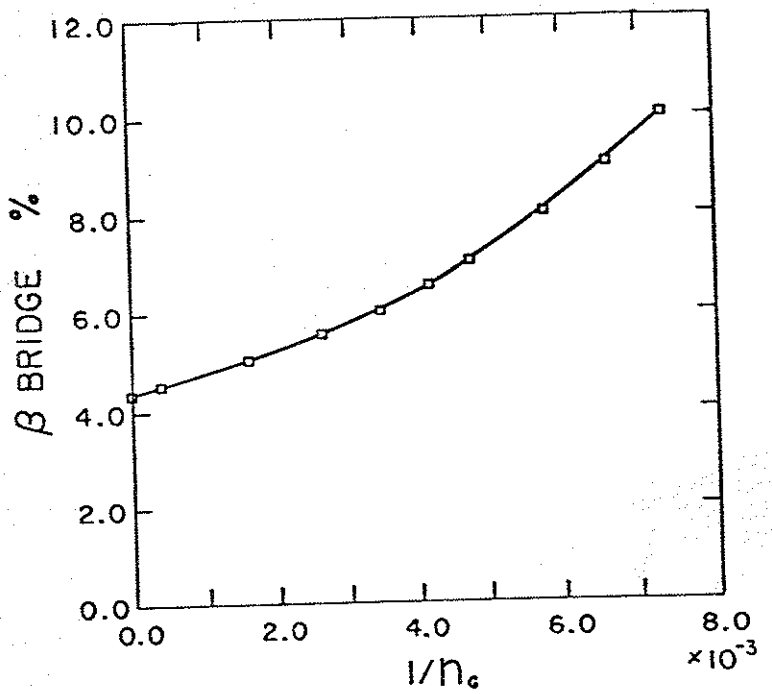

Fig. (3.5)

Fig. (3.6) X_0 Eigenfunction for $\beta = 5\%$

The X_0 eigenfunction of the marginally stable mode for $\beta = 5.0\%$. The eigenfunction peaks in the bad curvature region near the flux surface with the steepest pressure gradient. $n = 621$, $\psi_{sep} = 0.5275$, $\psi_{crit} = 0.8198$.

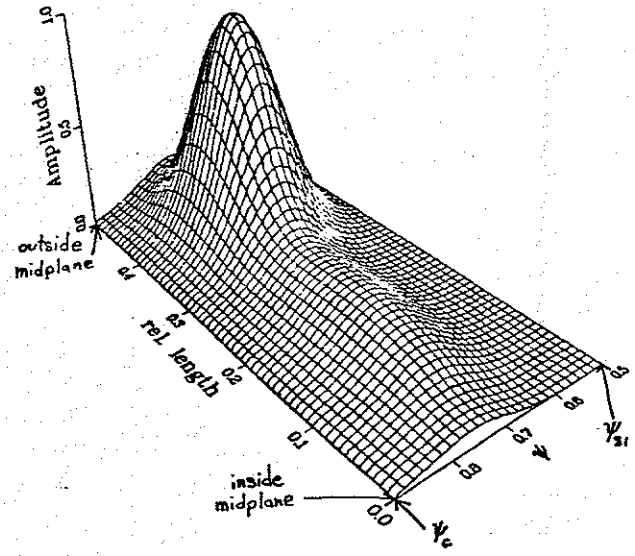
1.0
Amplitude
0.5
0.0
outside
midplane
0.4
0.3
rel length
0.2
0.1
inside
midplane
0.0
ψ_c
0.6
0.7
ψ
0.8
0.9
ψ_{s1}

Fig. (3.6)

Fig. (3.7) Radial Mode Structure of X_0 Eigenfunction

Projection of several marginally stable X_0 eigenfunctions on the constant χ plane for β = 4.5%, n =2525; β = 5.0%, n = 621; β = 5.5%, n = 378. The radial width of a mode is proportional to $1/\sqrt{n_c}$.

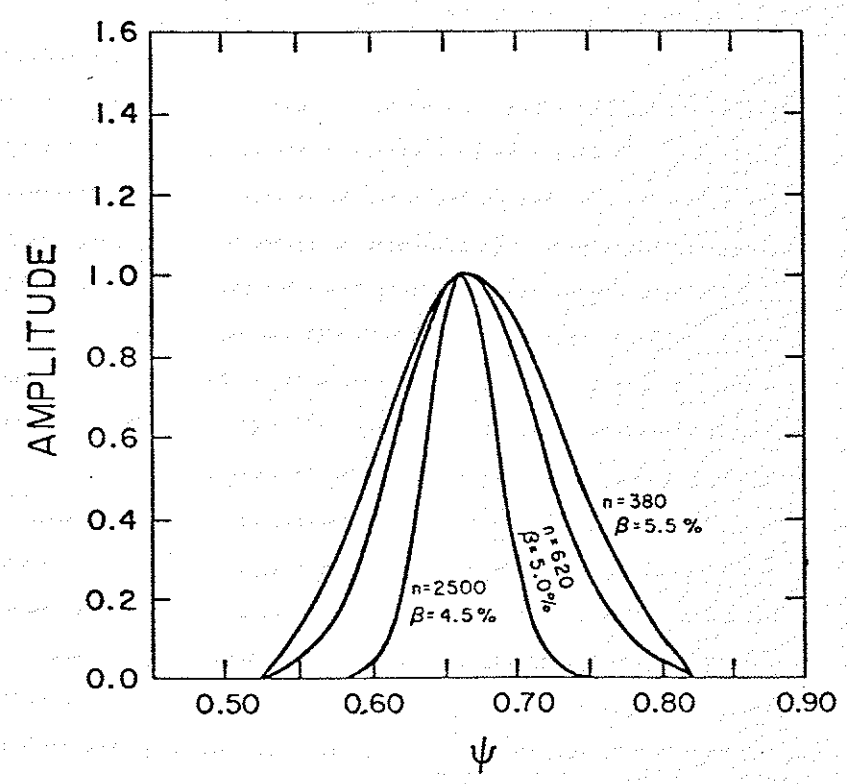

Fig. (3.7)

CHAPTER 4

The Low-Frequency Kinetic Equations for Multipoles

To find out how particle effects such as finite Larmor radius and trapped particles affect the ballooning mode one must use a kinetic treatment. In this chapter a system of kinetic equations for studying low frequency electromagnetic modes in an axisymmetric collisionless plasma is developed. The treatment presented here is applicable to systems with closed magnetic field lines but otherwise the equilibrium can be assumed arbitrary. As in the MHD analysis presented in Chapter 3 the orthogonal flux coordinate system (ψ, χ, θ) is used with the symbol $\mathcal{J}$ used to denote the Jacobian, $\mathcal{J}^{-1} = (\nabla\psi \times \nabla\chi)\cdot\nabla\theta$. A summary of this coordinate system can be found in Appendix A.

The ballooning mode is a low frequency electromagnetic mode allowing ω/Ω, where Ω is the gyrofrequency, to be used as an expansion parameter. The instability is characterized by long parallel wavelength and short perpendicular wavelengths, i.e., $k_\parallel \rho_i \sim 1$ and $k_\chi \rho_i \ll 1$ where k is the wave number and ρ_i is the ion Larmor radius. In Chapter 3 it was shown $k_\psi \sim \sqrt{n}$ in the limit of large toroidal mode number, n, while $k_\theta \sim n$. Hence $k_\theta \gg k_\psi$ is assumed. The equilibrium is assumed to vary on a scale much larger than the Larmor radius; $\rho/L_n \ll 1$, $\rho/L_B \ll 1$ where L_n and L_B are the density and magnetic scale lengths.

The kinetic analysis of electrostatic oscillations for closed field line systems such as multipoles was first formulated by Rutherford and Frieman[15] and Taylor and Hastie[16,18]. The derivation presented in this chapter is an extension of their work to electromagnetic modes. The derivation of the kinetic equations applicable to low frequency modes consists of a small frequency, $\omega/\Omega \ll 1$, small Larmor radius, $\rho/L_n \ll 1$, $\rho/L_B \ll 1$, expansion of the linear Vlasov equation to obtain the perturbed distribution function due to small electromagnetic perturbations. Moments of the distribution function are calculated and used in the quasi-neutrality condition and force balance equations to obtain a complete set of equations governing the modes. Two frequency regiemes are considered: a low frequency regime, $\omega \ll \omega_{bi} \ll \omega_{be}$ and an intermediate regime $\omega_{bi} \ll \omega \ll \omega_{be}$. Solutions to these two sets of equations will be the subject matter of Chapter 5 and Chapter 6. Similar analyses for tokamaks have been developed[25-29].

The field perturbations are doubly periodic in the χ and θ directions. Since the equilibrium magnetic field is shearless and points only in the χ direction the two periodicity conditions are separate. This makes the ballooning mode representation[23,24] used in tokamaks unnecessary and the perturbations can be simply Fourier analyzed in the θ direction. From now on perturbations will implicitly be understood to depend on θ, t by,

$$f_1 = f_1(\psi, \chi, \vec{v}) \exp(i\omega t - in\theta) .$$

where n is the toroidal mode number.

The small Larmor radius expansion of the equilibrium Vlasov equation is discussed in Chapter 2. To first order the equilibrium distribution function[ ] is found to be,

$$f_0 = f_m\left[1 + \frac{1}{n_0}\frac{\partial n_0}{\partial \psi}(\psi - \psi_0) + \frac{m}{T} v^* v_\theta\right] , \qquad (4.1)$$

where $v^* = -\frac{T}{q}\frac{r}{n_0}\frac{\partial n_0}{\partial \psi}$ is the diamagnetic drift velocity, f_m is the Maxwellian distribution function and n_0 is the particle density on the flux surface ψ_0. The temperature, T, is asssumed to be constant throughout the device but it can be different for different particle species. This equilibrium distribution function is defined locally on the flux surface ψ_0 with $\frac{1}{n_0}\frac{\partial n_0}{\partial \psi}$ evaluated on ψ_0. However the kinetic equations to be derived will be assumed to apply globally.

A. Small Larmor Radius Expansion

The collisionless linear Vlasov equation is,

$$\frac{\partial f_1}{\partial t} + \vec{v}\cdot\nabla f_1 + \frac{q}{m}\vec{v}\times\vec{B}_0\cdot\nabla_v f_1 = -\frac{q}{m}\left[\vec{E}_1 + \vec{v}\times\vec{B}_1\right]\cdot\nabla_v f_0 . \qquad (4.2)$$

where f_1 is the perturbed distribution function, $\vec{B}_0$ is the equilibrium magnetic field, $\vec{E}_1$ and $\vec{B}_1$ are the perturbed electric and magnetic fields and f_0 is the equilibrium distribution function. For

performing a small Larmor radius expansion on the Vlasov equation it helps to use the velocity coordinates $\varepsilon = \frac{1}{2}v_\chi^2 + \frac{1}{2}v_\perp^2$, $\mu = \frac{1}{2}\frac{v_\perp^2}{B}$ and $\zeta = \tan^{-1}\left(-\frac{v_\psi}{v_\theta}\right)$ where ε is the energy per unit mass, μ is the magnetic moment per unit mass and ζ is the gyrophase angle. Properties of these coordinates are summarized in Appendix A.

Define the operator $\mathfrak{b}$ by,

$$\mathfrak{b}f_1 \equiv \vec{v}\cdot\nabla f_1 + i\frac{n}{r}v_\perp\cos\zeta\, f_1 + \frac{d\mu}{dt}\frac{\partial f_1}{\partial\mu} + \left(\frac{d\zeta}{dt} - \Omega\right)\frac{\partial f_1}{\partial\zeta} .$$

with
$$\frac{d\mu}{dt} = -\frac{\mu}{B}\vec{v}\cdot\nabla B - \frac{v_\chi}{B}v_\perp\vec{\cdot}(\vec{v}\cdot\nabla)\hat{\chi}$$

$$= \frac{\Omega}{B}v_\perp\hat{m}(\hat{\chi}\times\vec{v}_D) + \mu v_\chi\left[\hat{\rho}\cdot(\hat{\varphi}\cdot\nabla)\hat{\chi} - \hat{m}(\hat{m}\cdot\nabla)\hat{\chi}\right] ,$$

$$\frac{d\zeta}{dt} = \Omega + \hat{\psi}\cdot(\vec{v}\cdot\nabla)\hat{\theta} + \frac{v_\chi}{v_\perp}\hat{\rho}\cdot(\vec{v}\cdot\nabla)\hat{\chi} ,$$

where $\hat{m} = -\sin\zeta\,\hat{\psi} + \cos\zeta\,\hat{\theta}$, $\hat{\rho} = \frac{\partial\hat{m}}{\partial\zeta}$,

and $\vec{v}_D = v_D\hat{\theta} = \hat{\chi}\times(\mu\nabla B + v_\chi^2\hat{\chi}\cdot\nabla\hat{\chi})/\Omega$.

Here $\vec{v}_D$ is the particle guiding center drift. The spatial derivative is taken holding ε, μ and ζ fixed and the derivatives with respect to ε and μ are taken holding $\vec{x}$ fixed. In terms of $\mathfrak{b}$ the collisionless Vlasov equation can be written,

$$i\omega f_1 + \mathfrak{b}f_1 + \Omega\frac{\partial f_1}{\partial\zeta} - i\frac{n}{r}v_\perp\cos\zeta\, f_1 = -\frac{1}{m}\vec{F}_1\cdot\nabla_v f_0 , \qquad (4.3)$$

where $\vec{F}_1 = q[\vec{E}_1 + \vec{v} \times \vec{B}_1]$. With the assumptions $\omega/\Omega \ll 1$, $\rho/L_n \ll 1$, $\rho/L_B \ll 1$ and $\rho k_\perp \sim 1$ the first and second terms in Eq. (2.3) are small compared with the third and fourth terms. To lowest order,

$$\Omega \frac{\partial f_1^0}{\partial \zeta} - i \frac{n}{r} v_\perp \cos\zeta \, f_1^0 = -\frac{1}{m} \vec{F}_1^0 \cdot \nabla_v f_0 \, , \tag{4.4}$$

where $$-\frac{1}{m} \vec{F}_1^0 \cdot \nabla_v f_0 = f_m \frac{q}{T} v_\perp \cos\zeta \, E_{1\theta} \left[1 + (\psi - \psi_0) \frac{1}{n_0} \frac{\partial n_0}{\partial \psi} \right] .$$

Solving Eq. (4.4) for f_1^0 yields,

$$f_1^0 = f_m \frac{q}{T} \left\{ i \frac{r}{n} E_{1\theta} \left[1 + (\psi - \psi_0) \frac{1}{n_0} \frac{\partial n_0}{\partial \psi} \right] + h \exp(ia \sin\zeta) \right] , \tag{4.5}$$

where $a \equiv \frac{v_\perp}{\Omega} \frac{n}{r}$ and h is a constant of integration, $h = h(\vec{x}, \mu, \varepsilon)$, yet to be determined. To first order in Eq. (4.3)

$$i\omega f_1^0 + \dot{\psi} f_1^0 + \Omega \exp(ia \sin\zeta) \frac{\partial}{\partial \zeta} \left[f_1^1 \exp(-ia \sin\zeta) \right] = -\frac{1}{m} \vec{F}_1 \cdot \nabla_v f_0 \, , \tag{4.6}$$

where $$-\frac{1}{m} \vec{F}_1^1 \cdot \nabla_v f_0 = f_m \frac{q}{T} \left\{ \left[E_{1\psi} v_\psi + E_{1\chi} v_\chi \right] \left[1 + (\psi - \psi_0) \frac{1}{n_0} \frac{\partial n_0}{\partial \psi} + \frac{m}{T} v_\theta v^* \right] - \left[E_{1\theta} \left(1 - \frac{m}{T} v_\theta^2 \right) - B_{1\psi} v_\chi + B_{1\chi} v_\psi \right] v^* \right] .$$

Multiplying Eq. (4.6) by $\exp(-ia \sin\zeta)$, integrating over ζ from 0 to 2π and requiring f_1^1 to be single valued in ζ annihilates the term involving on f_1^1 and gives an equation for h along the field line.

$$(\omega - \omega_D) h - i \vec{v}_\chi \cdot \nabla h = (\omega - \omega^*) \left\{ \left[-i \frac{r}{n} E_{1\theta} + i v_\chi \frac{r}{n} B_{1\psi} \right] J_0(a) + v_\perp \frac{r}{n} B_{1\chi} J_1(a) \right\} , \tag{4.7}$$

where $$\omega_D = \frac{n}{r} v_D = -\frac{n}{r} \frac{1}{\Omega} \left[\frac{1}{2} v_\perp^2 \frac{1}{B} \hat{\psi} \cdot \nabla B + v_\chi^2 \hat{\psi} \cdot (\hat{\chi} \cdot \nabla \hat{\chi}) \right] .$$

Here ω^* is the diamagnetic drift frequency $\omega^* = \frac{v^* n}{r} = -\frac{nT}{q} \frac{p'}{p}$. The quantity ω_D is the curvature and ∇B drift frequency and J_0 and J_1 are Bessel functions of the first kind. See Appendix C for useful Bessel function identities used in the derivations of this chapter. The local ψ dependence occurs in the term $(\omega - \omega^*)$ multiplying the right hand side of Eq. (4.7).

$$(\omega - \omega^*) \Rightarrow \left\{ \omega \left[1 + (\psi - \psi_0) \frac{1}{n_0} \frac{\partial n_0}{\partial \psi} \right] - \omega^* \right\} .$$

This local ψ dependence, which from now on will be assumed implicitly, is only important when we use the continuity equation later on to calculate the θ component of the velocity moment of f_1. As mentioned previously the resulting set of equations governing the modes will be assumed to apply globally to the system.

Before going any further it is best to introduce the representation of the perturbed fields that will be used for the remainder of the paper. The gauge condition for the perturbed fields is chosen so that $A_\chi = 0$. The remaining components of the vector potential are written in terms of the quantities X and Y defined by,

$$X \equiv rA_\theta \ ,$$

$$Y = i\frac{n}{r}\frac{A_\psi}{B} \ .$$

This representation is adopted because in the limit $\rho_i \to 0$ in the kinetic equations the notation will be similar to the traditional notation encountered in much of the earlier multipole stability literature. The representation is exact, no expansions are used. Thus, any other representation can be obtained by the gauge transformation $\hat{A}' = \hat{A} + \Delta\Lambda$ where Λ is an arbitrary gauge provided that Λ is single valued on a flux surface, i.e., $\frac{\partial}{\partial t}\int \hat{A}\cdot\hat{B}\,\mathcal{J}\,d\chi = 0$. In terms of X and Y the perturbed field components are,

$$B1_\psi = \frac{1}{\mathcal{J}rB}\frac{\partial X}{\partial \chi} \ ,$$

$$B1_\chi = -B\left(Y + \frac{\partial X_1}{\partial \psi}\right) \ ,$$

$$B1_\theta = i\frac{r}{n}\frac{1}{\mathcal{J}}\frac{\partial Y}{\partial \chi} \ ,$$

$$E1_\psi = -rB\frac{\partial \phi}{\partial \psi} - \omega\frac{r}{n}BY \ ,$$

$$E1_\chi = -\frac{1}{\mathcal{J}B}\frac{\partial \phi}{\partial \chi} \ ,$$

$$E1_\theta = i\frac{n}{r}\phi - i\frac{\omega}{r}X \ ,$$

where ϕ is the electric potential. See Appendix B for additional field relations.

For systems with closed field lines Eq. (4.7) has an exact solution. There are two types of solutions depending on whether the particles are trapped or untrapped in the magnetic wells. In addition the solution will depend on the sign of v_χ. The sign of v_χ will be denoted by a superscript, h^+ and h^-. For mirror trapped particles the boundary conditions are $h^+(\ell_1) = h^-(\ell_1)$ and $h^+(\ell_2) = h^-(\ell_2)$ where ℓ_1 and ℓ_2 are the turning points of the particle. This satisfies the requirement that the two solutions be the same when $v_\chi = 0$. For untrapped or circulating particles the boundary conditions are $h^+(\ell_1) = h^+(\ell_2)$ and $h^-(\ell_1) = h^-(\ell_2)$ where here ℓ_1 is an arbitrary starting point on a field line and $\ell_2 = \ell_1 + L$ where L is the length of the field line. For untrapped particles the two solutions are separately continuous around a field line. Denote the right hand side of Eq. (4.7) as Γ so that h satisfies,

$$(\omega - \omega_D)h^\pm \mp i|v_\chi|\hat{\chi}\cdot\nabla h^\pm = \Gamma^\pm \ , \tag{4.8}$$

where $\Gamma^\pm = (\omega - \omega^*)\{(\phi - \frac{\omega}{n}X \pm \frac{i}{n}|v_\chi|\hat{\chi}\cdot\nabla X)J_0(a)$

$$- v_\perp \frac{r}{n} B\left(Y + \frac{\partial X}{\partial \psi}\right) J_1(a)\Big\} \ .$$

The exact solution to the differential equation for h can be found by a straightforward application of the method of variation of parameters using the boundary conditions previously prescribed. The solution for trapped particles is,

$$h^{\pm}(\ell) = \frac{\exp\{\pm iQ(\ell,\ell_2)\}}{\sin\{Q(\ell_1,\ell_2)\}} \int_{\ell_1}^{\ell} d\ell' \frac{\Gamma^{\pm}(\ell')}{|v_\chi|} \cos\{Q(\ell_1,\ell')\}$$

$$+ \frac{\exp\{\mp iQ(\ell_1,\ell)\}}{\sin\{Q(\ell_1,\ell_2)\}} \int_{\ell}^{\ell_2} d\ell' \frac{\Gamma^{\pm}(\ell')}{|v_\chi|} \cos\{Q(\ell',\ell_2)\} \ , \quad (4.9)$$

where $Q(\ell_1,\ell_2) = \int_{\ell_1}^{\ell_2} d\ell' \frac{(\omega - \omega_D)}{|v_\chi|}$.

For untrapped particles the solution is,

$$h^{\pm}(\ell) = \frac{1}{2}\int_{\ell}^{\ell_2} d\ell' \frac{\Gamma^{\pm}(\ell')}{|v_\chi|} \frac{\exp\left[\pm iQ(\ell,\ell') \mp \frac{i}{2} Q(\ell_1,\ell_2)\right]}{\sin\left\{\frac{1}{2} Q(\ell_1,\ell_2)\right\}}$$

$$+ \frac{1}{2}\int_{\ell_1}^{\ell} d\ell' \frac{\Gamma^{\pm}(\ell')}{|v_\chi|} \frac{\exp\left[\mp iQ(\ell',\ell) \pm \frac{i}{2} Q(\ell_1,\ell_2)\right]}{\sin\left\{\frac{1}{2} Q(\ell_1,\ell_2)\right\}} \ . \quad (4.10)$$

Singularities appear in $h^{\pm}(\ell)$ when the sin function in the denominator is zero. This occurs when $Q = 0$, which corresponds to a drift resonance, and when $Q = 2\pi p$ where p is an integer which corresponds to bounce harmonic resonances.

To obtain a complete set of equations the velocity moments of f_1^0 are needed. Substituting Eq. (4.9) into Eq. (4.5) gives an expression for f_1^0. However, velocity moments of this expression for f_1^0 are difficult to calculate. The integration of $h^{\pm}$ over velocity can be made more tractable by finding approximate expressions for $h^{\pm}$. Two limits will be considered, a low frequency limit where $\omega \ll \omega_b$ where $\omega_b^{-1} = \pi \int \frac{d\ell}{|v_\chi|}$ and a higher frequency limit where $\omega \gg \omega_b$. However in taking these limits effects due to bounce particle resonances are lost.

B. Low Frequency Limit, $\omega \ll \omega_b$

For the low frequency expansion of h it is convenient to write h in the form,

$$h = - (\omega - \omega^*) \frac{X}{n} J_0(a) + h' \ , \quad (4.11)$$

where h′ satisfies,

$$(\omega - \omega_D) h'^{\pm} \mp i |v_\chi| \hat{\chi}\cdot\nabla h'^{\pm}$$

$$= (\omega - \omega^*)\left\{\left[\phi - \frac{\omega_D}{n} X\right] J_0(a) - v_\perp \frac{r}{n} B\left(Y + \frac{\partial X}{\partial \psi}\right) J_1(a)\right.$$

$$\left. \mp i \frac{X}{r} \frac{v_\perp}{\Omega} \frac{1}{2} \frac{1}{r^2 B} |v_\chi| \hat{\chi}\cdot\nabla(r^2 B) J_1(a)\right\} \ . \quad (4.12)$$

The last term will be neglected since it is of order ρ/L_B. To lowest order in ω/ω_b taking $\omega_D \sim \omega$ in Eq. (4.12) one finds $i\,|v_\chi|\,\hat{\chi}\cdot\nabla h\mathcal{J}^{\pm} = 0$. The next order expansion together with the boundary conditions yields a consistency condition which determines $h\mathcal{J}^{\pm}$.

$$h\mathcal{J}^{\pm} = \frac{\langle \mathcal{I}^{\pm} \rangle}{\omega - \langle \omega_D \rangle} , \tag{4.13}$$

where $$\langle \mathcal{I}^{\pm} \rangle = \frac{\int_{\ell_1}^{\ell_2} \frac{d\ell}{|v_\chi|}\, \Gamma^{\pm}}{\int_{\ell_1}^{\ell_2} \frac{d\ell}{|v_\chi|}}$$

The integral here is taken over the entire field line for untrapped particles and over the particle orbit along a field line for particles that are mirror trapped. It is useful to write down expressions of $h\mathcal{J}^{\pm}$ summed over $\pm v_\chi$ since this sum appears in the velocity integration.

$$\frac{1}{2}\,(h\mathcal{J}^{+} + h\mathcal{J}^{-}) = \frac{\omega - \omega^*}{\omega - \langle \omega_D \rangle} \left\langle \left(\phi - \frac{\omega_D}{n} X\right) J_0(a) - v_\perp \frac{r}{n} B\left(Y + \frac{\partial X}{\partial \psi}\right) J_1(a) \right\rangle , \tag{4.14}$$

$$\frac{1}{2}\,(h\mathcal{J}^{+} - h\mathcal{J}^{-}) = 0 . \tag{4.15}$$

C. Higher Frequency Limit, $\omega \gg \omega_b$

For frequencies much larger then a typical bounce frequency Eq. (4.8) can be expanded directly to obtain expressions for $h\bar{\mathcal{J}}^{+} + h\bar{\mathcal{J}}^{-}$ and $h\bar{\mathcal{J}}^{+} - h\bar{\mathcal{J}}^{-}$. To lowest order in ω_b/ω,

$$\frac{1}{2}\,(h\bar{\mathcal{J}}^{+} + h\bar{\mathcal{J}}^{-}) = \frac{\omega - \omega^*}{\omega - \omega_D} \left\{ \left[\phi - \frac{\omega}{n} X\right] J_0(a) - v_\perp \frac{r}{n} B\left(Y + \frac{\partial X}{\partial Y}\right) J_1(a) \right\} , \tag{4.16}$$

$$\frac{1}{2}\,(h\bar{\mathcal{J}}^{+} - h\bar{\mathcal{J}}^{-}) = -\,i\,\frac{\omega - \omega^*}{\omega - \omega_D}\,|v_\chi|\,\hat{\chi}\cdot\nabla\left[\frac{\omega_D}{\omega - \omega_D}\frac{X}{n} J_0(a)\right] . \tag{4.17}$$

Eq. (4.17) for $h\bar{\mathcal{J}}^{+} - h\bar{\mathcal{J}}^{-}$ is of order $\frac{\omega_b}{\omega}\frac{\omega_D}{\omega}$ smaller then Eq. (4.16) for $h\bar{\mathcal{J}}^{+} + h\bar{\mathcal{J}}^{-}$. Since $\omega_b/\omega \ll 1$ and $\omega_D/\omega \ll 1$ velocity moments that depend on $h\bar{\mathcal{J}}^{+} - h\bar{\mathcal{J}}^{-}$ will be neglected for this frequency range.

D. Complete Set of Equations

Three equations plus the gauge condition are needed to form a complete set of equations governing the modes. For low frequency modes of the type considered here the quasi-neutality condition provides one of the equations.

$$n_{1i} = n_{1e} , \tag{4.18}$$

where n_1 is the perturbed density, $n_1 = \int d^3v\, f_1$. The remaining two equations will be obtained from the force balance equation and Ampere's law. To construct these equations the zeroth and first moments of the linear Vlasov equation, Eq. (4.12), are needed. These are respectively,

$$\frac{\partial}{\partial t}\int d^3v\, f_1 + \nabla\cdot\left[\int d^3v\, \vec{v}\, f_1\right] = 0 \,, \tag{4.19}$$

and

$$\frac{\partial}{\partial t}\left[\, m\int d^3v\, \vec{v}\, f_1\right] + \nabla\cdot\left[m\int d^3v\, \vec{v}\vec{v}\, f_1\right] - \left[q\int d^3v\, f_1\right]\times \vec{B}_0 = q\,\vec{E}_1\int d^3v\, f_0 + \left[q\int d^3v\, \vec{v}\vec{v}\, f_0\right]\times \vec{B}_1 \,. \tag{4.20}$$

Summing the first moment over electron and ion species yields the force balance equation,

$$\frac{\partial}{\partial t}\left[\sum_{i,e} m\vec{v}_1\right] + \nabla\cdot\left[\sum_{i,e}\vec{P}\right] = \frac{1}{\mu_0}(\nabla\times\vec{B}_1)\times\vec{B}_0 + \frac{1}{\mu_0}(\nabla\times\vec{B}_0)\times\vec{B}_1 \,.$$

where

$$\vec{v}_1 \equiv \int d^3v\, \vec{v}\, f_1 \,, \quad \vec{P} \equiv m\int d^3v\, \vec{v}\vec{v}\, f_1 \,, \tag{4.21}$$

$$\nabla\times\vec{B}_1 = \mu_0\vec{j}_1 = \sum_{i,e} q\int d^3v\, f_1 \,.$$

Here $\vec{v}_1$ is used to denote the first velocity moment of f_1 and will be refered to as the perturbed velocity moment. The perturbed velocity moment is related to the perturbed fluid velocity, $\vec{u}_1$, by the relation $n_0\vec{u}_1 = n_1\vec{u}_0 + \vec{v}_1$ where $\vec{u}_0$ is the equilibrium fluid velocity. The

symbol $\vec{P}_1$ is used to denote the second velocity moment of f_1 and will be refered to as the perturbed pressure moment. It is related to the perturbed pressure tensor, $\vec{\Pi}_1$, by the relation $\vec{\Pi}_1 = \vec{P}_1 - m\vec{u}_0\vec{u}_1 - m\vec{u}_1\vec{u}_0$. Ampere's law was used to write the expression for $\vec{j}_1$ in terms of $\vec{B}_1$ in Eq. (4.21). The ψ and θ components of the force balance equation provide the remaining two equations to complete our set of equations. The χ component of the force balance equation turns out simply to be an identity.

The perturbed velocity moments n_1, $\vec{v}_1$ and $\vec{P}_1$ are summarized in Appendix D. They are calculated using Eq. (4.5) for f_1^q and Eq. (4.14) and Eq. (4.15) in Eq. (4.11) for h for the low frequency regime and Eq. (4.16) and Eq. (4.17) for h for the higher frequency regime.

Two sets of equations will be considered for two frequency regimes; a low frequency regime where $\omega \ll \omega_{bi} \ll \omega_{be}$ and an intermediate regime where $\omega_{bi} \ll \omega \ll \omega_{be}$, where ω_{bi} and ω_{be} are, respectively, the ion and electron bounce frequency. In both cases the electron Larmor radius will be considered small and neglected while finite ion Larmor radius effects will be retained.

1. Low frequency equations

For low frequencies $\omega \ll \omega_{bi} \ll \omega_{be}$ the appropriate forms for h for both the ions and electrons are Eq. (4.14) and Eq. (4.15). Using Eq. (D.8) for the perturbed density for the ions and the electrons in Eq. (4.18) gives the quasi-neutrality condition.

$$\phi\left(\frac{1}{\tau}+1\right) = \frac{p'}{p} X \left(1 - \frac{\omega}{\omega_i^*}\right)(1 - G_0)$$

$$+ \frac{1}{n_0} \sum_{i,e} \frac{e}{T} \int d^3v\, f_m\, J_0(a)\, \Xi \ , \qquad (4.22)$$

where

$$\Xi = \frac{\omega - \omega^*}{\omega - \langle\omega_D\rangle} \left\langle \left(\phi - \omega_D \frac{X}{n}\right) J_0(a) - v_\parallel \frac{r}{n} B\left(Y + \frac{\partial X}{\partial \psi}\right) J_1(a) \right\rangle \ ,$$

and $\Phi = \frac{e\phi}{T_i}$, $\tau = \frac{T_e}{T_i}$.

The function G_0 introduced in Eq. (4.20) and the functions G_1 and G_2 which will be introduced below include finite ion Larmor radius effects. These functions are defined by, effects.

$$G_0 \equiv \exp(-a_T^2)\, I_0(a_T^2) \ ,$$

$$G_1 \equiv \exp(-a_T^2)\, [I_0(a_T^2) - I_1(a^2{}_T)] \ ,$$

$$G_2 \equiv \exp(-a_T^2)\, [I_0(a_T^2)[1 - a_T^2] + a_T^2\, I_1(a^2{}_T)] \ ,$$

where $a_T \equiv k_\theta \rho_i = \frac{\rho_i n}{r}$. In the limit $a_T \to 0$ then $G_0 = G_1 = G_2 = 1$.

The first term appearing in the force balance equation, Eq. (4.21) is due to the rate of increase of momentum per unit volume. Since ion and electron fluid velocities are comparable the rate of increase of momentum is mainly due to the more massive ions and the

electron component will be neglected. To evaluate this term expressions for the components of the ion perturbed velocity moment are needed. The ψ - component can be evaluated directly using f_1^1; however, the θ -component of the perturbed velocity moment, $v1_\theta$, cannot be calculated from f_1^0 (the result is zero). One can either go to higher order and calculate f_1^1 or use the perturbed density and the other components of the perturbed velocity moment in the continuity equation, Eq. (4.19) to solve for $v1_\theta$. Either way the result to lowest order is the same. The perturbed velocity moments used in the force balance equation are,

$$v1_\psi = i n_0 (\omega - \omega^*) \frac{X}{rB} G_1$$

$$- i \frac{q}{T} \int d^3v\, f_m\, v_\parallel\, J_1(a)\, \Xi \ , \qquad (4.23)$$

$$= i n_0 (\omega - \omega^*) \frac{X}{rB} G_1$$

$$+ i n_0 \frac{n}{r} \frac{T}{q} \left(1 - \frac{\omega^*}{\omega}\right) \int_0^{1/B} \frac{d\alpha}{\sqrt{1 - \alpha B}}\, \alpha B \left\langle -\frac{3}{4} \frac{q\phi}{T} Z_3 \right.$$

$$\left. + \frac{15}{8} X\left[\left(1 - \frac{\alpha B}{2}\right) D + \alpha B \frac{\mu_0 p'}{B^2}\right] Z_4 + \frac{15}{8} \left(Y + \frac{\partial X}{\partial \psi}\right) \alpha B\, Z_5 \right\rangle \ ,$$

$$v1_\theta = - n_0 (\omega - \omega^*) \frac{r}{n} Y G_1$$

$$- \frac{r}{n} \frac{q}{T} \int d^3v\, f_m\, v_\parallel\, \hat{\psi} \cdot \nabla \left[J_1(a)\, \Xi \right] \ , \qquad (4.24)$$

$$= - n_0 (\omega - \omega^*) \frac{r}{n} Y G_1$$

$$+ n_0 \frac{T}{q}\left(1 - \frac{\omega^*}{\omega}\right)\int_0^{1/B} \frac{d\alpha}{\sqrt{1-\alpha B}}\,\alpha B\,\hat{\psi}\cdot\nabla\Big\{\Big\langle -\frac{3}{4}\frac{q\phi}{T}\,\mathcal{Z}_3$$

$$+ \frac{15}{8}\,X\Big[\Big(1 - \frac{\alpha B}{2}\Big)D + \alpha B\,\frac{\mu_0 p'}{B^2}\Big]\mathcal{Z}_4 + \frac{15}{8}\Big(Y + \frac{\partial X}{\partial\psi}\Big)\alpha B\,\mathcal{Z}_5\Big\rangle\Big\}\ .$$

where higher order finite Larmor radius terms were neglected in the equation for $v_{1\theta}$. By higher order finite Larmor radius terms we mean terms that include functions of the form $\exp(-a_T^2)\ I_p(a_T^2)$ where I_p is the modified Bessel functions of the first kind of order p where p is an integer greater then 2 or in general, terms that involve integrals over velocity space where the integrand contains the product $J_0(a)J_p(a)$ where p is an integer greater then 2. The functions $\mathcal{Z}$ are defined in Appendix D, Eqs. (D.6) and contain finite Larmor radius effects. In the limit $a_T \to 0$, $\omega_D/\omega \to 0$, then $\mathcal{Z} \to 1$.

The second term of the force balance equation, Eq. (4.21) is the divergence of the momentum flow. To evaluate this term the components of the total perturbed pressure moment tensor (the sum of the electron and ion perturbed pressure tensors) are needed. The components of the total perturbed pressure moment tensor are dominated by the diagonal elements $P_{\psi\psi}$, P_{XX}, $P_{\theta\theta}$ summarized below.

$$P_{\psi\psi} = P_{i\psi\psi} + P_{e\psi\psi}$$

$$= -\frac{p'}{1+\tau}\,X\,\Big[\tau + \frac{\omega}{\omega_i^*} + \Big(1 - \frac{\omega}{\omega_i^*}\Big)(2G_2 + G_1 - 2G_0)\Big]$$

$$+ \sum_{i,e} n\,\frac{q}{T}\int d^3v\ f_m\ v_\perp^2\ [J_0(a) - \frac{1}{a}J_1(a)]\,\Xi\ . \qquad (4.25)$$

$$P_{XX} = P_{iXX} + P_{eXX}$$

$$= -\frac{p'}{1+\tau}\,X\,\Big[\tau + \frac{\omega}{\omega_i^*} + \Big(1 - \frac{\omega}{\omega_i^*}\Big)G_0\Big]$$

$$+ \sum_{i,e} n\,\frac{q}{T}\int d^3v\ f_m\ v_X^2\ J_0(a)\,\Xi\ . \qquad (4.26)$$

$$P_{\theta\theta} = P_{i\theta\theta} + P_{e\theta\theta}$$

$$= -\frac{p'}{1+\tau}\,X\,\Big[\tau + \frac{\omega}{\omega_i^*} + \Big(1 - \frac{\omega}{\omega_i^*}\Big)G_1\Big]$$

$$+ \sum_{i,e} n\,\frac{q}{T}\int d^3v\ f_m\ v_\perp^2\ \frac{1}{a}J_1(a)\,\Xi\ . \qquad (4.27)$$

Here $p' = \partial p/\partial\psi$.

The two components of the divergence of the perturbed pressure moment tensor needed here are,

$$(\nabla\cdot\tilde{P}_1)_\theta = -i\,\frac{n}{r}\,P_{1\theta\theta}\ , \qquad (4.28)$$

$$(\nabla\cdot\tilde{P}_1)_\psi = rB\,\frac{\partial}{\partial\psi}P_{1\psi\psi} - (P_{1XX} - P_{1\psi\psi})\,\frac{rBD}{2}$$

$$+ (P_{1\psi\psi} - P_{1\theta\theta})\,B\,\frac{\partial r}{\partial\psi} + rB\,\frac{\partial}{\partial X}\Big(\frac{P_{1\psi X}}{rB^2}\Big)\ . \qquad (4.29)$$

where $D = -\frac{2}{rB}\hat{\psi}\cdot(\hat{\chi}\cdot\nabla)\hat{\chi} = -\frac{2\mu_0}{B^2}\frac{\partial}{\partial\psi}\left(p + \frac{B^2}{2\mu_0}\right)$.

The last two terms in the ψ component are small and will be neglected. The symbol D is the same as in Eq. (3.4) and has the same meaning as in the MHD analysis.

Using Eq. (4.24) and Eq. (4.28) the θ-component of the force balance equation, Eq. (4.21), can be written,

$$\frac{1}{n^2}\frac{\partial}{\partial\chi}\left(\frac{r^2}{\mathcal{F}}\frac{\partial Y}{\partial\chi}\right) = \mathcal{F}B^2\left(Y + \frac{\partial X}{\partial\psi}\right) + \mathcal{F}\mu_0 m_i\omega\frac{r}{n}v_{1i\theta}$$

$$+ \mathcal{F}\frac{\mu_0 p'}{1+\tau}X\left[\tau + \frac{\omega}{\omega_i^*} + \left(1 - \frac{\omega}{\omega_i^*}\right)G_1\right]$$

$$- \mathcal{F}\sum_{i,e}\mu_0 m\frac{q}{T}\int d^3v\, f_m\, v_\perp^2\,\frac{1}{a}J_1(a)\,\Xi \ . \qquad (4.30)$$

Substituting Eq. (4.24), Eq. (4.27) and Eq. (4.28) into the ψ component of Eq. (4.21) give an explicit expression for ψ-component of the force balance equation:

$$\frac{\partial}{\partial\chi}\left(\frac{1}{\mathcal{F}r^2B^2}\frac{\partial X}{\partial\chi}\right) + \frac{\partial}{\partial\psi}\left[\mathcal{F}B^2\left(Y + \frac{\partial X}{\partial\psi}\right)\right] - \mathcal{F}\mu_0 p'\left(Y + \frac{\partial X}{\partial\psi}\right)$$

$$= -\mathcal{F}\mu_0 n_0 m_i\omega\left(\omega - \omega_i^*\right)\frac{X}{r^2B^2}G_1 + \mathcal{F}\mu_0\omega\frac{m_i}{rB}\frac{e}{T_i}\int d^3v\, f_m\, v_\perp\, J_1(a)\,\Xi$$

$$- \mathcal{F}\frac{\partial}{\partial\psi}\left\{\frac{\mu_0 p'}{1+\tau}X\left[\tau + \frac{\omega}{\omega_i^*} + \left(1 - \frac{\omega}{\omega_i^*}\right)(2G_2 + G_1 - 2G_0)\right]\right\}$$

$$+ \mathcal{F}\frac{\partial}{\partial\psi}\left\{\sum_{i,e}\mu_0 m\frac{q}{T}\int d^3v\, f_m\, v_\perp^2\left[J_0(a) - \frac{1}{a}J_1(a)\right]\Xi\right\}$$

$$- \mathcal{F}D\frac{\mu_0 p'}{1+\tau}X\left(1 - \frac{\omega}{\omega_i^*}\right)\frac{1}{2}(2G_2 + G_1 - 3G_0) \qquad (4.31)$$

$$- \mathcal{F}D\sum_{i,e}\mu_0 m\frac{q}{T}\int d^3v\, f_m\,\frac{1}{2}\left[v_\chi^2 J_0(a) - v_\perp^2\left[J_0(a) - \frac{1}{a}J_1(a)\right]\right]\Xi \ .$$

It is often desirable to combine the ψ and θ components of the force balance equation.

$$\frac{\partial}{\partial\chi}\left(\frac{1}{\mathcal{F}r^2B^2}\frac{\partial X}{\partial\chi}\right) + \frac{1}{n^2}\frac{\partial}{\partial\psi}\frac{\partial}{\partial\chi}\left(\frac{r^2}{\mathcal{F}}\frac{\partial Y}{\partial\chi}\right) - \frac{1}{n^2}\frac{\mu_0 p'}{B^2}\frac{\partial}{\partial\chi}\left(\frac{r^2}{\mathcal{F}}\frac{\partial Y}{\partial\chi}\right)$$

$$= \frac{\partial}{\partial\psi}\left(\mathcal{F}\mu_0 m_i\omega\frac{r}{n}v_{1i\theta}\right) - \mathcal{F}\frac{\mu_0 p'}{B^2}\mu_0 m_i\omega\frac{r}{n}v_{1i\theta}$$

$$- \mathcal{F}\mu_0 n_0 m_i\omega\left(\omega - \omega_i^*\right)\frac{X}{r^2B^2}G_1 + \mathcal{F}\mu_0\omega\frac{m_i}{rB}\frac{e}{T_i}\int d^3v\, f_m\, v_\perp\, J_1(a)\,\Xi$$

$$+ \mathcal{F}D\frac{\mu_0 p'}{1+\tau}X\left[\tau + \frac{\omega}{\omega_i^*} + \left(1 - \frac{\omega}{\omega_i^*}\right)\left[G_1 - \frac{1}{2}(2G_2 + G_1 - 3G_0)\right]\right]$$

$$- \mathcal{F}D\sum_{i,e}\mu_0 m\frac{q}{T}\int d^3v\, f_m\,\frac{1}{2}\left[v_\chi^2 J_0(a) + v_\perp^2\left[\frac{3}{a}J_1(a) - J_0(a)\right]\right]\Xi$$

$$- \mathcal{F}\frac{\partial}{\partial\psi}\left\{\frac{\mu_0 p'}{1+\tau}X\left(1 - \frac{\omega}{\omega_i^*}\right)(2G_2 - 2G_0)\right]\right\}$$

$$+ \mathcal{F} \frac{\partial}{\partial \psi} \left\{ \sum_{i,e} \mu_0 \; m \frac{q}{T} \int d^3v \, f_m \, v_\perp^2 \; [J_0(a) - \frac{2}{a} J_1(a)] \Xi \right\} \quad . \quad (4.32)$$

The last two terms are of higher order in finite Larmor radius and will be neglected. Eq. (3.32) can be used to replace either the ψ component of the force balance equation of the θ component of the force balance equation.

The quasineutrality condition, Eq. (4.32), the θ component of the force balance equation, Eq. (4.30), and either ψ component of the force balance equation, Eq. (4.31), or the combined equation, Eq. (4.32), comprise the complete set of integro-differential equations for the study of low frequency modes, $\omega \ll \omega_{bi} \ll \omega_{be}$, in the multipole. The equations include finite ion Larmor radius, electron and ion drift resonance and heat flow along field lines.

2. Intermediate frequency equations

For the intermediate frequency regime $\omega_{bi} \ll \omega \ll \omega_{be}$ different forms for h are needed for each particle species. The appropriate forms for h for the electrons are Eq. (4.16) and Eq. (4.17). For the ions Eq. (4.14) and Eq. (4.15) are used for h.

Using Eq. (D.8) for the electron perturbed density and Eq. (D.23) for the ion perturbed density in Eq. (4.19) gives as the quasi-neutrality condition,

$$\left(\phi + \frac{\omega}{\omega_i^*} \frac{p'}{p} X\right) \left[\frac{1}{\tau} + 1 - \left(1 - \frac{\omega_i^*}{\omega}\right) Z_0\right]$$

$$= \frac{p'}{p} X \left(1 + \frac{1}{\tau} \frac{\omega}{\omega_i^*}\right) - \left(1 - \frac{\omega_i^*}{\omega}\right) \left(Y + \frac{\partial X}{\partial \psi}\right) Z_1$$

$$+ \frac{1}{n_0} \frac{e}{T_i} \frac{1}{\tau} \int d^3v \, f_m \, \Xi_e \qquad (4.33)$$

where

$$\Xi_e = \frac{\omega - \omega^*}{\omega - \langle \omega_D \rangle} \quad \phi - \omega_D \frac{X}{n} - \frac{1}{2} v_\perp^2 \frac{B}{\Omega} \left(Y + \frac{\partial X}{\partial \psi}\right) \quad .$$

Here the functions Z, Eqs. (D.21), include finite ion Larmor radius effects. In the limit $a_T^2 \to 0$, $\omega_D/\omega \to 0$ then $Z \to 1$.

The ψ and θ components of the ion perturbed velocity moment for $\omega \gg \omega_{bi}$ are,

$$v_{1\psi} = - i n_0 T \frac{n}{q} \frac{1}{rB} \left(1 - \frac{\omega^*}{\omega}\right) \left\{ \left(\frac{q\phi}{T} + \frac{\omega}{\omega^*} \frac{p'}{p} X\right) Z_1 \right.$$

$$\left. - 2 \left(Y + \frac{\partial X}{\partial \psi}\right) Z_2 \right] \quad , \qquad (4.34)$$

$$v_{1\theta} = \frac{r}{n} \omega n_0 \left\{ - \frac{q\phi}{T} - \frac{\omega}{\omega^*} \frac{p'}{p} X + \left(1 - \frac{\omega^*}{\omega}\right) \left[\left(\frac{q\phi}{T} + \frac{\omega}{\omega^*} \frac{p'}{p} X\right) Z_0 \right.\right.$$

$$- \left(Y + \frac{\partial X}{\partial \psi}\right) Z_1 \Big] \Big] - rn_0 \frac{T}{q} \frac{1}{\mathcal{F}} \frac{\partial}{\partial \psi} \Big[\mathcal{F} \Big(1 - \frac{\omega^*}{\omega}\Big) \Big[\Big(\frac{\Phi}{T} + \frac{\omega}{\omega^*} \frac{p'}{p} X\Big) Z_1$$

$$- 2\Big(Y + \frac{\partial X}{\partial \psi}\Big) Z_2 \Big] \Big] \ . \qquad (4.35)$$

The components of the perturbed pressure moment tensor for the intermediate frequency regime are,

$$P_{\psi\psi} = P_{i\psi\psi} + P_{e\psi\psi}$$

$$= \frac{p}{1+\tau} \Big(1 - \frac{\omega_i^*}{\omega}\Big) \Big[\Big(\Phi + \frac{\omega}{\omega_i^*} \frac{p'}{p} X\Big) (2Z_5 - Z_1)$$

$$- 2\Big(Y + \frac{\partial X}{\partial \psi}\Big) (2Z_6 - Z_2)$$

$$- \frac{p'}{1+\tau} X \Big(\tau + \frac{\omega}{\omega_i^*}\Big) - \frac{m_e}{\tau} \frac{e}{T_i} \int d^3v \, f_m \frac{1}{2} v_1^2 \, \Xi_e \ . \qquad (4.36)$$

$$P_{XX} = P_{iXX} + P_{eXX}$$

$$= \frac{p}{1+\tau} \Big(1 - \frac{\omega_i^*}{\omega}\Big) \Big[\Big(\Phi + \frac{\omega}{\omega_i^*} \frac{p'}{p} X\Big) Z_3 - \Big(Y + \frac{\partial X}{\partial \psi}\Big) Z_4 \Big]$$

$$- \frac{p'}{1+\tau} X \Big(\tau + \frac{\omega}{\omega_i^*}\Big) - \frac{m_e}{\tau} \frac{e}{T_i} \int d^3v \, f_m \, v_X^2 \, \Xi_e \ . \qquad (4.37)$$

$$P_{\theta\theta} = P_{i\theta\theta} + P_{e\theta\theta}$$

$$= \frac{p}{1+\tau} \Big(1 - \frac{\omega_i^*}{\omega}\Big) \Big[\Big(\Phi + \frac{\omega}{\omega_i^*} \frac{p'}{p} X\Big) Z_1 - 2\Big(Y + \frac{\partial X}{\partial \psi}\Big) Z_2 \Big]$$

$$- \frac{p'}{1+\tau} X \Big(\tau + \frac{\omega}{\omega_i^*}\Big) - \frac{m_e}{\tau} \frac{e}{T_i} \int d^3v \, f_m \frac{1}{2} v_1^2 \, \Xi_e \ . \qquad (4.38)$$

Substituting Eq. (4.35), Eq. (4.38) into the θ-component of Eq. (4.21) gives an explicit expression of the θ-component of the force balance equation,

$$\frac{1}{n^2} \frac{\partial}{\partial X} \Big(\frac{r^2}{\mathcal{F}} \frac{\partial Y}{\partial X} \Big) = \mathcal{F} B^2 \Big(Y + \frac{\partial X}{\partial \psi}\Big) + \mathcal{F} \mu_0 m_i \omega \frac{r}{n} v_{1\theta}$$

$$- \mathcal{F} \frac{\mu_0 p}{1+\tau} \Big(1 - \frac{\omega_i^*}{\omega}\Big) \Big[\Big(\Phi + \frac{\omega}{\omega_i^*} \frac{p'}{p} X\Big) Z_1 - 2\Big(Y + \frac{\partial X}{\partial \psi}\Big) Z_2 \Big]$$

$$+ \mathcal{F} \frac{\mu_0 p'}{1+\tau} X \Big(\tau + \frac{\omega}{\omega_i^*}\Big) + \mathcal{F} \mu_0 \frac{m_e}{\tau} \frac{e}{T_i} \int d^3v \, f_m \frac{1}{2} v_1^2 \, \Xi_e \ . \qquad (4.39)$$

Using Eq. (4.34), Eq. (4.36), Eq. (4.37) and Eq. (4.38) in Eq. (4.21) gives an expression for the ψ component of the force balance equation in the intermediate frequency regime,

$$\frac{\partial}{\partial X} \Big(\frac{1}{\mathcal{F} r^2 B^2} \frac{\partial X}{\partial X} \Big) + \frac{\partial}{\partial \psi} \Big[\mathcal{F} B^2 \Big(Y + \frac{\partial X}{\partial \psi}\Big) \Big] - \mathcal{F} \mu_0 p' \Big(Y + \frac{\partial X}{\partial \psi}\Big)$$

$$= \mathcal{J}\mu_0 n_0 m_i \omega \frac{nT_i}{e} \frac{1}{r^2 B^2} \left(1 - \frac{\omega_i^*}{\omega}\right)\left\{\left(\Phi + \frac{\omega}{\omega_i^*}\frac{p'}{p}X\right) Z_1 - 2\left(Y + \frac{\partial X}{\partial \psi}\right) Z_2\right\}$$

$$+ \mathcal{J} \frac{\partial}{\partial \psi}\left\{\frac{\mu_0 p}{1+\tau}\left(1 - \frac{\omega_i^*}{\omega}\right)\left[\left(\Phi + \frac{\omega}{\omega_i^*}\frac{p'}{p}X\right)(2Z_5 - Z_1)\right.\right.$$

$$\left.\left. - 2\left(Y + \frac{\partial X}{\partial \psi}\right)(2Z_6 - Z_2)\right]\right\} \qquad (4.40)$$

$$- \mathcal{J} \frac{\partial}{\partial \psi}\left\{\frac{\mu_0 p'}{1+\tau} X\left(\tau + \frac{\omega}{\omega_i^*}\right)\right\} - \mathcal{J} \frac{\partial}{\partial \psi}\left\{\mu_0 \frac{m_e}{\tau}\frac{e}{T_i}\int d^3v\, f_m \frac{1}{2}v_\parallel^2 \Xi_e\right\} ,$$

where higher order finite Larmor radius terms were dropped. Combining θ and ψ components of the force balance equation gives,

$$\frac{\partial}{\partial X}\left(\frac{1}{\mathcal{J} r^2 B^2}\frac{\partial X}{\partial X}\right) + \frac{1}{n^2}\frac{\partial}{\partial \psi}\frac{\partial}{\partial X}\left(\frac{r^2}{\mathcal{J}}\frac{\partial Y}{\partial X}\right) - \frac{1}{n^2}\frac{\mu_0 p'}{B^2}\frac{\partial}{\partial X}\left(\frac{r^2}{\mathcal{J}}\frac{\partial Y}{\partial X}\right)$$

$$= \frac{\partial}{\partial \psi}\left(\mathcal{J}\mu_0 m_i \omega \frac{r}{n} v_{1\parallel\theta}\right) - \mathcal{J}\frac{\mu_0 p'}{B^2}\mu_0 m_i \omega \frac{r}{n} v_{1\parallel\theta}$$

$$+ \mathcal{J}\frac{\mu_0 p' D}{1+\tau} X\left(\tau + \frac{\omega}{\omega_i^*}\right) + \mathcal{J}\mu_0 D \frac{m_e}{\tau}\frac{e}{T_i}\int d^3v\, f_m \frac{1}{2}v_\parallel^2 \Xi_e$$

$$+ \mathcal{J}\mu_0 n_0 m_i \omega \frac{nT_i}{e}\frac{1}{r^2 B^2}\left(1 - \frac{\omega_i^*}{\omega}\right)\left[\left(\Phi + \frac{\omega}{\omega_i^*}\frac{p'}{p}X\right) Z_1 - 2\left(Y + \frac{\partial X}{\partial \psi}\right) Z_2\right]$$

$$- \mathcal{J}\frac{\mu_0 pD}{1+\tau}\left(1 - \frac{\omega_i^*}{\omega}\right)\left[\left(\Phi + \frac{\omega}{\omega_i^*}\frac{p'}{p}X\right) Z_1 - 2\left(Y + \frac{\partial X}{\partial \psi}\right) Z_2\right]$$

$$+ \mathcal{J}\frac{\partial}{\partial \psi}\left\{\frac{\mu_0 p}{1+\tau}\left(1 - \frac{\omega_i^*}{\omega}\right)\left[\left(\Phi + \frac{\omega}{\omega_i^*}\frac{p'}{p}X\right)(2Z_5 - 2Z_1)\right.\right.$$

$$\left.\left. - 2\left(Y + \frac{\partial X}{\partial \psi}\right)(2Z_6 - 2Z_2)\right]\right\} . \qquad (4.41)$$

The last term of Eq. (4.41) is of higher order in the ion Larmor radius and will be neglected.

For the intermediate frequency regime $\omega_{bi} \ll \omega \ll \omega_{be}$ the complete set of equations governing electromagnetic modes are Eq. (4.33), the quasi-neutrality condition; Eq. (4.39), the θ-component of the force balance equation; and Eq. (4.40) the ψ-component of the force balance equation. The combined θ and ψ components of the force balance equation, Eq. (4.41) can be substituted for either the θ or ψ equations. These equations include finite ion Larmor radius, ion and electron drift resonances and electron heat flow along field lines.

In summary, the small Larmor radius expansion of the collisionless Vlasov equation was generalized to include electromagnetic perturbations as well as electrostatic perturbations. The perturbed distribution function was used together with the quasi-neutrality condition, the force balance equation and Ampere's law to construct two sets of three coupled, partial,

integro-differential equations governing low frequency, long parallel wave length modes. Two frequency regimes were considered: a low frequency regime where $\omega \ll \omega_{bi} \ll \omega_{be}$ and an intermediate regime where $\omega_{bi} \ll \omega \ll \omega_{be}$. For the low frequency regime the mode is considered slow enough that the majority of both the ions and the electrons execute many orbits along the field line while for the intermediate frequency regime the mode is assumed just slow enough that only the electrons are able to complete many parallel particle orbits. The frequency regime $\omega \gg \omega_{be}$ was not considered since in most devices this conflicts with the ordering $\omega \ll \Omega_i$. Properties and solutions to the two sets of equations will be discussed in the next two chapters. Chapter 5 will deal with the set of low frequency equations. We will see that in the limit of small ion Larmor radius the low frequency equations can be combined to give the Kruskal-Oberman energy principle[11,12]. Recently, it was also recognized that the low frequency equations in the limit of small real frequency predict the possibility of an unstable electromagnetic trapped particle mode[43]. Chapter 6 will deal with the set of equations for the intermediate frequency regime. In the limit $\omega_D/\omega \to 0$, $\omega^*/\omega \to 0$, $\rho_i \to 0$, these equations are related to the MHD equations.

CHAPTER 5

The Collisionless Energy Principle

In the collisionless kinetic equations derived in Chapter 4 the kinetic effects can be roughly divided into three categories, perpendicular kinetic effects, parallel kinetic effects and drift resonance effects. By perpendicular kinetic effects we mean those effects due to $v_\perp$ which include finite Larmor radius effects. By parallel particle effects we mean those due to particle dynamics along field lines including bounce resonance effects. The drift resonance involves both $v_\perp$ and v_x and so it is put in its own hybrid category. This chapter deals with the effect of parallel particle dynamics on the ballooning mode. Finite Larmor radius effects are considered in Chapter 6. Resonance effects will not be considered here.

Parallel particle dynamics are only important if the frequency of the mode under consideration is comparable to or less then the bounce frequency. In this chapter the low frequency equations are used $\omega \ll \omega_{bi} \ll \omega_{be}$. In these equations bounce resonance effects are neglected. In this frequency regime both the ions and the electrons are adiabatic. The guiding-center description of particle dynamics is valid. This means the magnetic moment, $\mu = \frac{mv_\perp^2}{2B}$, and the longitudinal invariant, $J = \oint d\ell \, |v_\parallel|$, are conserved[44]. In the hydromagnetic limit where $\omega_D/\omega \ll 1$ the particles can be considered stuck on a field line during the time scale of the mode. The particles can interact with the wave via Fermi acceleration. Changes in the volume of a flux

tube will cause the plasma to undergo collisionless adiabatic compression.

In section A of this chapter a low frequency collisionless variational principle is constructed from the complete set of equations for the low frequency regime that were derived in Chapter 4. In section B the hydrodynamic limit of this variational principle, $\omega^*/\omega \to 0$, $\omega_D/\omega \to 0$, $\rho_i \to 0$ is taken, resulting in the Kruskal-Oberman energy principle[11,12]. This energy principle is minimized in the same fashion as the MHD energy principle resulting in an integro-differential equation for the marginally stable mode. In section C this equation is solved for the Levitated Octupole configuration and compared with the MHD results.

A. Low Frequency Collisionless Variational Principle

For purposes of simplifying the algebra we will assume $a_I^2 = k_0^2\rho_i^2 \to 0$ in Eq. (4.22), Eq. (4.30) and Eq. (4.31), the equations governing low frequency modes. However, terms depending on ω^* will be retained. As will be seen in the next chapter the most important finite Larmor radius terms have been kept. In the limit $a_I^2 \to 0$, $G_0 = G_1 = G_2 = 1$, and the quasineutrality condition, Eq. (4.22), reduces to,

$$\Phi\left(\frac{1}{\tau} + 1\right) = \frac{1}{n_0}\sum_{i,e}\frac{e}{T}\int d^3v\, f_m\, \Xi \ , \tag{5.1}$$

where

$$\Xi = \frac{\omega - \omega^*}{\omega - \langle\omega_D\rangle}\left\langle \phi - \omega_D\frac{X}{n} - \frac{1}{2}v_I^2\frac{B}{\Omega}\left(Y + \frac{\partial X}{\partial\psi}\right)\right\rangle , \tag{5.2}$$

and $$\phi = \frac{e\phi}{T_i} \ , \quad \tau = \frac{T_e}{T_i} \ .$$

The θ-component of the force balance equation, Eq. (4.30), becomes in the limit $a_I^2 \to 0$,

$$\frac{1}{n^2}\frac{\partial}{\partial X}\left(\frac{r^2}{\mathcal{J}}\frac{\partial Y}{\partial X}\right) = \mathcal{J}B^2\left(Y + \frac{\partial X}{\partial\psi}\right) + \mathcal{J}\mu_0 m_I\omega\frac{r}{n}v_{1\theta}$$

$$+ \mathcal{J}\mu_0 p'\,X - \mathcal{J}\sum_{i,e}\mu_0 m\frac{q}{T}\int d^3v\, f_m\frac{1}{2}v_I^2\,\Xi \ . \tag{5.3}$$

where $$v_{1\theta} = -n_0(\omega - \omega_i^*)\frac{r}{n}Y \ . \tag{5.4}$$

Rounding out the set of equations the ψ-component of the force balance equation is, in the limit $a_I^2 \to 0$,

$$\frac{\partial}{\partial X}\left(\frac{1}{\mathcal{J}r^2B^2}\frac{\partial X}{\partial X}\right) + \frac{\partial}{\partial\psi}\left[\mathcal{J}B^2\left(Y + \frac{\partial X}{\partial\psi}\right)\right] - \mathcal{J}\mu_0 p'\left(Y + \frac{\partial X}{\partial\psi}\right)$$

$$= -\mathcal{J}\mu_0 n_0 m_I\omega(\omega - \omega_i^*)\frac{X}{r^2B^2} + \mathcal{J}\frac{\partial}{\partial\psi}\{\mu_0 p'\,X\}$$

$$+ \mathcal{J}\frac{\partial}{\partial\psi}\left\{\sum_{i,e}\mu_0 m\frac{q}{T}\int d^3v\, f_m\frac{1}{2}v_I^2\,\Xi\right\}$$

$$- \mathcal{J}D\sum_{i,e}\mu_0 m\frac{q}{T}\int d^3v\, f_m\frac{1}{2}\left\{v_X^2 - \frac{1}{2}v_I^2\right\}\Xi \ . \tag{5.5}$$

Multiplying Eq. (5.1) by $\frac{1}{2}\mu_0 n_0 e\phi^*$, Eq. (5.3) by $\frac{1}{2}Y^*$, Eq. (5.5) by $\frac{1}{2}X^*$, integrating each over volume and summing, the following variational principle is formed,

$$\pi \int d\psi\, d\chi\, \mathcal{J} \mu_0 n_0 m_i \omega (\omega - \omega_i^*) \left\{ \frac{X^2}{r^2 B^2} + \frac{r^2}{n^2} Y^2 \right\}$$

$$= \pi \int d\chi\, d\psi\, \mathcal{J} \frac{1}{\mathcal{J}^2 r^2 B^2} \left(\frac{\partial X}{\partial \chi}\right)^2 + \mu_0 p' D X^2$$

$$+ \frac{1}{n^2} \frac{r^2}{\mathcal{J}^2} \left(\frac{\partial Y}{\partial \chi}\right)^2 + B^2 \left[Y + \frac{\partial X}{\partial \psi} + \frac{\mu_0 p'}{B^2} X \right]^2 - \mu_0 n_0 \sum_{i,e} q^2 \frac{\phi^2}{T}$$

$$+ \mu_0 \sum_{i,e} \frac{q^2}{T} \int d^3v\, f_m \left[\phi - \frac{\omega_D}{n} X - \frac{1}{2} v_\perp^2 \frac{B}{\Omega} \left(Y + \frac{\partial X}{\partial \psi} \right) \right] \Xi \Big\} \quad . \tag{5.6}$$

Using the velocity coordinates ε, α and ζ (See Appendix A) the last term of Eq. (5.4) can be rewritten,

$$\pi \int d\psi\, d\chi\, \mathcal{J} \mu_0 \sum_{i,e} \frac{q^2}{T} \int d^3v\, f_m \left[\phi - \frac{\omega_D}{n} X - \frac{1}{2} v_\perp^2 \frac{B}{\Omega} \left(Y + \frac{\partial X}{\partial \psi} \right) \right] \Xi$$

$$= \pi \int d\psi\, d\chi\, \mathcal{J} \mu_0 \sum_{i,e} n_0 T \left(1 - \frac{\omega^*}{\omega} \right) \int_0^{1/B} \frac{d\alpha\, B}{\sqrt{1 - \alpha B}} \left\{ \frac{1}{2} \left\langle \frac{q\phi}{T} \right\rangle^2 Z_0 \right.$$

$$- \frac{3}{2} \left\langle \frac{q\phi}{T} \right\rangle \left\langle X \left[\left(1 - \frac{\alpha B}{2} \right) D + \alpha B \frac{\mu_0 p'}{B^2} \right] + \left(Y + \frac{\partial X}{\partial \psi} \right) \alpha B \right\rangle Z_1$$

$$\left. + \frac{15}{8} \left\langle X \left[\left(1 - \frac{\alpha B}{2} \right) D + \alpha B \frac{\mu_0 p'}{B^2} \right] + \left(Y + \frac{\partial X}{\partial \psi} \right) \alpha B \right\rangle^2 Z_4 \right\} \quad , \tag{5.7}$$

where

$$\frac{1}{2} n_0 Z_0 = 2\sqrt{2}\, \pi \int_0^\infty d\varepsilon\, \sqrt{\varepsilon}\, \frac{f_m}{1 - \frac{\langle \omega_D \rangle}{\omega}} \quad , \tag{5.8.1}$$

$$\frac{3}{4} n_0 \frac{T}{m} Z_1 = 2\sqrt{2}\, \pi \int_0^\infty d\varepsilon\, \sqrt{\varepsilon}\, \frac{\varepsilon\, f_m}{1 - \frac{\langle \omega_D \rangle}{\omega}} \quad , \tag{5.8.2}$$

$$\frac{15}{8} n_0 \left(\frac{T}{m}\right)^2 Z_4 = 2\sqrt{2}\, \pi \int_0^\infty d\varepsilon\, \sqrt{\varepsilon}\, \frac{\varepsilon^2\, f_m}{1 - \frac{\langle \omega_D \rangle}{\omega}} \quad . \tag{5.8.3}$$

The Z functions are the same as the functions defined in Appendix D, Eqs. (D.6), in the limit $a_T = \frac{v_\perp n}{\Omega r} \to 0$ and contain the effects due to drift resonance. The right hand side of Eq. (5.6) is the same as the variational principle of Rosenbluth and Sloan[21] used to study the finite beta stabilization of the collisionless trapped particle instability. The left hand side of Eq. (5.6) includes the perpendicular kinetic energy of the ions and the lowest order finite Larmor radius effects on the $\vec{E} \times \vec{B}$ drift of the ions.

We should note here that obtaining the full expression for the perpendicular kinetic energy without expanding to higher order in the perturbed distribution function, f_1, was dependent on the choice of using the force balance equations to complete the set of equations. If instead Ampere's Law had been used, only the term proportional to X^2 would be present. The advantage of using the force balance equations in the present formulation is that the most important effects of $\rho_i k_\psi$ are obtained without going to higher order in f_1.

It has been pointed out by Antonsen, Lane and Ramos[43] that in the limit $\omega/\omega^* \to 0$, $\omega/\omega_D \to 0$ the last term in Eq. (5.6) can drive an electromagnetic trapped particle mode if $\omega^*/\langle\omega_D\rangle$ is negative. In a

configuration that is stable to MHD modes ($\omega^*\omega_D < 0$) this term might have a destabilizing influence. One would generally expect that ω^* and $\langle\omega_D\rangle$ would have opposite signs in a system with a large fraction of the particles trapped in a bad curvature region. However the evaluation of the integration over pitch angle in the last term of Eq. (5.6) is sufficiently difficult and sensitive to the structure of the magnetic field that the sign of $\omega^*/\langle\omega_D\rangle$ is probably very configuration dependent.

B. Kruskal-Oberman Stability of the Multipole

In the hydromagnetic limit $\omega^*/\omega \to 0$, $\omega_D/\omega \to 0$ and for equal ion and electron temperature, $T_i = T_e$, the electrostatic terms (those terms proportional to ϕ) and the electromagnetic terms in Eq. (5.6) completely uncouple. Hence, terms proportional to ϕ can be dropped. This means the most unstable mode is one where $\vec{E}_1 \cdot \vec{B} = 0$. In this limit Eq. (5.6) can be written in the form,

$$\omega^2 \, \delta K_\perp = \delta W_{KO} \, , \tag{5.9}$$

where $$\delta K_\perp = \pi \int d\psi \, d\chi \, \mathcal{J} \mu_0 n_0 m_i \left\{ \frac{X^2}{r^2 B^2} + \frac{r^2}{n^2} Y^2 \right\} ,$$

and $$\delta W_{KO} = \pi \int d\chi \, d\psi \, \mathcal{J} \left\{ \frac{1}{\mathcal{J}^2 r^2 B^2} \left(\frac{\partial X}{\partial \chi}\right)^2 + p' D X^2 \right.$$

$$\left. + \frac{1}{n^2} \frac{r^2}{\mathcal{J}^2} \left(\frac{\partial Y}{\partial \chi}\right)^2 + B^2 \left[Y + \frac{\partial X}{\partial \psi} + \frac{\mu_0 p'}{B^2} X \right]^2 \right.$$

$$\left. + \frac{15}{2} \mu_0 p B \int_0^{1/B} \frac{d\alpha}{\sqrt{1 - \alpha B}} \frac{J^2}{K^2} \right\} ,$$

with $$J = \int dl \, \frac{1}{\sqrt{1 - \alpha B}} \left\{ \left(1 - \frac{\alpha B}{2}\right) \frac{XD}{2} + \frac{\alpha B}{2} \left[Y + \frac{\partial X}{\partial \psi} + \frac{\mu_0 p'}{B^2} X \right] \right\} ,$$

and $$K = \int dl \, \frac{1}{\sqrt{1 - \alpha B}} \, .$$

Here $\delta K_\perp$ is the perpendicular kinetic energy of the fluid and δW_{KO} is the potential energy due to the perturbations X and Y. Eq. (5.9) constitutes an energy principle. If δW_{KO} can be made negative for any choice of X and Y then the system is unstable. Eq. (5.9) is sometimes referred to as the Kruskal-Oberman energy principle or the collisionless energy principle. It was first published in a more general form for an anisotropic plasma by Kruskal and Oberman[11]. It was also published slightly later by Rosenbluth and Rostoker[12] for an isotropic plasma. The notation J and K is from the latter paper here written in X and Y representation. As can be seen in Eq. (5.9) δW_{KO} is similar to the MHD energy principle except the ideal adiabatic term is replaced with a kinetic term. The kinetic term includes effects due to the collisionless adiabatic compression of the plasma and the Fermi acceleration of the particles. It has been said elsewhere that the Kruskal-Oberman energy principle includes "heat flow along field lines". This is somewhat misleading since the word

"heat" generally brings to mind collisions and in the Kruskal-Oberman model the plasma is purely collisionless.

Some applications of the Kruskal-Oberman energy principle have been made to the problem of tokamak stability. In the tokamak only the trapped particles contribute to the integral in the kinetic term of Eq. (5.9). Using the Schwartz inequality Conner and Hastie[45] approximated the kinetic term and derived a criterion for the localized interchange mode. The new criterion predicted greater stability than the Mercier criterion. P. H. Rutherford et. al.[46] used a large aspect ratio model for the tokamak where the integrals over the pitch angle variable in the kinetic term could be solved analytically. They predicted an increase in the beta limit for ballooning modes but it was very slight. Their main conclusion was that the Kruskal-Oberman energy principle has little affect on the critical beta of the ballooning mode in tokamaks. However, in a multipole one would expect the Kruskal-Oberman energy principle to have a greater effect on the critical beta than in a tokamak. In a tokamak only the trapped particles contribute to the kinetic term. This is only a small percentage of the total number of particles. In the multipole all the particles contribute to the kinetic term.

The Kruskal-Oberman energy principle can be minimized in the same manner as the MHD energy principle. As in MHD the $n = \infty$ modes are the most unstable stable modes. Taking the limit $n \to \infty$ and minimizing Eq.(5.9) with respect to Y yields,

$$0 = \frac{B^2}{\mu_0}\left[Y + \frac{\partial X}{\partial \psi} + \frac{\mu_0 p' X}{B^2}\right] + \frac{15}{4} pB \int_0^{1/B} d\alpha \frac{\alpha B}{\sqrt{1-\alpha B}} \frac{J}{K} . \quad (5.10)$$

This is the same as the θ-component of the force balance equation in the limit $1/n \to 0$, $\rho_i \to 0$ and $\omega = 0$. For the multipole the last term will be small compared to the other terms. This is because the density scale length is much smaller then the magnetic field scale length implying $p' >> pD$. To lowest order Eq.(5.10) is then,

$$Y + \frac{\partial X}{\partial \psi} + \frac{\mu_0 p' X}{B^2} = 0 . \quad (5.11)$$

Using this expression in Eq. (5.9) to eliminate Y in δW_{KO} results in

$$\delta W_{KO} = \pi \int d\chi \, d\psi \, \mathcal{J}\left\{\frac{1}{\mu_0} \frac{1}{\mathcal{J}^2 r^2 B^2} \left(\frac{\partial X}{\partial \chi}\right)^2 + p' DX^2 \right.$$

$$\left. + \frac{15}{4} pB \int_0^{1/B_{min}} \frac{d\alpha}{\sqrt{1-\alpha B}} \frac{J^2}{K^2} \left(1 - \frac{\alpha B}{2}\right) XD\right\} \quad (5.12)$$

where $$J = \int \frac{d\ell}{\sqrt{1-\alpha B}} \left(1 - \frac{\alpha B}{2}\right) \frac{XD}{2} . \quad (5.13)$$

Minimizing Eq. (5.12) with respect to X gives a single integro-differential equation for X,

$$\frac{\partial}{\partial \chi}\left(\frac{1}{\mathcal{J} r^2 B} \frac{\partial X}{\partial \chi}\right) - \mu_0 p' \mathcal{J} DX$$

$$= \frac{15}{2}\mu_0 p\mathcal{J}\mathcal{B}D\int_0^{1/B}\frac{d\ell}{\sqrt{1-\alpha B}}\frac{J}{K}\left(1-\frac{\alpha B}{2}\right), \qquad (5.14)$$

or

$$\frac{\partial}{\partial\ell}\left(\frac{1}{r^2B}\frac{\partial X}{\partial\ell}\right) - \mu_0 p'\frac{D}{B}X$$

$$= \frac{15}{2}\mu_0 pD\int_0^{1/B}\frac{d\ell}{\sqrt{1-\alpha B}}\frac{J}{K}\left(1-\frac{\alpha B}{2}\right), \qquad (5.15)$$

where $d\ell$ is the line element along a field line and J is given in Eq. (5.13). Eq. (5.14) or Eq. (5.15) is solved on each flux surface for the eigenvalue p′. The quantity p′ gives the critical pressure gradient at which the mode is marginally stable. If the equilibrium pressure gradient is greater then p′ on any of the flux surfaces the system is unstable to ballooning modes.

The first two terms in Eq. (5.14) are the same as the n = ∞ MHD equation. The last term is the kinetic adiabatic term and replaces the ideal fluid adiabatic term in the MHD equation (the term proportional to γ in Eq. (3.1).) The new term is in general stabilizing. Note, that if X has odd symmetry with respect to the midplane i.e., $X(\ell) = -X(L-\ell)$ where L is the length of the field line, the integral over α is zero. Hence the kinetic term does not help stabilize odd modes. As far as odd modes are concerned Eq. (5.14) is the same as the MHD equation. This makes for the interesting possibility that the most unstable ballooning mode might be an odd mode instead of an even mode.

C. Numerical Procedure and Results

Eq. (5.15) was solved using a computer program that calculates the perturbation expansion to a specified order. The kinetic term involving the integral over α is taken to be the perturbing term. This is because except near a field null it is generally true that $p' \gg pD$ meaning the kinetic term is much smaller then the second term in Eq. (5.15). Let's rewrite Eq. (5.15) in the form,

$$\frac{\partial}{\partial\ell}\left(\frac{1}{r^2B}\frac{\partial X}{\partial\ell}\right) = \mu_0 p'\frac{D}{B}X + LX, \qquad (5.16)$$

where $$LX = \frac{15}{2}\mu_0 pD\int_0^{1/B}\frac{d\ell}{\sqrt{1-\alpha B}}\frac{J}{K}\left(1-\frac{\alpha B}{2}\right).$$

The operator L is of order ϵ. We seek a perturbative solution to Eq. (5.16) of the form,

$$X = \sum_{m=0}^{\infty} X_m \epsilon^m, \quad p' = \sum_{m=0}^{\infty} p'_m \epsilon^m.$$

Substituting these expressions into Eq. (5.15) and comparing powers of ϵ gives the following sequence of equations,

$$\frac{\partial}{\partial\ell}\left(\frac{1}{r^2B}\frac{\partial X_m}{\partial\ell}\right) - \mu_0 p'_0\frac{D}{B}X_m$$

$$= \sum_{j=1}^{m}\mu_0 p'_j\frac{D}{B}X_{m-j} + LX_{m-1}. \qquad (5.17)$$

To lowest order Eq. (5.17) is the same as the infinite n MHD equation. If Eq. (5.17) is multiplied by X_0 and integrated over $d\ell$ an equation

for the coefficient p_m' is obtained in terms of lower order coefficients p_j' and X_j.

$$p_m' = -\frac{\sum_{j=1}^{m-1} p_j' \int X_0 \frac{D}{B} X_{m-j}\, d\ell + \int X_0\, LX_{m-1}\, d\ell}{\int X_0 \frac{D}{B} X_0\, d\ell} . \qquad (5.18)$$

After the lowest order term, X_0, of Eq. (5.16) has been found the higher order terms can be solved by the reduction of order technique. Substituting the expression $X_m(\chi) = u_m(\chi)X_0(\chi)$ into Eq. (5.16) and then multiplying by X_0 and integrating twice gives a formula for $u_m(\chi)$,

$$u_m = \int_0^{\ell} \frac{Br^2}{X_0^2}\, d\ell' \int_0^{\ell'} X_0 \left[\sum_{j=1}^{m} p_j' \frac{D}{B} X_{m-j} + LX_{m-1} \right] d\ell . \qquad (5.19)$$

Eq. (5.18) and Eq. (5.19) together constitute an iterative procedure for calculating the coefficients of the perturbation series. The integral over α occurring in the operator L is evaluated directly. The integrand in the expressions for J and K have integrable singularities where $B(\ell) = 1/\alpha$ at the end points. For the particular case $B(\ell) = B_0 + B_1 \cos^2(\ell)$ an analytic expression for K can be written in terms of elliptic integrals. The functions J and K can then be expected to behave like elliptic functions. Both J and K have a singularity whenever the limits of integration are such that $dB/d\ell = 0$ at the endpoints. This is due to the infinite period of particles

having a pitch angle such that $v_\chi = 0$ at a local maximum in the magnetic field. Both J and K have a nonzero value when $\alpha = 1/B_{min}$, where B_{min} is one of the minima of the magnetic field. This is due to the fixed frequency of particles executing small oscillations at the bottom of the magnetic well. The ratio J/K is finite but has discontinuities at points where $\alpha = 1/B_{min}$.

For the case of the Levitated Octupole the results of the stability calculation for even modes are shown in Fig. (5.1). Plotted in Fig. (5.1) is the critical pressure gradient of the even mode for Kruskal-Oberman stability, the critical pressure gradient of the even mode for MHD stability and the equilibrium pressure gradient. The beta of the equilibrium was chosen to be self consistent with the stability calculation. For marginal stability this means the critical pressure gradient must equal the critical pressure gradient at least at one point and must be less then the critical pressure gradient everywhere else. As expected the Kruskal-Oberman critical pressure gradient is always greater then the MHD critical pressure gradient. At the critical flux surface the two cases are degenerate. The critical beta for the $n = \infty$ even mode for Kruskal-Oberman stability is 4.70% compared to 4.33% for the MHD case. This represents a relative increase of 9% in the beta limit. For the calculation presented here the perturbation series was taken to 5th order. The 5th order correction to p' was only about 2% of the sum of the first four terms.

Except near the separatrix, the assumption that the kinetic term is small is justified. Near the separatrix the critical p′ for the Kruskal-Oberman case appears to diverge. This is due to the infinite inverse radius of curvature of the field lines near the null. In the MHD case the mode minimizes the effect of the infinite inverse radius of curvature by going to zero at the null. In the Kruskal-Oberman case the curvature is averaged by the parallel particle motion so even though the perturbation goes to zero at the null the effect of the infinite inverse radius of curvature is still felt. However, this is just an anomaly of the Kruskal-Oberman equation. Near the null the assumption that ρ/L_n and $\rho k_\parallel$ are small breaks down and the equations are no longer valid. This is of no great consequence to us. Since the equilibrium pressure gradient goes to zero at the separatrix the immediate region around the separatrix is not an important consideration for the ballooning mode which is centered around the peak pressure gradient region.

Fig. (5.2) shows the X eigenfunction for both the Kruskal-Oberman and MHD cases. Recall X is proportional to the fluid perturbation in the ψ direction in units of flux. Another way of looking at X is that it is proportional to rE_{l_θ}. The eigenfunction is a delta function of the variable ψ. The flux surface for Fig. (5.2) is the surface half way between the critical flux surface and the separatrix. Both the MHD and Kruskal-Oberman cases are similar. The eigenfunction peaks in the bad curvature region chacteristic of the ballooning mode. For the

Kruskal-Oberman case the X eigenfunction is peaked a little bit more in the bad curvature region.

For odd modes Eq. (5.14) is the same as the MHD equation for marginal stability and there is no improvement in the critical pressure gradient from the kinetic term. The result of the stability calculation for the odd mode for $\beta = 4.70\%$ is shown in Fig. (5.3). This plot shows the critical pressure gradient for both the even and odd modes calculated from the $n = \infty$ MHD analysis and the equilibrium pressure gradient plotted vs ψ. Here the odd mode is unstable since the equilibrium pressure gradient is greater then the critical pressure gradient of the odd mode on some of the flux surfaces. Hence, for the Levitated Octupole configuration the Kruskal-Oberman stability analysis says the odd mode is the most unstable mode.

In conclusion, the effect of parallel particle dynamics on ballooning modes was investigated and shown to produce a small increase in the beta limit of the Levitated Octupole. The effect is proportional to beta so if additional effects such as finite Larmor radius effects are included the stabilization due to the parallel motion of the particles would be proportionally greater. It was also found at least in the case of the $n = \infty$ mode that the odd mode is the most unstable mode. One would expect, however, that if the mode were sufficiently nonlocalized as in the case of finite n that the even mode would again be the most unstable. This is because the critical pressure gradient of the even mode is less than the critical pressure gradient of the odd mode out near the critical flux surface. This

means for betas somewhat greater then 4.70% the equilibrium pressure gradient will be greater then the critical pressure gradient of the even mode over more flux surfaces than the critical pressure gradient of the odd mode.

Fig. (5.1) Critical p′ vs ψ for Kruskal-Oberman and MHD Stability

The critical pressure gradient of the even mode for the Kruskal-Oberman stability analysis and the MHD stability analysis plus the equilibrium pressure gradient calculated using an MHD equilibrium with $\beta = 4.70\%$. $\psi_{sep} = 0.5294$, $\psi_{crit} = 0.8219$.

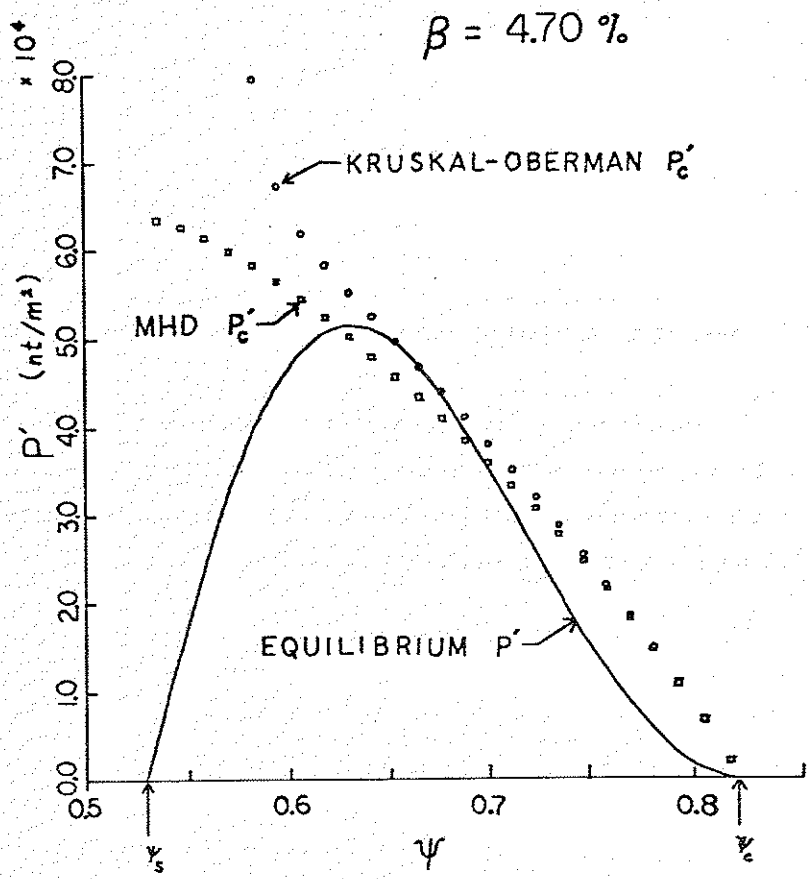

Fig. (5.1)

Fig. (5.2) X Eigenfunction for Kruskal Oberman and MHD Stability

The X eigenfunction of the even mode representing the fluid perturbation in the ψ direction in units of flux plotted against the relative distance along the field line for $\psi = 0.6754$.

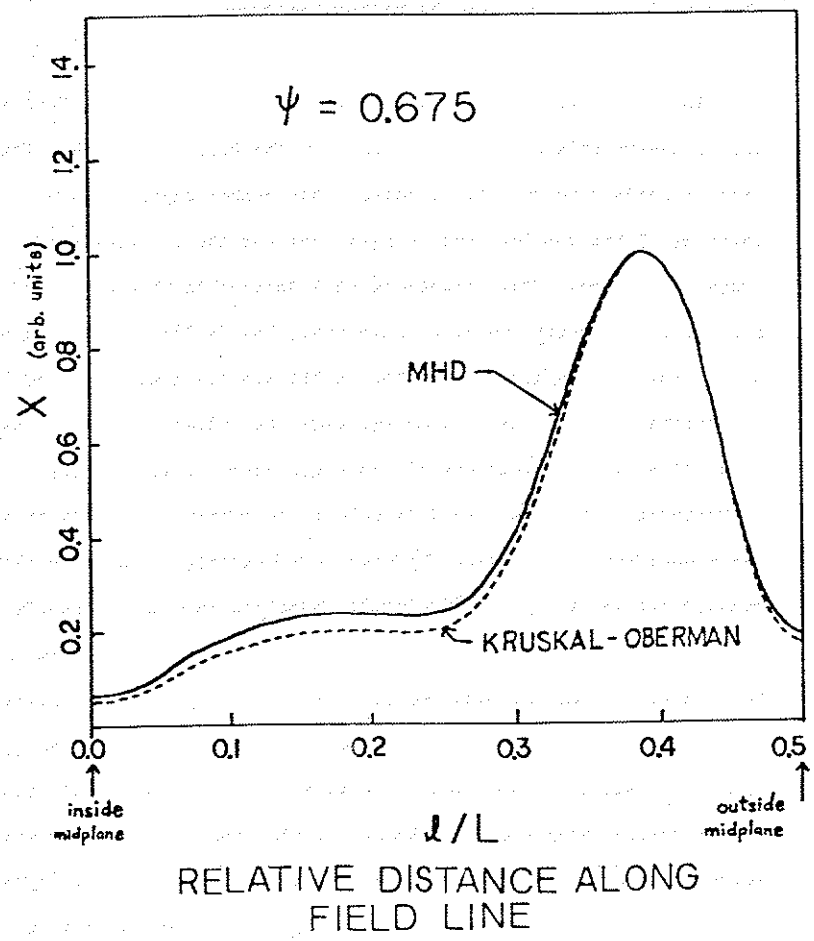

Fig. (5.2)

Fig. (5.3) Critical p′ vs ψ for Odd Mode Kruskal Oberman Stability

The critical pressure gradient of the odd mode for Kruskal-Oberman stability (which is the same in this case as the MHD stability) for $\beta = 4.70\%$. Also plotted is the critical pressure gradient of the even mode for MHD stability and the equilibrium pressure gradient. $\psi_{sep} = 0.5294$, $\psi_{crit} = 0.8219$.

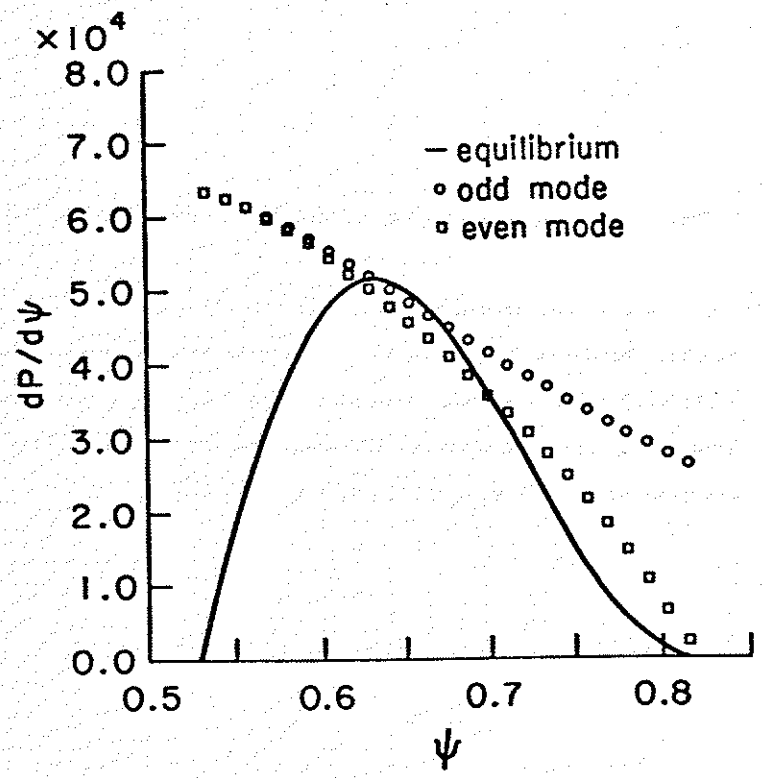

Fig. (5.3)

CHAPTER 6

Finite Larmor Radius Effects on the Ballooning Mode

The objective is to get an adequate solution including finite Larmor radius effects for the problem of the ballooning mode. This section deals with the high toroidal mode number expansion and solution of the complete set of equations for the intermediate frequency regime. These equations were derived in Chapter 4 and consist of the quasineutrality condition, Eq. (4.33), the θ-component of the force balance equation, Eq. (4.39) and the combined ψ and θ components of the force balance equation, Eq. (4.41). Ideally one would like to solve this set of equations exactly, without any perturbation expansion. In principle it is probably feasable to solve these equations numerically; however, even numerically solving three coupled partial integro-differential equations in a not-so-simple geometry is quite a horrendous task. With the high n expansion, the three equations can be combined to form a single partial differential equation. This approach has also been used for simplifying the kinetic equations in tokamaks[29]. This partial differential equation can be solved using a method similar to that was used to in Chapter 3 solve the high n MHD equation. For the multipole the high n expansion is actually a very good approximation. Generally, one runs into problems with ρ_i/L_n not being small (which makes the entire set of equations suspect) before the high n approximation breaks down.

The equations for the intermediate frequency regime, $\omega_{bi} \ll \omega \ll \omega_{be}$, are used since this most closely models the situation in the octupole when ballooning modes occur. With kinetic modifications, the real part of the frequency of the ballooning mode is on the order of the ion diamagnetic drift frequency, $\omega \sim \omega_i^*$. This frequency is somewhat larger then the typical ion bounce frequency, although not a great deal larger. For this frequency regime the ions are fluid-like in behavior. The electrons are adiabatic in the kinetic sense that there are constants of motion for each particle that are conserved. In Chapter 5 where both ions and electrons were adiabatic it was found that the increase in the critical beta was slight. In the case of the Levitated Octupole the beta limit increased from 4.3% to 4.7%. This represents a relative increase in the critical beta by a factor of 9%. For equal ion and electron temperatures, if there is only one adiabatic species present, one would expect the adiabatic terms to improve the critical beta by less then a factor of 5%. For this reason and also for numerical expediency the electron adiabatic terms will be neglected in this chapter.

A. High Toroidal Mode Number Expansion

Ignoring the terms involving integrals along the field lines (the electron adiabatic terms) Eq. (4.33) for the quasineutrality condition is,

$$\Phi + \frac{\omega}{\omega_i^*}\frac{p'}{p}X = \frac{\omega}{\omega_i^*}\frac{p'}{p}X\,\frac{1+\tau\,\frac{\omega_i^*}{\omega}}{1+\tau-\tau\left(1-\frac{\omega_i^*}{\omega}\right)Z_0} - \left(Y+\frac{\partial X}{\partial\psi}\right)Z_1\,\frac{\tau\left(1-\frac{\omega_i^*}{\omega}\right)}{1+\tau-\tau\left(1-\frac{\omega_i^*}{\omega}\right)Z_0} \quad . \tag{6.1}$$

where $\Phi = e\phi/T_i$ and $\tau = T_e/T_i$. Likewise, ignoring the adiabatic terms, the θ-component of the force balance equation is,

$$\frac{1}{n^2}\frac{\partial}{\partial X}\left(\frac{r^2}{\mathcal{J}}\frac{\partial Y}{\partial X}\right) = \mathcal{J}B^2\left(Y+\frac{\partial X}{\partial\psi}\right) + \mathcal{J}\mu_0 m_i\omega\,\frac{r}{n}\,v_{1\theta}$$

$$- \mathcal{J}\,\frac{\mu_0 p}{1+\tau}\left(1-\frac{\omega_i^*}{\omega}\right)\left[\left(\Phi+\frac{\omega}{\omega_i^*}\frac{p'}{p}X\right)Z_1 - 2\left(Y+\frac{\partial X}{\partial\psi}\right)Z_2\right]$$

$$+ \mathcal{J}\,\frac{\mu_0 p'}{1+\tau}\,X\left(\tau+\frac{\omega}{\omega_i^*}\right) \quad . \tag{6.2}$$

The combining ψ and θ components of the force balance equation results in the equation,

$$\frac{\partial}{\partial X}\left(\frac{1}{\mathcal{J}r^2B^2}\frac{\partial X}{\partial X}\right) + \frac{1}{n^2}\frac{\partial}{\partial\psi}\frac{\partial}{\partial X}\left(\frac{r^2}{\mathcal{J}}\frac{\partial Y}{\partial X}\right) - \frac{1}{n^2}\frac{\mu_0 p'}{B^2}\frac{\partial}{\partial X}\left(\frac{r^2}{\mathcal{J}}\frac{\partial Y}{\partial X}\right)$$

$$= \frac{\partial}{\partial\psi}\left(\mathcal{J}\mu_0 m_i\omega \frac{r}{n} v_{1i\theta}\right) - \mathcal{J}\frac{\mu_0 p'}{B^2}\mu_0 m_i\omega \frac{r}{n} v_{1i\theta}$$

$$+ \mathcal{J}\mu_0 n m_i\omega \frac{nT_i}{e}\frac{1}{r^2B^2}\left(1 - \frac{\omega_i^*}{\omega}\right)\left[\left(\Phi + \frac{\omega}{\omega_i^*}\frac{p'}{p}X\right)Z_1 - 2\left(Y + \frac{\partial X}{\partial\psi}\right)Z_2\right]$$

$$- \mathcal{J}\frac{\mu_0 pD}{1+\tau}\left(1 - \frac{\omega_i^*}{\omega}\right)\left[\left(\Phi + \frac{\omega}{\omega_i^*}\frac{p'}{p}X\right)Z_1 - 2\left(Y + \frac{\partial X}{\partial\psi}\right)Z_2\right]$$

$$+ \mathcal{J}\frac{\mu_0 p'D}{1+\tau}X\left(\tau + \frac{\omega}{\omega_i^*}\right) \quad . \tag{6.3}$$

Eq. (6.1) can be used to eliminate Φ in Eq. (6.2). For large toroidal mode number an expansion in orders of $1/n^2$ of Eq. (6.2) yields to lowest order,

$$Y = -\frac{\partial X}{\partial\psi} - \frac{\mu_0 p'}{B^2}S_1 X \quad , \tag{6.4}$$

where $$S_0 \equiv \frac{1 + \tau\dfrac{\omega_i^*}{\omega}}{1 + \tau - \tau\left(1 - \dfrac{\omega_i^*}{\omega}\right)G_0} \quad ,$$

$$S_1 \equiv \frac{1}{1+\tau}\left[\tau + \frac{\omega}{\omega_i^*} + \left(1 - \frac{\omega}{\omega_i^*}\right)S_0 G_1\right] \quad .$$

Here G_0 and G_1 contain finite ion Larmor radius effects and are defined in Eqs. (D.7). In deriving this expression for Y it was

assumed that $\omega_D/\omega \ll 1$ and the Z functions were expanded to first order in ω_D/ω (See Eqs. (D.22)). The first term on the right hand side of Eq. (6.4) is by far the largest term. The second term is smaller then the first by less then a factor of β since $\frac{\partial X}{\partial\psi} > \frac{p'}{p}X$. Terms of order β^2 or greater are neglected. The functions S_0 and S_1 contain finite Larmor radius effects and have the property that in the limit $\rho_i \to 0$, $S_0 = S_1 = 1$.

An expression for the θ-component of the perturbed velocity moment in terms of X is found by substituting Eq. (6.1) for Φ and Eq. (6.4) for Y into Eq. (4.35):

$$v_{1\theta} = \frac{r}{n} n_0 (\omega - \omega_i^*)\left(\frac{\partial X}{\partial\psi} + \frac{\mu_0 p'}{B^2}S_1 X\right)S_0 G_1 \quad , \tag{6.5}$$

where terms of order β^2 or greater were neglected as well as higher order finite Larmor radius effects. Using Eq. (6.1) for Φ, Eq. (6.4) for Y and Eq. (6.5) for $v_{1\theta}$ in Eq. (6.3) gives a single partial differential equation for X:

$$\frac{\partial}{\partial\chi}\left(\frac{1}{\mathcal{J}r^2B^2}\frac{\partial X}{\partial\chi}\right) - \frac{1}{n^2}\frac{\partial}{\partial\psi}\frac{\partial}{\partial\chi}\left[\frac{r^2}{\mathcal{J}}\frac{\partial}{\partial\chi}\left(\frac{\partial X}{\partial\psi} + \frac{\mu_0 p'}{B^2}S_1 X\right)\right]$$

$$+ \frac{1}{n^2}\frac{\mu_0 p'}{B^2}\frac{\partial}{\partial\chi}\left[\frac{r^2}{\mathcal{J}}\frac{\partial}{\partial\chi}\left(\frac{\partial X}{\partial\psi} + \frac{\mu_0 p'}{B^2}S_1 X\right)\right] - \mathcal{J}\mu_0 p' D S_1 X$$

$$= -\mathcal{J}\mu_0 n m_i\omega(\omega - \omega_i^*)\frac{X}{r^2B^2}S_0 G_1$$

$$+\frac{1}{n^2}\frac{\partial}{\partial\psi}\left[\mu_0 n_0 m_i \omega(\omega-\omega_i^*)\,\mathcal{J}r^2 S_0 G_1\left(\frac{\partial X}{\partial\psi}+\frac{\mu_0 p'}{B^2}S_1 X\right)\right]$$

$$-\frac{1}{n^2}\frac{\mu_0 p'}{B^2}\mu_0 n_0 m_i \omega(\omega-\omega_i^*)\,\mathcal{J}r^2 S_0 G_1\left(\frac{\partial X}{\partial\psi}+\frac{\mu_0 p'}{B^2}S_1 X\right) \quad . \quad (6.6)$$

This is a partial differential equation governing high n modes. It contains terms to first order in $1/n^2$. The boundary condition is $X = 0$ on conducting surfaces. In the limit $\rho_i \to 0$, $\frac{\omega_i^*}{\omega} \to 0$ Eq. (6.6) is almost term for term identical with the high n MHD equation, Eq. (3.14). The only difference is Eq. (6.6) lacks the ideal fluid adiabatic term. Thus, in the fluid limit Eq. (6.6) reduces to a high n incompressible hydromagnetic equation.

It is instructive to examine Eq. (6.6) locally. Letting $\frac{\partial}{\partial\psi} \to -i\frac{k_\psi}{rB}$, $\frac{\partial}{\partial X} \to -i\mathcal{J}Bk_X$, $\frac{n}{r} \to k_\theta$ and neglecting terms involving $\frac{\mu_0 p'}{B^2}$ (which are very small) we can write Eq. (6.6) in the form

$$\omega(\omega-\omega_i^*)S_0 G_1 + \frac{2\omega_i^*\omega_D S_1}{\rho_i^2 k_\perp^2} - k_X^2 v_A^2 = 0 \quad , \quad (6.7)$$

where $k_\perp^2 = k_\psi^2 + k_\theta^2$, $\rho_i = \frac{T_i}{m}\frac{1}{\Omega_i^2}$ and $v_A^2 = \frac{B^2}{\mu_0 n_0 m_i}$ is the Alfven velocity. The frequency of the mode is mainly determined by the combination $\omega(\omega-\omega_i^*)$ in the first term. The frequency dependence appearing elsewhere in the terms S_0 and S_1 is of higher order in Larmor radius. Eq. (6.7) is essentially a quadratic equation in ω if the frequency the dependence of S_0 and S_1 is taken to be small.

Solving Eq. (6.7) for ω one finds that for a marginally stable or unstable mode the real part of the frequency is given by $\mathrm{Re}(\omega) = \omega_i^*/2$. There is also a stabilizing component proportional to $\omega_i^{*2}/4$. For $k_X = 0$, $\omega = \omega_i^*/2$ and $\rho_i k_\theta < 1$ in Eq. (6.7) the terms $S_0 G_1$ multiplying the first term and S_1 multiplying the second term are slightly destabilizing for $\omega_i^*\omega_D$ positive. In real geometry, where ω_D changes sign along a field line the net effect of these terms is hard to determine but is smaller then the effect of ω^* in the first term. Neglecting the higher order finite Larmor radius effects (setting $G_0 = G_1 = 1$) and taking $k_X = 0$ reduces Eq. (6.7) to the familiar interchange dispersion relation including the lowest order FLR effects on the ion $\vec{E} \times \vec{B}$ drift[14].

There are five scalar parameters in Eq. (6.6) n, ω, n_0, τ and T_i. The ion temperature does not occur explicitly but is present in p, p' and a_T. The ratio of temperatures, τ, appears in the pressure and is usually just specified. One of the remaining parameters can be designated the eigenvalue in Eq. (6.6). This still leaves three parameters in this equation, hence, three additional constraints are needed. We are interested in calculating the beta limit of a device, so we want to find the boundary between stable plasmas and unstable ones. One way of finding points on this boundary is to solve Eq. (6.6) with an equilibrium of a specified β and look for the marginally stable mode with the largest ion temperature. This gives three additional constraints and the problem is fully determined. This is the approach that will be followed here.

B. Approximate Solution

In this section an approximate solution to Eq. (6.6) is formulated. The method is similar to that used in Chapter 3 for solving the high n MHD equation. The method involves a perturbation expansion about the $n = \infty$ solution. The difference is here the limit $n = \infty$ will be taken holding $a_T^2 = \rho_i n/r$ and ω_i^* fixed. The alternate method of Spies[42] who solves the high n equations by expanding in terms of a complete set of eigenfunctions along a field line could also be applied here. However, using the method presented below, it is easier to obtain explicit solutions to the problem. In operator notation Eq. (6.6) can be written in the form,

$$L_0 X + \frac{1}{n^2} L_1 X - \mathcal{J}\mu_0 p' D S_1 X$$

$$= -\mu_0 n_0 m_i \omega (\omega - \omega_i^*) M_0 X - \frac{1}{n^2} M_1 X \quad , \tag{6.8}$$

where $L_0 X = \frac{\partial}{\partial \chi}\left(\frac{1}{\mathcal{J} r^2 B^2} \frac{\partial X}{\partial \chi}\right)$,

$$L_1 X = -\frac{\partial}{\partial \psi}\frac{\partial}{\partial \chi}\left[\frac{r^2}{\mathcal{J}} \frac{\partial}{\partial \chi}\left(\frac{\partial X}{\partial \psi} + \frac{\mu_0 p'}{B^2} S_1 X\right)\right]$$

$$+ \frac{\mu_0 p'}{B^2}\frac{\partial}{\partial \chi}\left[\frac{r^2}{\mathcal{J}} \frac{\partial}{\partial \chi}\left(\frac{\partial X}{\partial \psi} + \frac{\mu_0 p'}{B^2} S_1 X\right)\right] \quad ,$$

$$M_0 X = \mathcal{J} \frac{X}{R^2 B^2} S_0 G_1 \quad ,$$

$$M_1 X = -\frac{\partial}{\partial \psi}\left[\mu_0 n_0 m_i \omega (\omega - \omega_i^*) \mathcal{J} r^2 S_0 G_1 \left(\frac{\partial X}{\partial \psi} + \frac{\mu_0 p'}{B^2} S_1 X\right)\right]$$

$$+ \frac{\mu_0 p'}{B^2} \mu_0 n_0 m_i \omega (\omega - \omega_i^*) \mathcal{J} r^2 S_0 G_1 \left(\frac{\partial X}{\partial \psi} + \frac{\mu_0 p'}{B^2} S_1 X\right) \quad .$$

If we treat $1/n^2$ as the perturbing parameter in Eq. (6.8) the lowest order equation is,

$$L_0 X_0 - \mathcal{J}\mu_0 p' D S_1 X_0 = -\omega_0^2 M_0 X_0 \quad . \tag{6.9}$$

Eq. (6.9) is a Sturm-Liouville type of equation and is solved using periodic boundary conditions. In a device with up-down symmetry solutions to Eq. (6.9) have either even or odd symmetry with respect to reflection on the midplane. The quantities n, ω, n_0, τ and T_i must be specifed to determine $S_0 G_1$ and S_1. Either p' or ω_0^2 can be specified in Eq. (6.9) with the other solved for as an eigenvalue. Setting ω_0^2 to zero and solving for p', one finds the finite Larmor radius equivalent of the critical pressure gradient, p'_{crit}. If p' is less then p'_{crit} on all the flux surfaces, then ω_0^2 is always positive and instability cannot occur for the values of n, ω, n_0 and T_i specified. If p' is greater then p'_{crit} on any of the flux surfaces, ω_0^2 is negative on those flux surfaces and it is possible for an instability to occcur for certain values of n, ω, n_0 and T_i.

The solution X_0 of Eq. (6.9) is defined only up to an arbitrary multiplicative constant. Let us write X_0 in terms of two functions $X_0 = R_0(\psi) U_0(\psi, \chi)$ where $U_0(\psi, \chi)$ is a solution to Eq. (6.9) and in

addition satisfies a normalizing condition which fully determines $U_0(\psi,\chi)$. The normalizing condition is completely arbitrary. The final solution for X_0 does not depend on it. An equation for $R_0(\psi)$ is found by going to the next highest order in $1/n^2$. To first order in $1/n^2$, Eq. (6.8) becomes

$$L_0 X_1 + \frac{1}{n^2} L_1 R_0(\psi) U_0 - \mathcal{J}\mu_0 p_1' DS_1 X_1 - \mathcal{J}\mu_0 p_1' DS_1 R_0(\psi) U_0$$

$$= -\omega_0^2 M_0 X_1 - \omega_1^2 M_0 R_0(\psi) U_0 - \frac{1}{n^2} M_1 R_0(\psi) U_0 \quad . \tag{6.10}$$

where $p_1' = p' - p_0'$, $\omega_1^2 = \mu_0 n_0 m_i \omega(\omega - \omega_i^*) - \omega_0^2$. p' is the equilibrium pressure gradient, and $R_0(\psi)$ is the ψ correction to the zeroth order solution. For this perturbation expansion to be valid it is necessary to choose p_0' so that both p_1' and ω_1^2 are small. Generally a value of p_0' about half way between the critical pressure gradient of Eq. (6.9) and the equilibrium pressure gradient is chosen. Since L_0 is self-adjoint, multiplying Eq. (6.10) by U_0 and integrating over χ eliminates terms involving X_1 and gives an equation for for $R_0(\psi)$:

$$\frac{1}{n^2}\oint U_0 L_1 R_0(\psi) U_0 \, d\chi - \mu_0 p_1' \oint \mathcal{J} DS_1 R_0(\psi) U_0^2 \, d\chi$$

$$= -\omega_1^2 \oint U_0 M_0 R_0(\psi) U_0 \, d\chi - \frac{1}{n^2}\oint U_0 M_1 R_0(\psi) U_0 \, d\chi \quad . \tag{6.11}$$

The nature of this equation is more apparent when the individual terms are written out explicitly using Eqs. (6.8),

$$\oint U_0 L_1 R_0(\psi) U_0 \, d\chi = \frac{d}{d\psi}\left[\oint \frac{\partial U_0}{\partial \chi} \frac{r^2}{\mathcal{J}} \frac{\partial U_0}{\partial \chi} \, d\chi \, \frac{dR_0(\psi)}{d\psi}\right]$$

$$+ R_0(\psi)\left\{\frac{\partial}{\partial\psi}\left[\oint \frac{\partial U_0}{\partial \chi} \frac{r^2}{\mathcal{J}} \frac{\partial}{\partial \chi}\left(\frac{\partial U_0}{\partial \psi} + \frac{\mu_0 p'}{B^2} S_1 U_0\right) d\chi\right]\right.$$

$$\left. - \oint \frac{\partial}{\partial \chi}\left(\frac{\partial U_0}{\partial \psi} + \frac{\mu_0 p'}{B^2} S_1 U_0\right) \frac{r^2}{\mathcal{J}} \frac{\partial}{\partial \chi}\left(\frac{\partial U_0}{\partial \psi} + \frac{\mu_0 p'}{B^2} S_1 U_0\right) d\chi\right\} \quad , \tag{6.12.1}$$

$$\oint U_0 M_0 R_0(\psi) U_0 \, d\chi = R_0(\psi) \oint \mathcal{J} \frac{U_0^2}{r^2 B^2} S_0 G_1 \, d\chi \quad , \tag{6.12.2}$$

$$\oint U_0 M_1 R_0(\psi) U_0 \, d\chi$$

$$= -\frac{d}{d\psi}\left[\oint \mu_0 n_0 m_i \omega(\omega - \omega_i^*) \mathcal{J} r^2 S_0 G_1 U_0^2 \, d\chi \, \frac{dR_0(\psi)}{d\psi}\right]$$

$$+ R_0(\psi)\left\{\oint \mu_0 n_0 m_i \omega(\omega - \omega_i^*) \mathcal{J} r^2 S_0 G_1 \left(\frac{\partial U_0}{\partial \psi} + \frac{\mu_0 p'}{B^2} S_1 U_0\right)^2 d\chi\right.$$

$$\left. - \frac{d}{d\psi}\left[\oint \mu_0 n_0 m_i \omega(\omega - \omega_i^*) U_0 \mathcal{J} r^2 S_0 G_1 \left(\frac{\partial U_0}{\partial \psi} + \frac{\mu_0 p'}{B^2} S_1 U_0\right) d\chi\right]\right] \quad . \tag{6.12.3}$$

Since the notation by now is hopeless anyway let's at least make it convenient for the person who has to debug the computer code used to solve these equations. If we substituting Eqs. (6.12) into Eq. (6.11) the latter can be rewritten in the form,

$$\frac{d}{d\psi}\left\{[a_1 - \mu_0 n_0 m_i \omega(\omega - \omega_i^*) a_2] \frac{dR_0(\psi)}{d\psi}\right\} + [a_3 - a_4] R_0(\psi)$$

$$= n^2 \{[\omega_0^2 - \mu_0 n_0 m_i \omega (\omega - \omega_i^*)] a_0 + a_5\} R_0(\psi) \quad . \tag{6.13}$$

where a_0, a_1, a_2, a_3, a_4 and a_5 are functions of ψ defined as follows,

$$a_0 = \oint \mathcal{J} \frac{U_0^2}{r^2 B^2} S_0 G_1 \, d\chi \quad , \tag{6.14.1}$$

$$a_1 = \oint \frac{\partial U_0}{\partial \psi} \frac{r^2}{\mathcal{J}} \frac{\partial U_0}{\partial \chi} \, d\chi \quad , \tag{6.14.2}$$

$$a_2 = \oint \mathcal{J} r^2 S_0 G_1 \, U_0^2 \, d\chi \quad , \tag{6.14.3}$$

$$a_3 = \frac{d}{d\psi}\left[\oint \frac{\partial U_0}{\partial \chi} \frac{r^2}{\mathcal{J}} \frac{\partial}{\partial \chi}\left(\frac{\partial U_0}{\partial \psi} + \frac{\mu_0 p'}{B^2} S_1 U_0\right) d\chi\right]$$
$$- \oint \frac{\partial}{\partial \chi}\left(\frac{\partial U_0}{\partial \psi} + \frac{\mu_0 p'}{B^2} S_1 U_0\right) \frac{r^2}{\mathcal{J}} \frac{\partial}{\partial \chi}\left(\frac{\partial U_0}{\partial \psi} + \frac{\mu_0 p'}{B^2} S_1 U_0\right) d\chi \quad , \tag{6.14.4}$$

$$a_4 = \frac{d}{d\psi}\left[\mu_0 n_0 m_i \omega (\omega - \omega_i^*) \oint U_0 \mathcal{J} r^2 S_0 G_1 \left(\frac{\partial U_0}{\partial \psi} + \frac{\mu_0 p'}{B^2} S_1 U_0\right) d\chi\right]$$
$$- \mu_0 n_0 m_i \omega (\omega - \omega_i^*) \oint \mathcal{J} r^2 S_0 G_1 \left(\frac{\partial U_0}{\partial \psi} + \frac{\mu_0 p'}{B^2} S_1 U_0\right)^2 d\chi\Big] \quad , \tag{6.14.5}$$

$$a_5 = \mu_0 (p' - p\phi') \oint \mathcal{J} D S_1 \, U_0^2 \, d\chi \quad . \tag{6.14.6}$$

The Eq. (6.13) is a second order ordinary differential equation for

$R_0(\psi)$. The boundary conditions are that R_0 go to zero on conducting surfaces.

As was stated earlier, two additional constraints are needed to determine the solution to Eq. (6.6). To obtain these constraints, a variational principle is constructed using Eq. (6.13) by multiplying by $R_0(\psi)$ and integrating over ψ.

$$- \int [a_1 - \mu_0 n_0 m_i \omega (\omega - \omega_i^*) a_2] \left(\frac{dR_0(\psi)}{d\psi}\right)^2 d\psi$$
$$+ \int [a_3 - a_4] R_0^2(\psi) \, d\psi$$
$$- n^2 \int \{[\omega_0^2 - \mu_0 n_0 m_i \omega (\omega - \omega_i^*)] a_0 + a_5\} R_0^2(\psi) \, d\psi = 0 \quad . \tag{6.15}$$

This equation is quadratic in ω, i.e., it is of the form $a\omega^2 + b\omega + c = 0$. The requirement that the solution be marginally stable means that the discriminant, $b^2 - 4ac$, of Eq. (6.15) must be equal to zero. This condition is satisfied by,

$$\left[\int \mu_0 n_0 m_i \omega_i^* \, a_2 \left(\frac{dR_0(\psi)}{d\psi}\right)^2 d\psi \right.$$
$$\left. + n^2 \int \mu_0 n_0 m_i \omega_i^* \, a_0 \, R_0^2(\psi) \, d\psi\right]^2$$
$$= 4\left[\int \mu_0 n_0 m_i \, a_2 \left(\frac{dR_0(\psi)}{d\psi}\right)^2 d\psi + n^2 \int \mu_0 n_0 m_i \, a_0 \, R_0^2(\psi) \, d\psi\right]$$
$$\times\left[- \int a_1 \left(\frac{dR_0(\psi)}{d\psi}\right)^2 d\psi + \int [a_3 - a_4] R_0^2(\psi) \, d\psi \right.$$
$$\left. - n^2 \int [\omega_0^2 a_0 + a_5] R_0^2(\psi) \, d\psi\right] \quad . \tag{6.16}$$

Using the relations $n0 = \frac{p}{T_i}\frac{1}{1+\tau}$ and $\omega_i^* = -\frac{nT_i}{e}\frac{p'}{p}$ Eq. (6.16) gives an equation for the ion temperature in terms of n^2.

$$\frac{T_i}{e^2}\frac{1}{1+\tau} = \frac{4[c4 + n^2 c2][c0 - n^2 c1]}{n^2[c5 + c3]^2} \quad , \tag{6.17}$$

where

$$c0 = -\int a_1 \left(\frac{dR_0(\psi)}{d\psi}\right)^2 d\psi + \int [a_3 - a_4] R_0^2(\psi)\, d\psi \quad , \tag{6.18.1}$$

$$c1 = \int [\omega_0^2 a_0 + a_5] R_0^2(\psi)\, d\psi \quad , \tag{6.18.2}$$

$$c2 = \int \mu_0 m_i p\, a_0 R_0^2(\psi)\, d\psi \quad , \tag{6.18.3}$$

$$c3 = \int \mu_0 m_i p'\, a_0 R_0^2(\psi)\, d\psi \quad , \tag{6.18.4}$$

$$c4 = \int \mu_0 m_i p\, a_2 \left(\frac{dR_0(\psi)}{d\psi}\right)^2 d\psi \quad , \tag{6.18.5}$$

$$c5 = \int \mu_0 m_i p'\, a_2 \left(\frac{dR_0(\psi)}{d\psi}\right)^2 d\psi \quad . \tag{6.18.6}$$

The second requirement is that the solution be a maximum, i.e. the marginally stable solution with the largest temperature. To find the extremum the derivative of the temperature with respect to n^2 in Eq. (6.17) is taken and set equal to zero. This gives the following polynomial whose roots determine the toroidal mode number corresponding to the largest temperature,

$$p^3 \times c0 \times c4 \times c5 + p^2 \times 3 \times c0 \times c3 \times c4 + p \times (2 \times c0 \times c2 \times c3 + c1 \times c2 \times c5 - 2 \times c1 \times c3 \times c4) - c1 \times c2 \times c3 = 0 \quad . \tag{6.19}$$

where $p = 1/n^2$. For betas just above the MHD critical beta the modes are localized in ψ, the coefficients c4 and c5 are small and the n^2 corresponding to the largest temperature is approximately $n^2 = 2\, c0/c1$. By numerically evaluating the coefficients it can be shown that there is at most only one positive root to Eq. (6.19) and this root is a maximum.

At marginal stability the mode has the real part of the frequency given by,

$$\omega = -\frac{n}{2}\frac{T_i}{e}\frac{c5 + n^2\, c3}{c4 + n^2\, c2} \tag{6.20}$$

$$= -\frac{n}{2}\frac{T_i}{e}\frac{\int p'\, a_2 \left(\frac{dR_0(\psi)}{d\psi}\right)^2 d\psi - n^2 \int p'\, a_0 R_0^2(\psi)\, d\psi}{\int p\, a_2 \left(\frac{dR_0(\psi)}{d\psi}\right)^2 d\psi - n^2 \int p\, a_0 R_0^2(\psi)\, d\psi} \quad .$$

In the case where the mode is highly localized in ψ it can be seen from Eq. (6.20) that $\omega = \frac{1}{2}\omega_i^*$ where ω_i^* is the local diamagnetic frequency, $\omega_i^* = -\frac{nT_i}{e}\frac{p'}{p}$.

The lowest order solution to the problem consists of solving five simultaneous equations: Eq. (6.9), an ordinary differential equation in χ which must be solved on each flux surface and determines the structure of the mode along the field lines; Eq. (6.13) which is an ordinary differential equation determining the structure of the mode perpendicular the field lines; Eq. (6.19) the equation determining the toroidal mode number; Eq. (6.17) for the ion temperature and

Eq. (6.20) for the frequency of the mode. In theory Eq. (6.19) is not needed. If the remaining equations are satisfied self-consistently, n is determined uniquely. In practice the equations are solved numerically using an iteration scheme and Eq. (6.19) is a necessary intermediate step for the procedure to converge to the desired solution.

C. Numerical Results

The scheme used here is to calculate the maximum temperature of a marginally stable mode using an equilibrium of a specified beta. The equilibria were calculated using the MHD equilibrium code described in Chapter 2 and equilibrium quantities were mapped out in flux coordinates for subsequent use in the stability calculation. By calculating the stability of a sequence of equilibria with different beta, the boundary between stable and unstable regions is mapped out.

The even mode is more unstable then the odd mode when finite Larmor radius effects are included. With finite ion Larmor radius the mode is more spread out in the ψ direction. Over the extent of the mode the average critical pressure gradient for the even mode is almost always smaller then the critical pressure gradient of the odd mode. The only exception occurs when the adiabatic terms are retained in the analysis where in the limit of $\rho_i \to 0$ the odd mode might be more unstable then the even mode for certain pressure profiles. This

situation only occurs for betas slightly above the MHD critical beta. Only the even mode will be considered here.

Eq. (6.9), Eq. (6.13), Eq. (6.19), Eq. (6.19) and Eq. (6.20) are solved by a procedure consisting of two iterations, an inner iteration nested inside an outer iteration. The outer iteration starts with a guess at the values of T_i, ω and n. With these quantities and the equilibrium quantities ω_i^*, ρ_i and n_0 can be computed and hence, are known as functions of ψ and χ. Eq. (6.9) is solved on a number of equally spaced flux surfaces between the two conducting boundaries or whatever flux surfaces are designated the boundaries of the mode. The lowest order pressure gradient, p' is chosen with the strategy of keeping p' and ω_0^2 small. Here $p' = (p'_{crit} + p')/2$ was used where p'_{crit} is the critical pressure gradient found by setting ω_0^2 to zero in Eq. (6.9) and solving for p' as the eigenvalue. With this choice of p', Eq. (6.9) is solved for U_0 and ω_0^2. The quantities a_0, a_1, a_2, a_3, a_4 and a_5 are calculated on each flux surface and so are known as functions of ψ.

It turns out U_0 and ω_0 have only a relatively weak dependence on T_i, ω and n. This is because the finite Larmor radius effects of the functions $S_0 G_1$ and S_1 tend to cancel each other. In the inner iteration Eq. (6.13) and Eq. (6.19), Eq. (6.19) and Eq. (6.20) are solved self consistently keeping the functions a_0, ... etc., fixed. First, Eq. (6.13) is solved for $R_0(\psi)$ and the eigenvalue n. The toroidal mode number, n, is then recalculated using Eq. (6.19). With this value of n, Eq. (6.19) is evaluated for T_i and Eq. (6.20) for ω.

From these new values of T_i, ω and n the quantities ω_i^* and n_0 can be calculated and the inner iteration starts over. The inner iteration is tested for convergence by comparing the value of n found as the eigenvalue of Eq. (6.13) with the n corresponding to the largest T_i calculated from Eq. (6.19). If these two values agree to within a relative error of 10^{-4} the outer iteration is started over using the new values of T_i, ω and n. The outer iteration is tested for convergence by comparing two consecutive values of T_i. When the two values agree to within a relative error of 10^{-3}, the solution is assumed to have converged. Usually 15 inner iterations are needed and 5 outer iterations are needed to arrive at a solution.

For calculations using the Levitated Octupole configuration the mode was made to go to zero near the critical flux surface and the separatrix. This is a reasonable approximation since the critical flux surface lies close to the outside wall in this device. Actually the mode was made to go to zero slightly inside the critical flux surface because of a reoccurring problem with interchange modes. Initially one would think that interchange modes would be stablized with the addition of finite ion Larmor radius due to ω_i^*[14]. This is not true for the equilibrium used in this calculation because the finite ion Larmor radius causes the critical flux surface to move inside the MHD critical flux surface. The critical flux surface is defined as the point where the average good curvature is zero. The average curvature drift of the ions is not changed much with larger ρ_i (Remember for equal ion and electron temperature the average curvature

drift is the same for ions and electrons.) What is changed is the amount of charge separation that is allowed to build up since the ions average the perturbation over a Larmor radius and so see a smaller perturbation than the electrons. The ion Larmor radius is largest where the magnetic field is weakest which, in the case of the octupole, happens to be the good curvature region. Thus, the finite ion Larmor radius has the effect of lessening the stabilizing contribution due to the good curvature. This effect can be demonstrated by looking at $p\phi'_{crit}$, the FLR critical pressure gradient. In Fig. (6.1) are plotted the equilibrium pressure gradient, MHD critical pressure gradient and the FLR critical pressure gradient. Notice the FLR critical pressure gradient goes to zero before the equilibrium pressure gradient and the MHD critical pressure gradient out near ψ_{crit}. The flux surfaces outside this point are interchange unstable. There is some conflicting experimental evidence for this effect. The pressure profile is observed to be much more sharply peaked on the separatrix for plasmas with large ion Larmor radius. However, this might also be due to obstructions close to the separatrix limiting the plasma.

The mode was chosen to go to zero at the separatrix. The reason is that in the private flux region the field lines have totally good curvature. Inside the separatrix the critical pressure gradient jumps by a factor of ten. Thus, the ψ extent of the mode would be expected to die off rapidly inside the separatrix.

The stability criterion for the Levitated Octupole is shown in Fig. (6.2). In this calculation the ions were assumed to be protons. Instead of plotting β vs T_i, the marginally stable mode with the largest ion temperature, it is better to plot β vs ρ_i, where $\rho_i = \sqrt{\frac{T_i}{m}} \frac{1}{\Omega_i}$, because β vs ρ_i is independent of the magnitude of the equilibrium magnetic field. In Fig. (6.2) β and ρ_i are defined locally on the separatrix in the bridge region. The bridge region here is defined as the region between the outside ring and the outer wall. This point is chosen for ease in comparison with experimental results. This plot shows that even for a moderate average ion Larmor radius there is a substantial increase in the critical beta above the MHD result of 4.3%. Plotting β vs ρ_i depends on the shape of the equilibrium pressure profile. The plot of β vs ρ_i/L_n, Fig. (6.3), is independent of the detailed shape of the pressure profile. The quantity L_n is the density scale length defined here as the distance between the separatrix and a point halfway down the pressure profile in the bridge region.

A summary of the pertinent results of the stability runs for the Levitated Octupole can be found in Appendix E. For the calculations presented here, the equilibria were self-consistent for values of beta ranging between 5% and 17%. For betas of 18% to 20%, the MHD equilibrium for β = 17% was used and the pressure was scaled appropriately. This definition was again chosen for easy comparison with experimental results. For the pressure profile used in this

calculation L_n is 1.4 cm. for a β of 14% and slightly wider for smaller betas.

The X_0 eigenfunctions for the marginally stable mode with the largest ion temperature for betas of 4.5%, 5.0% and 10.0% are shown in Figs. (6.4), (6.5) and (6.6), respectively. The quantity X is proportional to $rE_{1\theta}$. The term $E_{1\theta}$ is the largest component of the electric field for this mode. Typical of the ballooning mode the X_0 eigenfunction is peaked in the outside bad curvature region in the area of the steepest pressure gradient. This sequence of figures shows that as ρ_i is raised the ψ extent of the mode initally spreads out rapidly and then doesn't change much.

A given β and ρ_i uniquely define the ion density, n_i. This gives another way of plotting the stability criteria. Fig. (6.7) is a plot of the ion density vs β. For a given beta the ballooning mode sets a density limit on the machine that does not depends on the strength of the magnetic field or the temperature of the plasma. In the Levitated Octupole as beta gets larger the critical density levels off at slightly less then 10^{13} particles/cm^3. Below 4.3% there is no critical density imposed by the ballooning mode.

By far the largest finite Larmor radius effect stabilizing the plasma is due to ω_i^*. This is the same effect that stabilizes the interchange mode in the analysis of Rosenbluth, Krall and Rostoker[14]. A good way to illustrate this is to calculate the stablility criteria keeping terms that depend on ω_i^* but letting $\rho_i \to 0$ in the remaining terms. The result of such a calculation is shown in

Fig. (6.8). The remaining FLR terms have the net effect of destabilizing the plasma but only by a small amount.

In summary, using a high n expansion a method was formulated for solving the ballooning mode problem including finite Larmor radius effects in multipoles. The largest stabilizing effect is due to the difference in the $\vec{E} \times \vec{B}$ drift of the ions and the electrons, the same effect that stabilizes interchange modes. This has a dramatic effect on stabilizing the ballooning mode and increasing the beta limit.

Fig. (6.1) MHD and FLR Critical Pressure Gradient

p' vs ψ for $\beta = 6$ % for the equilibrium presssure gradient, MHD critical pressure gradient and FLR critical pressure gradient. The FLR critical pressure gradient was calculated using quantities of the marginally stable mode with the maximum pressure gradient, $n_{0_i} = 453$, $T_i = 24.5$ eV, and $\omega = 4.65 \times 10^5$ sec^{-1}. This plot shows the FLR term S_1 has a slight destabilizing effect and ψ_{crit} moves inward meaning the equilibrium is interchange unstable at the edge.

$\psi_{crit} = 0.812838$, $\psi_{sep} = 0.521315$.

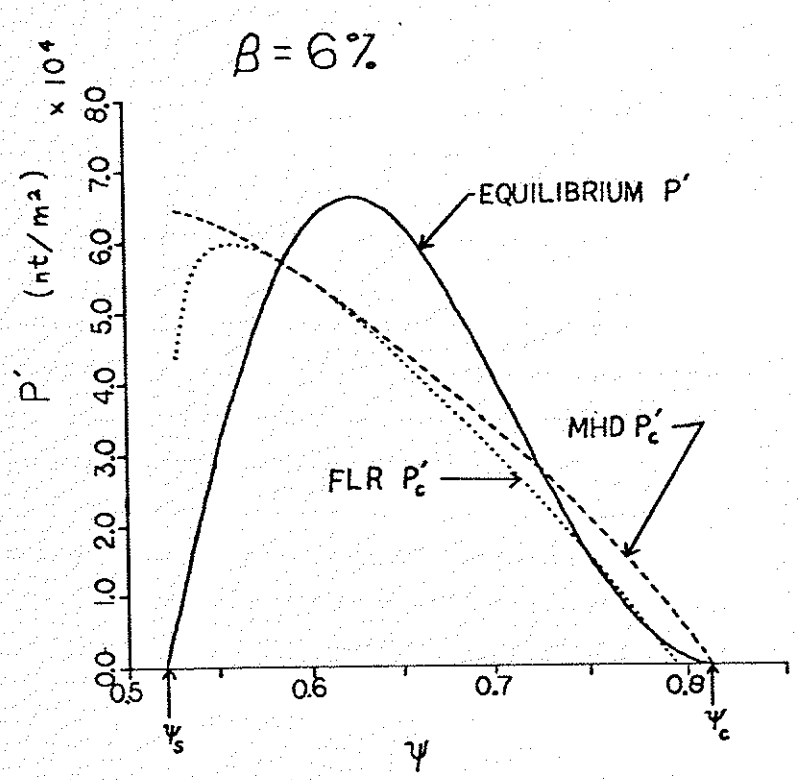

Fig. (6.1)

Fig. (6.2) Stability Criteria for the Levitated Octupole, β vs ρ_i

Stability Criteria for the Levitated Octupole plotted as β vs ρ_i where $\rho_i = \sqrt{\frac{T_i}{m_i}} \frac{1}{\Omega_i}$. Both β and ρ_i are evaluated on the separatrix in the bridge region. The plot shows that even a small increase in the ion Larmor radius can substantially increase the beta limit of the octupole.

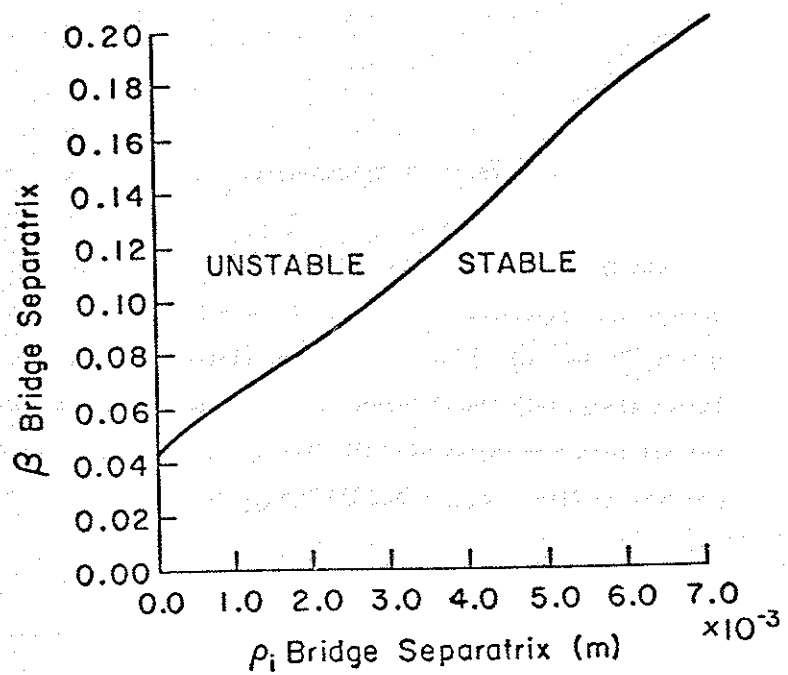

Fig. (6.2)

Fig. (6.3) Stability Criteria for the Levitated Octupole, β vs ρ_i/L_n

Stability criteria for the Levitated Octupole plotted as β vs ρ_i/L_n where β, ρ_i and L_n are evaluated on the separatrix in the bridge region. The density scale length is defined here as the distance from the separatrix to a point half way down the pressure profile on the unstable side. This plot is relatively invariant to changes in the shape of the pressure profile. For comparing theory with experiment this plot should be used.

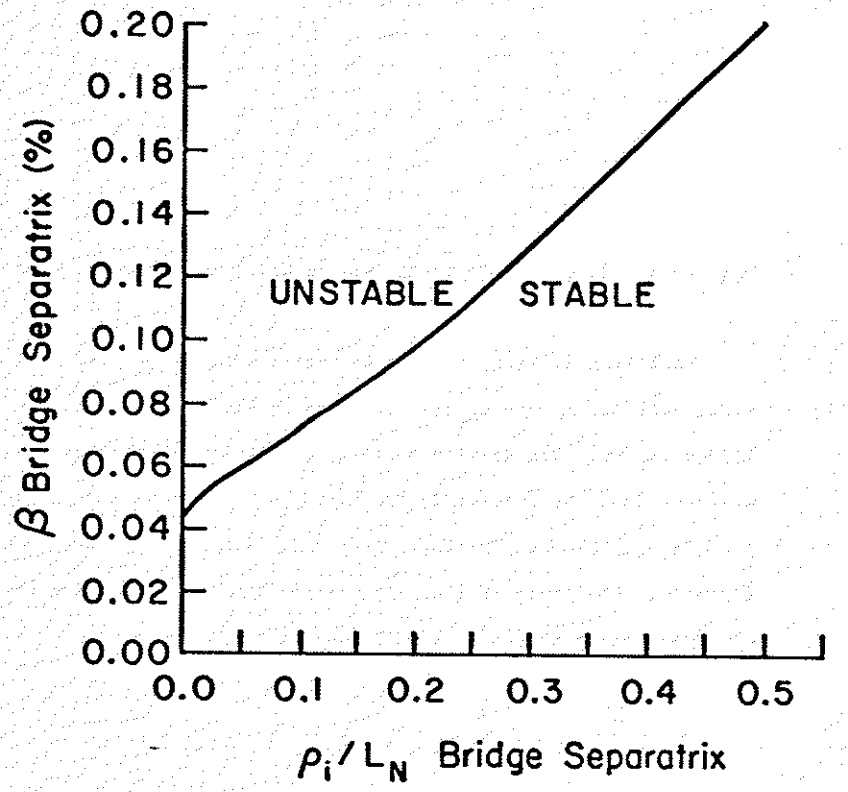

Fig. (6.3)

Fig. (6.4) X_0 Eigenfunction for β = 4.5 %

The X_0 eigenfunction for the marginally stable mode with the largest ion temperature for β = 4.5 %. n = 3428, $n_0 = 3.0 \times 10^{23}$ /m^3, $\rho_i = 4.4 \times 10^{-5}$ m, plotted vs ψ and relative length along field line. Typical of a ballooning mode, X_0 peaks in the bad curvature region near the flux surface with the steepest pressure gradient. $\psi_{sep} = 0.530687$, $\psi_{crit} = 0.823312$.

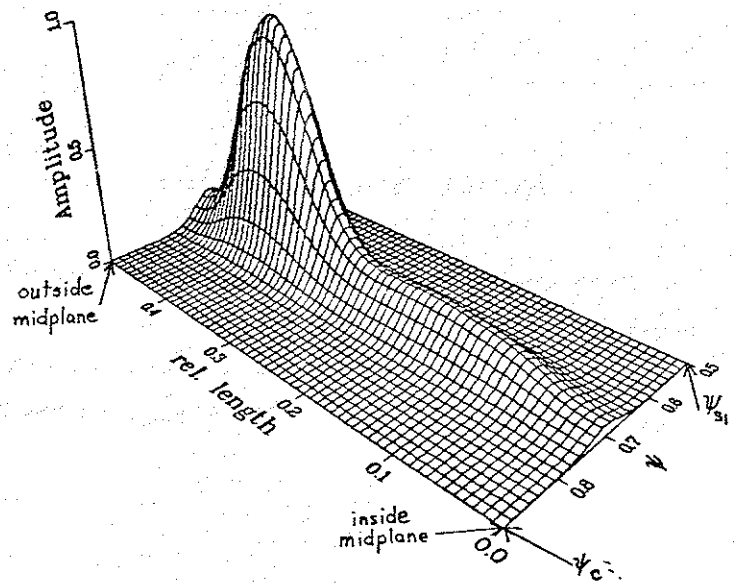

Fig. (6.4)

Fig. (6.5) X_0 Eigenfunction for β = 5.0 %

The X_0 eigenfunction for the marginally stable mode with the largest ion temperature for β = 5.0 %. n = 942, $n_0 = 1.4 \times 10^{22}$ /m^3, $\rho_i = 2.2 \times 10^{-4}$ m, plotted vs ψ and relative length along field lines. As the toroidal mode number decreases the mode has a longer ψ wavelength. $\psi_{sep} = 0.527545$, $\psi_{crit} = 0.819758$.

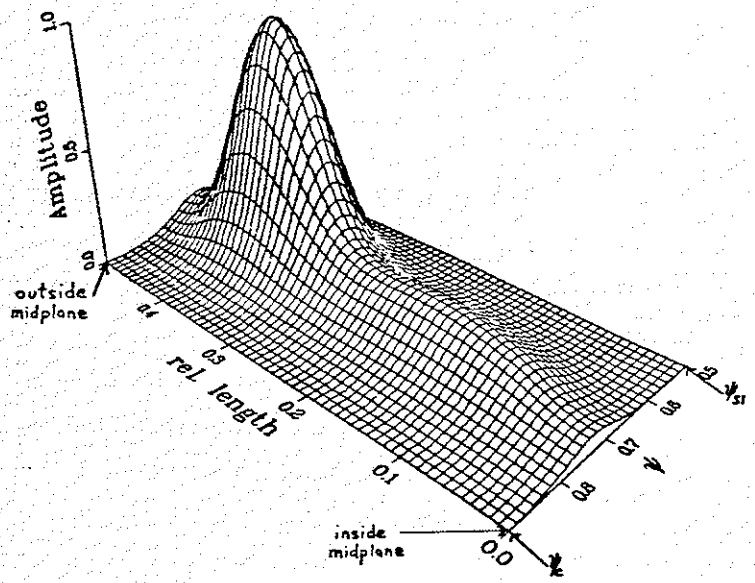

Fig. (6.5)

Fig. (6.6) X_0 Eigenfunction for β = 10.0 %

The X_0 eigenfunction for the marginally stable mode with the largest ion temperature for β = 10.0 %. n = 236, $n_0 = 1.5 \times 10^{20}$ /m^3, $\rho_i = 2.9 \times 10^{-5}$ m, plotted versus ψ and relative length along field lines. $\psi_{sep} = 0.496626$, $\psi_{crit} = 0.784459$.

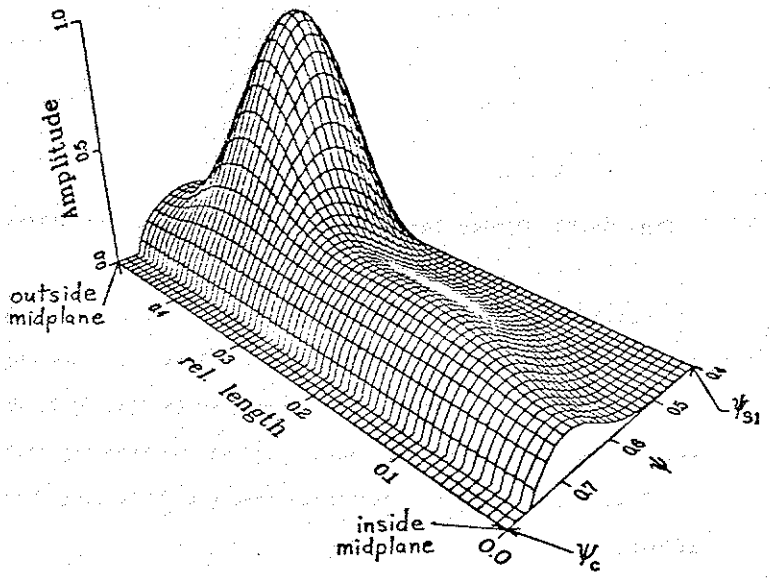

Fig. (6.6)

Fig. (6.7) Stability Criteria for the Levitated Octupole, $n_0 i$ vs β

Stability Criteria for the Levitated Octupole plotted as $n_0 i$ vs β. The quantity $n_0 i$ is the peak ion density and β is the beta defined locally on the separatrix in the bridge region. This plot shows above β = 4.33 % for a given β there is a critical density above which the octupole is ballooning mode unstable.

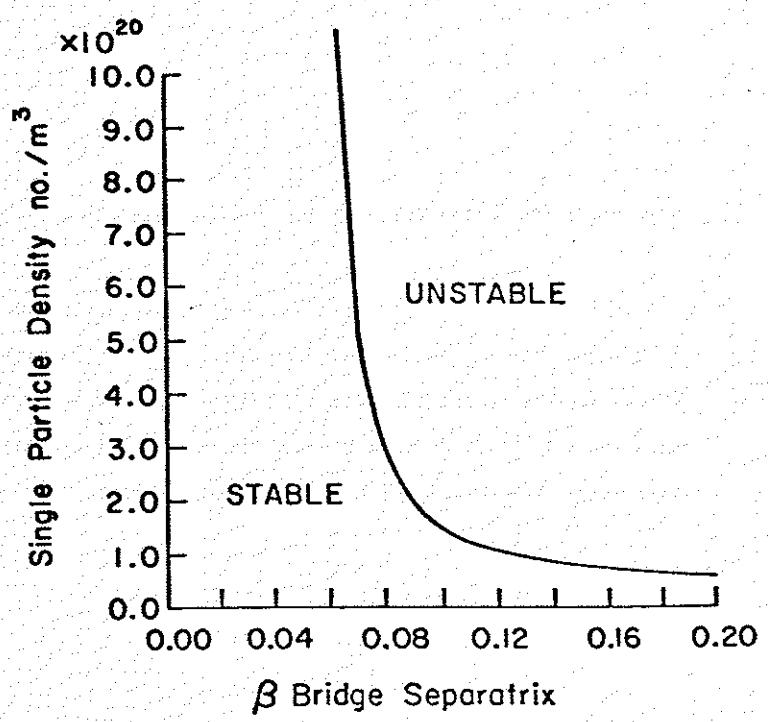

Fig. (6.7)

Fig. (6.8) Finite Larmor Radius Effects on the Stability Criteria

Stability criteria for the Levitated Octupole calculated keeping terms that depend on ω_i^* but letting $\rho_i \to 0$ in the remaining terms compared to the stability criteria plotted in Fig. (6.2) where all terms were kept. This plot shows the main stabilizing effect is due to ω_i^* with the remaining FLR terms having a small destabilizing effect.

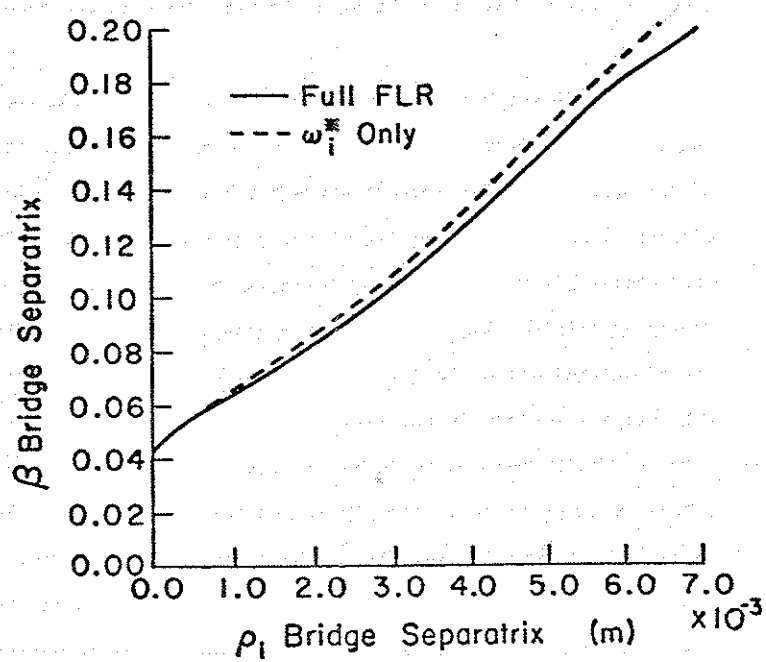

Fig. (6.8)

CHAPTER 7

Conclusions

A. Summary of Results

Let's summarize the ballooning mode and beta limit calculation for the Levitated Octupole. In Chapter 2 a procedure for calculating MHD equilibrium in multipoles was discussed. A computer code using this procedure was developed to calculate the MHD equilibrium of a wide variety of multipole configurations. For the Levitated Octupole configuration it was found that there are two main effects of high beta. As the beta increases the plasma pushes flux out from the center of the plasma thereby increasing the minimum average B well. This has a stabilizing effect on the ballooning instability. However, another opposing effect occurs. As beta is increased the distance, measured in flux, between the separatrix and the critical flux surface shortens. This steepens the pressure gradient and has a destabilizing effect on the ballooning instability. The net result of these two effects is that high beta has a small destabilizing effect on the critical beta calculated from ideal MHD.

The ideal MHD stability was investigated in Chapter 3. The most unstable mode is the one with the smallest wavelength in the toroidal direction. This is the mode where the limit of the toroidal mode number goes to infinity, $n \to \infty$. This mode is the most unstable because it minimizes the stabilizing contribution that would result if

the field lines were bent in the toroidal direction. For $n \to \infty$ and marginal stability the mode is incompressible. In the limit $n \to \infty$ modes are localized to a flux surface. The radial extent of the mode is a delta function of the variable ψ. The most unstable mode generally occurs near the flux surface with the steepest pressure gradient. The most unstable mode is the even mode because it bends the field line in the ψ direction the least. The critical beta for the $n \to \infty$ mode in the Levitated Octupole is $\beta_c = 4.33\%$ where β_c is the local beta on the separatrix in the bridge region.

Also in Chapter 3 modes with high but not infinite toroidal mode number were considered. For an equilibrium beta greater than β_c there exists a critical mode number, n_c. Modes with toroidal mode number greater than n_c are unstable and modes with n less than n_c are stable. The radial extent of a high but not infinite n mode is no longer localized to a flux surface. For the case of the marginally stable mode the radial extent of the mode spreads rapidly with increasing beta and eventually the mode covers the entire region between the separatrix and the critical flux surface.

An attempt was made in Chapter 3 to approximate the effect of finite Larmor radius on the ballooning mode. It was assumed MHD modes get converted into drift type waves in a manner similar to flute modes. The ballooning mode was found to be stablized if $\omega_i^{*2} > -4\omega^2_{MHD}$ where ω_i^* is the diamagnetic drift frequency and ω^2_{MHD} is the MHD frequency of the mode. From this condition one can solve for the marginally stable mode with the largest value of ρ_i/rL_n. For a given

beta the critical value of ρ_i/rL_n is found to be $\left(\frac{\rho_i}{rL_n}\right)^2_c = \frac{32}{27}\frac{\rho_m\gamma^2}{n_c p}$ where γ is the growth rate of the most unstable MHD mode, $\gamma^2 = -\omega^2_{MHD\ min}$. For this value of ρ_i/rL_n the marginally stable mode has $n = \frac{3}{2} n_c$. For $\rho_i/L_n = 0.2$ in the Levitated Octupole where ρ_i is measured on the separatix in the bridge and L_n is the density scale length of the plasma in the bridge the beta limit is predicted to be about 8%.

Two different kinetic effects on the ballooning mode were considered. In Chapter 5 we looked at the Kruskal-Oberman stability of the multipole. The Kruskal-Oberman energy principle includes the effects of the parallel motion of the particles along field lines. This energy principle always predicts greater stability than the MHD energy principle. The Kruskal-Oberman energy principle is similar to the MHD energy principle except the ideal fluid adiabatic term in the MHD energy principle is replaced with a kinetic term. The new kinetic term is stabilizing and includes effects due to collisionless adiabatic compression of the plasma and the Fermi acceleration of the particles. In the Kruskal-Oberman analysis the $n \to \infty$ mode is still the most unstable mode. The critical beta of the Levitated Octupole for the even mode increases modestly to 4.70%. This represents a relative increase of 9% in the beta limit. The kinetic terms in the Kruskal-Oberman energy principle are proportional to beta so if the beta limit is increased by some other means the increase in the beta limit due to the Kruskal-Oberman term is proportionally greater. For $\beta = 4.70\%$ the odd mode is slightly unstable. The kinetic terms in the

Kruskal-Oberman equations help stablize only even modes. Hence, for Kruskal-Oberman stability the odd mode is the most unstable mode in the Levitated Octupole.

Another kinetic effect, finite ion Larmor radius, was considered in Chapter 6. In this analysis the effects of the parallel particle dynamics were neglected. The derivation of the high n equations governing low frequency modes followed along lines similar to that of the high n MHD equations. The largest finite Larmor radius effect is due to the presence of ω_i^* in the equations. This term appears from a discrepancy between the $\vec{E} \times \vec{B}$ drift of the ions and electrons. This discrepancy is due to the difference in size of the ion and electron Larmor radius. The effect of ω_i^* on the MHD mode is similar to the finite Larmor radius stabilization of the flute mode[14] but here an electromagnetic drift type mode is excited instead of an electrostatic drift type mode. The increase in the beta limit due to ω_i^* is large. In the Levitated Octupole for an ρ_i/L_n of 0.20 in the bridge region the beta limit increases to about 10%.

A given β and ρ_i uniquely define an ion density. This means for a given beta the ballooning mode sets a density limit on the machine. This density limit depends only on β and ρ_i and not specifically on the magnetic field strength or the temperature of the plasma. In the Levitated Octupole as the beta gets large the critical density levels off at about 8.0×10^{13} particles/cm^3.

Another effect of finite Larmor radius is to move the critical flux surface in closer to the separatrix. This means that a plasma with large ion Larmor radius has a narrower, more sharply peaked, pressure profile then a plasma with small Larmor radius.

B. Final Comments

In this thesis kinetic effects on the linear stability of the ballooning mode were considered. However, the kinetic equations that were derived for this study are fairly general and can be used to study other low frequency modes as well. For calculating the stability criteria only one type of unstable mode was considered, the ballooning mode. One should keep in mind, other types of modes might possibly occur before the beta limit, that was calculated here, is reached. Because of the complexity of the low frequency kinetic equations there is the potential for other types of unstable modes.

There are many different questions concerning ballooning modes that would be interesting to study if time permitted. Drift and bounce resonances were not considered in the calculations here. The spectrum of bounce frequencies in the multipole is fairly broad so one would expect to find some resonant effects. Another thing that was not done here but might be interesting is to consider a multispecies plasma. Fusion reactors are expected to have at least a small amount of some heavier ion species. A question that should be addressed is

whether a minority species with a large Larmor radius can significantly stabilize the ballooning mode.

The multipole configuration has been suggested as a possible advanced fuel fusion reactor. One interesting application of the computer codes developed for studying the Levitated Octupole would be to optimize the multipole design to achieve a higher beta limit. It is not inconceivable that ideal MHD critical betas of up to 10% in the bridge region could be achieved for the octupole configuration.

For studying the ballooning mode the kinetic equations were expanded in high n. For the ballooning mode the high n approximation is usually pretty good. In the case of the Levitated Octupole one runs into problems of the quantity ρ_i/L_n not being small before the high n approximation becomes questionable. This leaves the topic low n, low frequency modes in the multipole unaddressed. Whether or not low n modes are important needs further study.

In the analysis presented here the plasma is considered to be collisionless. A collisionless theory has relevance to fusion reactor plasmas. The plasma in a fusion reactor will be hot enough to be within the collisionless regime. However, most experimental plasmas are to some degree collisional. Analyses including the effect of a small collision frequency have been done elsewhere[25,26]. As far as the ballooning mode is concerned collisions only have an appreciable effect when the collision frequency becomes greater than or comparable to the MHD growth rate. Many experimental plasmas have a fairly large collision frequency particularly at high beta. A theory is needed to

treat these situations. Also in the analysis presented here the Larmor radius is considered small and the quantity ρ_i/L_n is used as expansion parameter. Situations occur frequently in plasma devices such as mirrors and multipoles where ρ_i/L_n is not small. In the multipole ρ_i/L_n can not be considered small near the field null and for large betas. Fortunate for our analysis ρ_i/L_n is smallest in the bridge region where the ballooning mode is localized. For the Levitated Octupole values of ρ_i/L_n up to 0.5 are calculated for the stability criterion. This is admittedly stretching things a bit. However, for lack af a better theory the calculation was extended into the high beta region so that the experimentalist would have something to compare their data with. Since the beta limit of high beta plasma devices is important a theory applicable to high ρ_i/L_n is needed.

What really happens when a ballooning mode occurs is not known. The ballooning mode has yet to manifest itself experimentally. In this study only the linear stability of the ballooning mode was considered. Linear stability theory is an extremely valuable tool for finding out the types of waves and instabilities that can occur in a plasma. Linear stability theory is also fairly good at predicting the point where a mode becomes unstable. However, linear stability theory often fails to predict the long term evoultion of an unstable mode. For this the nonlinear stability of the mode must be calculated. A nonlinear kinetic theory of ballooning modes could answer many of the questions concerning what happens when a ballooning mode occurs.

APPENDIX A

Coordinates

Spatial Coordinates

The right handed coordinate system used throughout this paper consists of the terms ψ, χ, and θ. The term θ is the angle in the toroidal direction. The term ψ is related to the poloidal magnetic flux by $\psi = 2\pi\,\psi_p$ and is perpendicular to a field line in a constant θ plane. The term χ measures along field lines.

Volume element $dV = \mathcal{J}\, d\psi\, d\chi\, d\theta$, where $\mathcal{J}$ is the Jacobian.

$$\frac{1}{\mathcal{J}}\frac{\partial}{\partial\psi}(\mathcal{J}B^2) = -\mu_0\frac{\partial p}{\partial\psi} \quad . \tag{A.1}$$

Line element:

$$dL^2 = \frac{1}{r^2B^2}\,d\psi^2 + B^2\mathcal{J}^2\,d\chi^2 + r^2\,d\theta^2 \quad . \tag{A.2}$$

Divergence:

$$\nabla\cdot\vec{A} = \frac{1}{\mathcal{J}}\left[\frac{\partial}{\partial\psi}(\mathcal{J}rBA_\psi) + \frac{\partial}{\partial\chi}\left(\frac{1}{B}A_\chi\right) + \frac{1}{r}\frac{\partial}{\partial\theta}(\mathcal{J}A_\theta)\right] \quad . \tag{A.3}$$

Gradient:

$$\nabla f = rB\frac{\partial f}{\partial\psi}\hat{\psi} + \frac{1}{\mathcal{J}B}\frac{\partial f}{\partial\chi}\hat{\chi} + \frac{1}{r}\frac{\partial f}{\partial\theta}\hat{\theta} \quad . \tag{A.4}$$

Curl:

$$(\nabla\times\vec{A})_\psi = \frac{1}{\mathcal{J}rB}\left[\frac{\partial}{\partial\chi}(rA_\theta) - \frac{\partial}{\partial\theta}(\mathcal{J}BA_\chi)\right] \quad . \tag{A.5.1}$$

$$(\nabla\times\vec{A})_\chi = B\left[\frac{\partial}{\partial\theta}\left(\frac{1}{rB}A_\psi\right) - \frac{\partial}{\partial\psi}(rA_\theta)\right] \quad . \tag{A.5.2}$$

$$(\nabla\times\vec{A})_\theta = \frac{r}{\mathcal{J}}\left[\frac{\partial}{\partial\psi}(\mathcal{J}A_\chi) - \frac{\partial}{\partial\chi}\left(\frac{1}{rB}A_\psi\right)\right] \quad . \tag{A.5.3}$$

Laplacian:

$$\nabla^2\phi = \frac{1}{\mathcal{J}}\left[\frac{\partial}{\partial\psi}\left(\mathcal{J}r^2B^2\frac{\partial\phi}{\partial\psi}\right) + \frac{\partial}{\partial\chi}\left(\frac{1}{\mathcal{J}B}\frac{\partial\phi}{\partial\chi}\right) + \frac{\mathcal{J}}{r^2}\frac{\partial^2\phi}{\partial\theta^2}\right] \quad . \tag{A.6}$$

Components of $(\vec{A}\cdot\nabla)\vec{B}$:

$$(\vec{A}\cdot\nabla\vec{B})_\psi = A_\psi\, rB\frac{\partial B_\psi}{\partial\psi} + A_\chi\frac{1}{\mathcal{J}B}\frac{\partial B_\psi}{\partial\chi} + A_\theta\frac{1}{r}\frac{\partial B_\psi}{\partial\theta} \tag{A.7.1}$$

$$+ A_\psi B_\chi\frac{r}{\mathcal{J}}\frac{\partial}{\partial\chi}\left(\frac{1}{rB}\right) - A_\chi B_\chi\frac{r}{\mathcal{J}}\frac{\partial}{\partial\psi}(\mathcal{J}B) - A_\theta B_\theta B\frac{\partial r}{\partial\psi} \quad .$$

$$(\hat{A}\cdot\nabla\hat{B})_\chi = A_\psi\, rB\frac{\partial B_\chi}{\partial\psi} + A_\chi\frac{1}{\mathcal{J}B}\frac{\partial B_\chi}{\partial\chi} + A_\theta\frac{1}{r}\frac{\partial B_\chi}{\partial\theta} \qquad (A.7.2)$$

$$- A_\psi B_\psi\frac{r}{\mathcal{J}}\frac{\partial}{\partial\chi}\left(\frac{1}{rB}\right) + A_\chi B_\psi\frac{r}{\mathcal{J}}\frac{\partial}{\partial\psi}(\mathcal{J}B) - A_\theta B_\theta\frac{1}{\mathcal{J}rB}\frac{\partial r}{\partial\chi} \ .$$

$$(\hat{A}\cdot\nabla\hat{B})_\theta = A_\psi\, rB\frac{\partial B_\theta}{\partial\psi} + A_\chi\frac{1}{\mathcal{J}B}\frac{\partial B_\theta}{\partial\chi} + A_\theta\frac{1}{r}\frac{\partial B_\theta}{\partial\theta} \qquad (A.7.3)$$

$$+ A_\theta B_\psi\, B\frac{\partial r}{\partial\psi} + A_\theta B_\chi\frac{1}{\mathcal{J}rB}\frac{\partial r}{\partial\chi} \ .$$

Divergence of a Tensor:

$$(\nabla\cdot\bar{\bar{P}})_\psi = \frac{1}{\mathcal{J}}\frac{\partial}{\partial\psi}\left(\mathcal{J}rB\ P_{\psi\psi}\right) + \frac{1}{\mathcal{J}}\frac{\partial}{\partial\chi}\left(\frac{1}{B}P_{\chi\psi}\right) + \frac{1}{r}\frac{\partial}{\partial\theta}\left(P_{\theta\psi}\right) \qquad (A.8.1)$$

$$+ P_{\psi\chi}\frac{r}{\mathcal{J}}\frac{\partial}{\partial\chi}\left(\frac{1}{rB}\right) - P_{\chi\chi}\frac{r}{\mathcal{J}}\frac{\partial}{\partial\psi}\left(\mathcal{J}B\right) - P_{\theta\theta}\, B\frac{\partial r}{\partial\psi} \ .$$

$$(\nabla\cdot\bar{\bar{P}})_\chi = \frac{1}{\mathcal{J}}\frac{\partial}{\partial\psi}\left(\mathcal{J}rB\ P_{\psi\chi}\right) + \frac{1}{\mathcal{J}}\frac{\partial}{\partial\chi}\left(\frac{1}{B}P_{\chi\chi}\right) + \frac{1}{r}\frac{\partial}{\partial\theta}\left(P_{\theta\chi}\right) \qquad (A.8.2)$$

$$- P_{\psi\psi}\frac{r}{\mathcal{J}}\frac{\partial}{\partial\chi}\left(\frac{1}{rB}\right) + P_{\chi\psi}\frac{r}{\mathcal{J}}\frac{\partial}{\partial\psi}\left(\mathcal{J}B\right) - P_{\theta\theta}\frac{1}{\mathcal{J}rB}\frac{\partial r}{\partial\psi} \ .$$

$$(\nabla\cdot\bar{\bar{P}})_\theta = \frac{1}{\mathcal{J}}\frac{\partial}{\partial\psi}\left(\mathcal{J}rB\ P_{\psi\theta}\right) + \frac{1}{\mathcal{J}}\frac{\partial}{\partial\chi}\left(\frac{1}{B}P_{\chi\theta}\right) + \frac{1}{r}\frac{\partial}{\partial\theta}\left(P_{\theta\theta}\right) \qquad (A.8.3)$$

$$+ P_{\theta\psi}\, B\frac{\partial r}{\partial\psi} + P_{\theta\chi}\frac{1}{\mathcal{J}rB}\frac{\partial r}{\partial\chi} \ .$$

Velocity Coordinates:

Below is a summary of the velocity coordinates used in this paper.

$$\vec{v} = v_\chi\hat{\chi} + v_\psi\hat{\psi} + v_\theta\hat{\theta} \ . \qquad (A.9)$$

$(v_\chi, v_\perp, \zeta)$ coordinates:

$$\vec{v} = v_\chi\hat{\chi} + v_\perp\hat{m} \ , \qquad (A.10)$$

where $\vec{v_\perp} \equiv v_\perp\hat{m}$, $v_\perp^2 = v_\psi^2 + v_\chi^2$, $\hat{m} = -\sin\zeta\,\hat{\psi} + \cos\zeta\,\hat{\theta}$,

and $\tan\zeta \equiv -\dfrac{v_\psi}{v_\theta}$.

Integration over velocity:

$$\int d^3v\, f = \sum_{\pm}\int_0^{2\pi} d\zeta\int_0^\infty dv_\chi\int_0^\infty dv_\perp\, v_\perp\, f \ . \qquad (A.11)$$

where the sum is over the sign of v_χ.

$(\varepsilon, \mu, \zeta)$ coordinates:

When gyroaveraging the linear Vlasov equation the coordinates ε, μ, ζ are useful, where ζ has been defined previously and,

$$\varepsilon \equiv \frac{1}{2}v_\chi^2 + \frac{1}{2}v_\perp^2 \ , \qquad (A.12)$$

$$\mu \equiv \frac{1}{2}\frac{v_\perp^2}{B} \quad . \tag{A.13}$$

Integration over velocity:

$$\int d^3v\, f = \sum_{\pm} \int_0^{2\pi} d\zeta \int_0^{\infty} d\varepsilon \int_0^{\varepsilon/B} du\, \frac{B}{|v_\chi|} \tag{A.14}$$

$$= \frac{1}{\sqrt{2}} \sum_{\pm} \int_0^{2\pi} d\zeta \int_0^{\infty} d\varepsilon \int_0^{\varepsilon/B} du\, \frac{B}{\sqrt{\varepsilon - \mu B}} \quad .$$

For an equilibrium with $\vec{E} = 0$, $\partial\vec{A}/\partial t = 0$ where $\vec{A}$ is the vector potential, $\vec{B} = \nabla \times \vec{A}$, the following time derivatives hold:

$$\frac{d\varepsilon}{dt} = 0 \quad . \tag{A.15}$$

$$\frac{du}{dt} = -\frac{\mu}{B}\vec{v}\cdot\nabla B - \frac{v_\chi}{B} v_\perp \vec{\rho}\cdot(\vec{\rho}\cdot\nabla)\hat{\chi} \tag{A.16}$$

$$= \frac{\Omega}{B} v_\perp \hat{m}\cdot(\hat{\chi} \times \vec{v}_D) + \mu v_\chi \left[\hat{\rho}\cdot(\hat{\rho}\cdot\nabla)\hat{\chi} - \hat{m}\cdot(\hat{m}\cdot\nabla)\hat{\chi}\right] \quad .$$

where $\hat{\rho} = \cos\zeta\,\hat{\psi} + \sin\zeta\,\hat{\theta} = \dfrac{\partial \hat{m}}{\partial \zeta}$,

and $\vec{v}_D = v_D\hat{\theta} = \hat{\chi} \times (\mu\nabla B + v_\chi^2\, \hat{\chi}\cdot\nabla\hat{\chi})/\Omega$.

$$\frac{d\zeta}{dt} = \Omega + \hat{\psi}\cdot(\vec{v}\cdot\nabla)\hat{\theta} + \frac{v_\chi}{v_\perp}\hat{\rho}\cdot(\vec{\rho}\cdot\nabla)\hat{\chi} \quad . \tag{A.17}$$

The following moments of $\frac{du}{dt}$ and $\frac{d\zeta}{dt}$ with respect to ζ are useful for deriving the equation for f_1.

$$\frac{1}{2\pi}\int_0^{2\pi} \frac{du}{dt}\, d\zeta = 0 \quad , \tag{A.18.1}$$

$$\int_0^{\zeta} \frac{du}{dt}\, d\zeta = \frac{\Omega}{B} v_\perp \hat{\rho}\cdot(\hat{\chi} \times \vec{v}_D) - \mu v_\chi \hat{\rho}\cdot(\hat{m}\cdot\nabla)\hat{\chi} \quad , \tag{A.18.2}$$

$$\frac{1}{2\pi}\int_0^{2\pi} \hat{\rho}\, \frac{du}{dt}\, d\zeta = -\mu \vec{v}_D \quad , \tag{A.18.3}$$

$$\frac{1}{2\pi}\int_0^{2\pi} \cos\zeta\, \frac{du}{dt}\, d\zeta = 0 \quad , \tag{A.18.4}$$

$$\frac{1}{2\pi}\int_0^{2\pi} \sin\zeta\, \frac{du}{dt}\, d\zeta = -\frac{v_\perp}{2}\frac{\Omega}{B} v_D \quad , \tag{A.18.5}$$

$$\frac{1}{2\pi}\int_0^{2\pi} \sin\zeta\, \cos\zeta\, \frac{du}{dt}\, d\zeta = 0 \quad , \tag{A.18.6}$$

$$\frac{1}{2\pi}\int_0^{2\pi} \left(\frac{d\zeta}{dt} - \Omega\right) d\zeta = 0 \quad , \tag{A.18.7}$$

$$\frac{1}{2\pi}\int_0^{2\pi} \cos\zeta \left(\frac{d\zeta}{dt} - \Omega\right) d\zeta = \frac{1}{2} v_\perp \hat{\psi}\cdot(\hat{\theta}\cdot\nabla)\hat{\theta} + \frac{1}{2}\frac{v_\chi^2}{v_\perp}\hat{\psi}\cdot(\hat{\chi}\cdot\nabla)\hat{\chi} \quad , \tag{A.18.8}$$

$$\frac{1}{2\pi}\int_0^{2\pi} \sin\zeta \left(\frac{d\zeta}{dt} - \Omega\right) d\zeta = 0 \quad , \tag{A.18.9}$$

$$\frac{1}{2\pi}\int_0^{2\pi} \sin\zeta \cos\zeta \left(\frac{d\zeta}{dt} - \Omega\right) d\zeta = 0 \quad , \tag{A.18.10}$$

$$\frac{1}{2\pi}\int_0^{2\pi} \sin^2\zeta \left(\frac{d\zeta}{dt} - \Omega\right) d\zeta = 0 \quad . \tag{A.18.11}$$

$(\varepsilon, \alpha, \zeta)$ coordinates:

It is useful when integrating over pitch angle to use the coordinate α instead of μ, where α is defined by,

$$\alpha \equiv \frac{\mu}{\varepsilon} \quad . \tag{A.19}$$

Integration over velocity:

$$\int d^3v\, f = \frac{1}{\sqrt{2}} \sum_{\pm} \int_0^{2\pi} d\zeta \int_0^{\infty} d\varepsilon \int_0^{1/B} d\alpha \frac{\sqrt{\varepsilon}\, B}{\sqrt{1 - \alpha B}} \quad . \tag{A.20}$$

APPENDIX B

Perturbed Field Representation

Below are some useful identities of the perturbed field representation used in the derivation of some of the equations in the text. The components of the perturbed vector potential are written in terms of the quantities X and Y where $X \equiv rA_\theta$ and $Y \equiv i\, nA_\psi / rB$. The χ-component of the vector potential is retained here for completeness but in the text the gauge condition is choosen so that $A_\chi = 0$. The (ψ, χ, θ) coordinate system is used. Components of the perturbed magnetic and electric field:

$$Bl_\psi = \frac{1}{\mathcal{J} rB} \frac{\partial X}{\partial \chi} + i \frac{n}{r} A_\chi \quad , \tag{B.1.1}$$

$$Bl_\chi = - B\left(Y + \frac{\partial X}{\partial \psi}\right) \quad , \tag{B.1.2}$$

$$Bl_\theta = i \frac{r}{n} \frac{1}{\mathcal{J}} \frac{\partial Y}{\partial \chi} + \frac{r}{\mathcal{J}} \frac{\partial}{\partial \psi}(\mathcal{J} B A_\chi) \quad , \tag{B.1.3}$$

$$El_\psi = - rB \frac{\partial \phi}{\partial \psi} - \omega \frac{r}{n} BY \quad , \tag{B.1.4}$$

$$El_\chi = - \frac{1}{\mathcal{J} B} \frac{\partial \phi}{\partial \chi} - i\omega A_\chi \quad , \tag{B.1.5}$$

$$El_\theta = i \frac{n}{r} \phi - i \frac{\omega}{r} X \quad . \tag{B.1.6}$$

Components of the perturbed current density written in terms of the perturbed magnetic field, $\tilde{B}l$, using Ampere's law:

$$\mu_0 j_{1\psi} = \frac{i}{\mathcal{J} r B}\left\{\frac{1}{n}\frac{\partial}{\partial\chi}\left(\frac{r^2}{\mathcal{J}}\frac{\partial Y}{\partial\chi}\right) - n\,\mathcal{J}B^2\left(Y + \frac{\partial X}{\partial\psi}\right)\right.$$

$$\left. - \frac{\partial}{\partial\chi}\left[\frac{r^2}{\mathcal{J}}\frac{\partial}{\partial\psi}(\mathcal{J}B\; iA_\chi)\right]\right\} \quad , \tag{B.2.1}$$

$$\mu_0 j_{1\chi} = -\,inB\left\{\frac{1}{\mathcal{J} r^2 B^2}\frac{\partial X}{\partial\chi} + \frac{1}{n^2}\frac{\partial}{\partial\psi}\left(\frac{r^2}{\mathcal{J}}\frac{\partial Y}{\partial\chi}\right)\right.$$

$$\left. - \frac{1}{n}\frac{\partial}{\partial\psi}\left[\frac{r^2}{\mathcal{J}}\frac{\partial}{\partial\psi}(\mathcal{J}B\; iA_\chi)\right] + \frac{n}{r^2 B}\, iA_\chi\right\} \quad , \tag{B.2.2}$$

$$\mu_0 j_{1\theta} = \frac{r}{\mathcal{J}}\left\{\frac{\partial}{\partial\chi}\left(\frac{1}{\mathcal{J} r^2 B^2}\frac{\partial X}{\partial\chi}\right)\right.$$

$$\left. - \frac{\partial}{\partial\psi}\left[\mathcal{J}B^2\left(Y + \frac{\partial X}{\partial\psi}\right)\right] + \frac{\partial}{\partial\chi}\left(\frac{n}{r^2 B}\, iA_\chi\right)\right\} \quad . \tag{B.2.3}$$

Components of the perturbed force density:

$$(\mu_0 \vec{j}_0 \times \vec{B}_1 + \mu_0 \vec{j}_1 \times \vec{B}_0)_\psi = rB\left\{\frac{1}{\mathcal{J}}\frac{\partial}{\partial\chi}\left(\frac{1}{\mathcal{J} r^2 B^2}\frac{\partial X}{\partial\chi}\right)\right.$$

$$\left. + \frac{1}{\mathcal{J}}\frac{\partial}{\partial\psi}\left[\mathcal{J}B^2\left(Y + \frac{\partial X}{\partial\psi}\right)\right] - \mu_0 p'\left(Y + \frac{\partial X}{\partial\psi}\right) + \frac{\partial}{\partial\chi}\left(\frac{n}{r^2 B}\, iA_\chi\right)\right\} \quad , \tag{B.3.1}$$

$$(\mu_0 \vec{j}_0 \times \vec{B}_1 + \mu_0 \vec{j}_1 \times \vec{B}_0)_\chi = -\,\mu_0 p'\left[\frac{1}{\mathcal{J}B}\frac{\partial X}{\partial\chi} + n\, iA_\chi\right] \quad , \tag{B.3.2}$$

$$(\mu_0 \vec{j}_0 \times \vec{B}_1 + \mu_0 \vec{j}_1 \times \vec{B}_0)_\theta = \frac{i}{\mathcal{J} r}\left\{\frac{1}{n}\frac{\partial}{\partial\chi}\left(\frac{r^2}{\mathcal{J}}\frac{\partial Y}{\partial\chi}\right)\right.$$

$$\left. - n\,\mathcal{J}B^2\left(Y + \frac{\partial X}{\partial\psi}\right) - \frac{\partial}{\partial\chi}\left[\frac{r^2}{\mathcal{J}}\frac{\partial}{\partial\psi}(\mathcal{J}B\; iA_\chi)\right]\right\} \quad . \tag{B.3.3}$$

APPENDIX C

Bessel Function

Identities and Integral Relations

$$J_p(a) = \frac{1}{2\pi i^p}\int_0^{2\pi} d\zeta\, \exp(ip\theta - ia\cos\zeta) \quad , \tag{C.1}$$

where p is an integer.

$$\exp(\pm\, ia\sin\zeta) = \sum_{p=-\infty}^{\infty}(-1)^p J_p(a)\, e^{\pm ip\zeta} \tag{C.2}$$

$$= J_0(a) + 2\sum_{p=1}^{\infty} I_p(a)\cos(p\zeta)$$

$$+ 2i\sum_{p=0}^{\infty} J_{2p+1}(a)\sin[(2p+1)\zeta] \quad .$$

$$\frac{1}{2\pi}\int_0^{2\pi} d\zeta\, \cos(p\zeta)\exp(-ia\sin\zeta) \tag{C.3}$$

$$= \begin{cases} J_p(a) & \text{for } p \text{ even} \\ 0 & \text{for } p \text{ odd} \end{cases} \quad .$$

$$\frac{1}{2\pi}\int_0^{2\pi} d\zeta\, \sin(p\zeta)\exp(-ia\sin\zeta) \tag{C.4}$$

$$= \begin{cases} 0 & \text{for } p \text{ even} \\ -\,i\,J_p(a) & \text{for } p \text{ odd} \end{cases} \quad .$$

$$\frac{1}{2\pi}\int_0^{2\pi} d\zeta\, \cos^2\zeta\exp(-ia\sin\zeta) = \frac{1}{a}J_1(a) \quad . \tag{C.5}$$

$$\frac{1}{2\pi}\int_0^{2\pi} d\zeta\, \sin\zeta\cos\zeta\exp(-ia\sin\zeta) = 0 \quad , \tag{C.6}$$

$$\frac{1}{2\pi}\int_0^{2\pi} d\zeta\ \sin^2\zeta\ \exp(-ia\sin\zeta) = J_0(a) - \frac{1}{a}J_1(a)\ . \qquad (C.7)$$

$$\frac{1}{2\pi}\int_0^{2\pi} d\zeta\ \cos^3\zeta\ \exp(-ia\sin\zeta) = 0\ . \qquad (C.8)$$

$$\frac{1}{2\pi}\int_0^{2\pi} d\zeta\ \cos^2\zeta\ \sin\zeta\ \exp(-ia\sin\zeta) = -\frac{i}{a}J_2(a)\ . \qquad (C.9)$$

$$\frac{1}{2\pi}\int_0^{2\pi} d\zeta\ \cos\zeta\ \sin^2\zeta\ \exp(-ia\sin\zeta) = 0\ . \qquad (C.10)$$

$$\frac{1}{2\pi}\int_0^{2\pi} d\zeta\ \sin^3\zeta\ \exp(-ia\sin\zeta) = \frac{i}{4}\left[J_3(a) - 3J_1(a)\right]\ . \qquad (C.11)$$

$$\int_0^\infty dv\ v\ J_p^2(v\,b)\ \exp\left(-\frac{mv^2}{2T}\right) = \frac{T}{m}\exp\left(-\frac{T}{m}b^2\right)\ I_p\left(\frac{T}{m}b^2\right)\ , \qquad (C.12)$$

where p is an integer.

$$\int_0^\infty dv\ v^2\ J_0(vb)\ J_1(vb)\ \exp\left(-\frac{mv^2}{2T}\right) \qquad (C.13)$$

$$= \left(\frac{T}{m}\right)^2 b\ \exp\left(-\frac{T}{m}b^2\right)\left[I_0\left(\frac{T}{m}b^2\right) - I_1\left(\frac{T}{m}b^2\right)\right]\ .$$

$$\int_0^\infty dv\ v^3\ J_0^2(vb)\ \exp\left(-\frac{mv^2}{2T}\right) \qquad (C.14)$$

$$= 2\left(\frac{T}{m}\right)^2\ \exp\left(-\frac{T}{m}b^2\right)\left\{I_0\left(\frac{T}{m}b^2\right)\left[1 - \frac{T}{m}b^2\right]\right.$$

$$\left. + \frac{T}{m}b^2\ I_1\left(\frac{T}{m}b^2\right)\right\}\ .$$

$$\int_0^\infty dv\ v^3\ J_1^2(vb)\ \exp\left(-\frac{mv^2}{2T}\right) \qquad (C.15)$$

$$= 2\left(\frac{T}{m}\right)^3 b^2\ \exp\left(-\frac{T}{m}b^2\right)\left[I_0\left(\frac{T}{m}b^2\right) - I_1\left(\frac{T}{m}b^2\right)\right]\ .$$

$$\int_0^\infty dv\ v^4\ J_0(vb)\ J_1(vb)\ \exp\left(-\frac{mv^2}{2T}\right) \qquad (C.16)$$

$$= 2\left(\frac{T}{m}\right)^2 b\ \exp\left(-\frac{T}{m}b^2\right)\left\{2I_0\left(\frac{T}{m}b^2\right)\left[1 - \frac{T}{m}b^2\right]\right.$$

$$\left. - I_1\left(\frac{T}{m}b^2\right)\left[1 - 2\frac{T}{m}b^2\right]\right\}\ .$$

$$\int_0^\infty dv\ v^5\ J_1^2(vb)\ \exp\left(-\frac{mv^2}{2T}\right) \qquad (C.17)$$

$$= 4\left(\frac{T}{m}\right)^3 b^2\ \exp\left(-\frac{T}{m}b^2\right)\left[3I_0\left(\frac{T}{m}b^2\right) - 2I_1\left(\frac{T}{m}b^2\right)\right]\ .$$

APPENDIX D

Moments of the Perturbed Distribution Function

Below is a list of the velocity moments of the perturbed distribution function, f_1^0.

$$f_1^0 = \frac{q}{T} f_m \{-\phi + \frac{\omega}{n} X + h \exp(ia \sin\zeta)\}, \tag{D.1}$$

where h is a solution to,

$$(\omega - \omega_D)h - iv_\chi \hat{\chi}\cdot\nabla h = (\omega - \omega^*)\left\{(\phi - \frac{\omega}{n} X + \frac{i}{n} v_\chi \hat{\chi}\cdot\nabla X)J_0(a) - v_\perp \frac{r}{n} B(Y + \frac{\partial X}{\partial \psi})J_1(a)\right\}, \tag{D.2}$$

with $a = \frac{v_\perp n}{\Omega r}$.

Two frequency regimes will be considered, $\omega << \omega_b$ and $\omega >> \omega_b$, with the appropriate approximation of h adopted for each regime. Here ω_b is defined as $\omega_b^{-1} \equiv \pi \int_{X1}^{X2} \frac{B\mathcal{J}\, dX}{|v_\chi|}$ where X_1 and X_2 are the end points of a particle trapped in one of the magnetic wells.

Low Frequency Regime, $\omega << \omega_b$

For frequencies much less then a typical bounce frequency it is useful to write h in the form,

$$h = -(\omega - \omega^*)\frac{X}{n} J_0(a) + h' \tag{D.3}$$

where h' is a solution to,

$$(\omega - \omega_D)h' - iv_\chi \hat{\chi}\cdot\nabla h' = (\omega - \omega^*)\left\{(\phi - \frac{\omega_D}{n} X)J_0(a) - v_\perp \frac{r}{n} B(Y + \frac{\partial X}{\partial \psi})J_1(a) - iv_\chi v_\perp \frac{X}{2r\Omega}\frac{1}{r^2 B}\hat{\chi}\cdot\nabla(r^2 B)\, J_1(a)\right\}. \tag{D.4}$$

The last term is of order ρ_i/L_B and will be neglected. In integrating over velocity the expression for h' will be summed over $\pm v_\chi$. To lowest order in ω/ω_b the expression for h' is,

$$\frac{1}{2}(h'^{+} + h'^{-}) = \frac{\omega - \omega^*}{\omega - \langle\omega_D\rangle}\left\langle(\phi - \frac{\omega_D}{n} X)J_0(a) - v_\perp \frac{r}{n} B(Y + \frac{\partial X}{\partial \psi})J_1(a)\right\rangle, \tag{D.5}$$

where h' has been summed over the sign of v_χ and

$$\langle A\rangle \equiv \frac{\int_{X1}^{X2} \frac{A\, BJ\, dX'}{|v_\chi|}}{\int_{X1}^{X2} \frac{BJ\, dX'}{|v_\chi|}} .$$

First some preliminary definitions. Define the functions $\tilde{z}$ as follows:

$$\frac{1}{2} n_0 z_0 = 2\sqrt{2}\,\pi \int_0^\infty d\varepsilon\, \sqrt{\varepsilon}\, f_m \frac{J_0(a)J_0(a')}{1 - \frac{\langle\omega_D\rangle}{\omega}}, \tag{D.6.0}$$

$$\frac{3}{4} n_0 \frac{T}{m} z_1 = 2\sqrt{2}\,\pi \int_0^\infty d\varepsilon\, \sqrt{\varepsilon}\, \varepsilon\, f_m \frac{J_0(a)J_0(a')}{1 - \frac{\langle\omega_D\rangle}{\omega}}, \tag{D.6.1}$$

$$\frac{3}{4} n_0 \frac{T}{m} \frac{aB'}{\Omega'} z_2 = 2\sqrt{2}\,\pi \int_0^\infty d\varepsilon\, \sqrt{\varepsilon}\, f_m \frac{J_0(a)J_1(a')\frac{v_\perp' r'}{n}}{1 - \frac{\langle\omega_D\rangle}{\omega}}, \tag{D.6.2}$$

$$\frac{3}{4} n_0 \frac{T}{m} \frac{\alpha B}{\Omega} Z_3 = 2\sqrt{2}\,\pi \int_0^\infty d\varepsilon\, \sqrt{\varepsilon}\, f_m \frac{J_1(a)\frac{v_\perp r}{n} J_0(a')}{1 - \frac{\langle\omega_D\rangle}{\omega}} \quad , \tag{D.6.3}$$

$$\frac{15}{8} n_0 \left(\frac{T}{m}\right)^2 \frac{\alpha B}{\Omega} Z_4 = 2\sqrt{2}\,\pi \int_0^\infty d\varepsilon\, \sqrt{\varepsilon}\, \varepsilon\, f_m \frac{J_1(a)\frac{v_\perp r}{n} J_0(a')}{1 - \frac{\langle\omega_D\rangle}{\omega}} \quad , \tag{D.6.4}$$

$$\frac{15}{8} n_0 \left(\frac{T}{m}\right)^2 \frac{\alpha B}{\Omega} \frac{\alpha B'}{\Omega'} Z_5 = 2\sqrt{2}\,\pi \int_0^\infty d\varepsilon\, \sqrt{\varepsilon}\, f_m \frac{J_1(a)\frac{v_\perp r}{n} J_1(a')\frac{v_\perp' r'}{n}}{1 - \frac{\langle\omega_D\rangle}{\omega}} \quad , \tag{D.6.5}$$

$$\frac{15}{8} n_0 \left(\frac{T}{m}\right)^2 Z_6 = 2\sqrt{2}\,\pi \int_0^\infty d\varepsilon\, \sqrt{\varepsilon}\, \varepsilon^2\, f_m \frac{J_0(a) J_0(a')}{1 - \frac{\langle\omega_D\rangle}{\omega}} \quad , \tag{D.6.6}$$

$$\frac{15}{8} n_0 \left(\frac{T}{m}\right)^2 \frac{\alpha B'}{\Omega'} Z_7 = 2\sqrt{2}\,\pi \int_0^\infty d\varepsilon\, \sqrt{\varepsilon}\, \varepsilon\, f_m \frac{J_0(a) J_1(a')\frac{v_\perp' r'}{n}}{1 - \frac{\langle\omega_D\rangle}{\omega}} \quad . \tag{D.6.7}$$

The prime over a term indicates it should be evaluated at χ', i.e.,

$$\left\langle \frac{1}{2} \frac{q\phi}{T} Z_0 \right\rangle = 2\sqrt{2}\,\pi \int_0^\infty d\varepsilon\, \sqrt{\varepsilon}\, f_m \frac{J_0(a)}{1 - \frac{\langle\omega_D\rangle}{\omega}} \left\langle \frac{1}{2} \frac{q\phi}{T} J_0(a) \right\rangle .$$

In the limit $\rho \to 0$, $\omega_D/\omega \to 0$, $Z_0 = Z_1 = Z_2 = Z_3 = Z_4 = Z_5 = Z_6 = Z_7 = 1$. In the limit $\rho \to \infty$, $Z_0 = Z_1 = Z_2 = Z_3 = Z_4 = Z_5 = Z_6 = Z_7 = 0$. The Z functions contain finite Larmor radius effects and the drift

resonance. Let's also define the following finite Larmor radius terms:

$$a_T \equiv \sqrt{\frac{T}{m}} \frac{1}{\Omega} \frac{n}{r} = \frac{\rho}{\lambda_\theta} \quad ,$$

$$G_0 \equiv \frac{1}{n_0} \int d^3v\, f_m\, J_0^2(a) = \exp(-a_T^2)\, I_0(a_T^2) \quad , \tag{D.7.0}$$

$$G_1 \equiv \frac{1}{n_0} \frac{m}{T} \int d^3v\, f_m \frac{v_\perp^2}{a} J_0(a) J_1(a) = \exp(-a_T^2)\,[I_0(a_T^2) - I_1(a_T^2)] \quad , \tag{D.7.1}$$

$$G_2 \equiv \frac{1}{n_0} \frac{m}{T} \int d^3v\, f_m \frac{1}{2} v_i^2\, J_0^2(a) = \exp(-a_T^2)\,\{I_0(a_T^2)[1 - a_T^2] + a_T^2\, I_1(a_T^2)\} \quad . \tag{D.7.2}$$

Zeroth moment of f_1^0:

$$\begin{aligned} n_1 &= \int d^3v\, f_1^0 \qquad\qquad (D.8) \\ &= n_0 \frac{q}{T} \left\{ -\phi + \omega \frac{X}{n} - (\omega - \omega^*) \frac{X}{n} G_0 \right\} \\ &\quad + \frac{q}{T} \left(1 - \frac{\omega^*}{\omega}\right) \int d^3v\, f_m \frac{J_0(a)}{1 - \frac{\langle\omega_D\rangle}{\omega}} \left\langle [\phi - \omega_D \frac{X}{n}] J_0(a) \right. \\ &\quad \left. - v_\perp \frac{r}{n} B\left(Y + \frac{\partial X}{\partial \psi}\right) J_1(a) \right\rangle \\ &= n_0 \left\{ \frac{-q\phi}{T} - \frac{\omega}{\omega_{*p}} \frac{p'}{p} X - \left(1 - \frac{\omega}{\omega_*}\right) \frac{p'}{p} X\, G_0 \right\} \\ &\quad - n_0 \left(1 - \frac{\omega^*}{\omega}\right) \int_0^{1/B} \frac{d\alpha\, B}{\sqrt{1 - \alpha B}} \left\langle -\frac{1}{2} \frac{q\phi}{T} Z_0 \right. \\ &\quad \left. + \frac{3}{4} X\left[\left(1 - \frac{\alpha B}{2}\right) D + \alpha B \frac{\mu_0 p'}{B^2}\right] Z_1 + \frac{3}{4} \left(Y + \frac{\partial X}{\partial \psi}\right) \alpha B\, Z_2 \right\rangle \quad . \end{aligned}$$

First moments of f_1^0 :

$$v_{1_\psi} = \int d^3v\, f_1^0\, v_\psi = -\int d^3v\, f_1^0\, v_\perp \sin\zeta \qquad (D.9)$$

$$= i\, n_0(\omega - \omega^*)\frac{X}{rB}\, G_1 - i\,\frac{q}{T}\,(1 - \frac{\omega^*}{\omega}) \int d^3v\, f_m \frac{v_\perp J_1(a)}{1 - \frac{\langle\omega_D\rangle}{\omega}}$$

$$\times \left\langle [\phi - \omega_D \frac{X}{n}] J_0(a) - v_\perp \frac{r}{n} B(Y + \frac{\partial X}{\partial \psi}) J_1(a) \right\rangle$$

$$= i\, n_0(\omega - \omega^*)\frac{X}{rB}\, G_1 + i\, n_0 \frac{n}{r}\frac{T}{q}(1 - \frac{\omega^*}{\omega}) \int_0^{1/B} \frac{d\alpha}{\sqrt{1 - \alpha B}}\, \alpha B$$

$$\times \left\langle -\frac{3}{4}\frac{q\phi}{T}\, Z_3 + \frac{15}{8} X[(1 - \frac{\alpha B}{2})D + \alpha B \frac{\mu_0 p'}{B^2}]\, Z_4 \right.$$

$$\left. + \frac{15}{8}(Y + \frac{\partial X}{\partial \psi})\alpha B\, Z_5 \right\rangle \quad .$$

To calculate v_{1_X} an expression for $h'^+ - h'^-$ is needed. Summing Eq. (D.4) over positive and negative v_X gives an equation for $h'^+ - h'^-$.

$$(\omega - \omega_D)\,\frac{1}{2}\,(h'^+ + h'^-) - i\,|v_X|\,\hat{X}\cdot\nabla\,\frac{1}{2}\,(h'^+ - h'^-)$$

$$= (\omega - \omega^*)\left\{[\phi - \omega_D \frac{X}{n}] J_0(a) - v_\perp \frac{r}{n} B(Y + \frac{\partial X}{\partial \psi}) J_1(a)\right\}. \qquad (D.10)$$

The term v_{1_X} appears in the continuity equation and in the χ component of Ampere's law (after dividing by B and taking the derivative with respect to χ) in the form $i\frac{\partial}{\partial X}(\frac{v_{1_X}}{B})$. This term can be calculated directly from Eq. (D.10) by multiplying it by $J_0(a)$ and integrating over velocity.

$$v_{1_X} = \int d^3v\, f_1^0\, v_X = \frac{q}{T} \int d^3v\, f_m\, |v_X|\, J_0(a)\, \frac{1}{2}(h'^+ - h'^-) \ .$$

$$i\,\frac{\partial}{\partial X}(\frac{v_{1_X}}{B}) = \mathcal{F}\, n_0(\omega - \omega^*)\left\{-\frac{q\phi}{T}\, G_0 + X[D\,\frac{1}{2}(G_0 + G_2)\right.$$

$$\left. + \frac{\mu_0 p'}{B^2} G_2] + (Y + \frac{\partial X}{\partial \psi}) G_1\right\}$$

$$+ \mathcal{F}\,\frac{q}{T}\,(1 - \frac{\omega^*}{\omega}) \int d^3v\, f_m \frac{J_0(a)}{1 - \frac{\langle\omega_D\rangle}{\omega}}\,(\omega - \omega_D)$$

$$\times \left\langle [\phi - \omega_D \frac{X}{n}] J_0(a) - v_\perp \frac{r}{n} B(Y + \frac{\partial X}{\partial \psi}) J_1(a) \right\rangle$$

$$= \mathcal{F}\, n_0(\omega - \omega^*)\left\{-\frac{q\phi}{T}\, G_0 + X[D\,\frac{1}{2}(G_0 + G_2)\right.$$

$$\left. + \frac{\mu_0 p'}{B} G_2] + (Y + \frac{\partial X}{\partial \psi}) G_1\right\}$$

$$- \mathcal{F}\,\omega n_0 (1 - \frac{\omega^*}{\omega}) \int_0^{1/B} \frac{d\alpha\, B}{\sqrt{1 - \alpha B}} \left\langle -\frac{1}{2}\frac{q\phi}{T} Z_0 \right.$$

$$\left. + \frac{3}{4} X[(1 - \frac{\alpha B}{2})D + \alpha B \frac{\mu_0 p'}{B^2}]\, Z_1 + \frac{3}{4}(Y + \frac{\partial X}{\partial \psi})\alpha B\, Z_2 \right\rangle$$

$$+ \mathcal{F}\, n_0 T \frac{n}{q}(1 - \frac{\omega^*}{\omega}) \int_0^{1/B} \frac{d\alpha\, B}{\sqrt{1 - \alpha B}}\, [(1 - \frac{\alpha B}{2})D + \alpha B \frac{\mu_0 p'}{B^2}]$$

$$\times \left\langle -\frac{3}{4}\frac{q\phi}{T} Z_1 + \frac{15}{8} X[(1 - \frac{\alpha B}{2})D + \alpha B \frac{\mu_0 p'}{B^2}]\, Z_6 \right.$$

$$\left. + \frac{15}{8}(Y + \frac{\partial X}{\partial \psi})\alpha B\, Z_7 \right\rangle \quad . \qquad (D.11)$$

where use was made of Eq. (D.5) for $h'^+ - h'^-$.

The term v_{1_θ} can not be calculated directly from f_1^* unless higher order terms are kept. Although the procedure for finding the next higher order expansion in ρ_i/L_n of f_1 is straight forward it involves considerably more algebra. An easier way of finding v_{1_θ} is to use the

continuity equation plus the expressions for the other velocity moments above.

$$\frac{\partial n_1}{\partial t} + \nabla\cdot\vec{v}_1 = 0 \quad .$$

Solving for v_{1_θ} remembering $(\omega - \omega^*) = [\omega[1 + \frac{p'}{p}(\psi - \psi_0)] - \omega^*\}$ we get,

$$v_{1_\theta} = \frac{r}{n}\omega n_1 - \frac{r}{n}\frac{i}{\mathcal{J}}\frac{\partial}{\partial\psi}(\mathcal{J}rBv_{1_\psi}) - \frac{r}{n}\frac{i}{J}\frac{\partial}{\partial\chi}(\frac{v_{1_\chi}}{B})$$

$$= \frac{r}{n}\omega n_0\left\{-\frac{q\phi}{T} - \frac{\omega}{\omega^* p}p'X - (1 - \frac{\omega}{\omega^*})\frac{p'}{p}X\ G_0\right\}$$

$$+ \frac{r}{n}n_0(\omega - \omega^*)\frac{1}{\mathcal{J}}\frac{\partial}{\partial\psi}(\mathcal{J}X\ G_1) + \frac{r}{n}n_0\omega\frac{p'}{p}X\ G_1$$

$$+ \frac{T}{q}\frac{1}{\mathcal{J}}\frac{\partial}{\partial\psi}\left\{n_0(1 - \frac{\omega^*}{\omega})\ \mathcal{J}rB\int_0^{1/B}\frac{d\alpha}{\sqrt{1 - \alpha B}}\alpha B\right.$$

$$\times\left\langle -\frac{3}{4}\frac{q\phi}{T}z_3 + \frac{15}{8}X[(1 - \frac{\alpha B}{2})D + \alpha B\frac{\mu_0 p'}{B^2}]\ z_4\right.$$

$$\left.\left. + \frac{15}{8}(Y + \frac{\partial X}{\partial\psi})\alpha B\ z_5\right\rangle\right\} - \frac{r}{n}n_0(\omega - \omega^*)\left\{-\frac{q\phi}{T}G_0\right.$$

$$\left. + X[D\frac{1}{2}(G_0 + G_2) + \frac{\mu_0 p'}{B^2}G_2] + (Y + \frac{\partial X}{\partial\psi})G_1\right\}$$

$$- \frac{r}{n}n_0 T\frac{n}{q}(1 - \frac{\omega^*}{\omega})\int_0^{1/B}\frac{d\alpha\ B}{\sqrt{1 - \alpha B}}[(1 - \frac{\alpha B}{2})D + \alpha B\frac{\mu_0 p'}{B^2}]$$

$$\times\left\langle -\frac{3}{4}\frac{q\phi}{T}z_1 + \frac{15}{8}X[(1 - \frac{\alpha B}{2})D + \alpha B\frac{\mu_0 p'}{B^2}]\ z_6\right.$$

$$\left. + \frac{15}{8}(Y + \frac{\partial X}{\partial\psi})\alpha B\ z_7\right\rangle \quad . \qquad (D.12)$$

Neglecting higher order finite Larmor radius terms (like $G_1 - G_2$) that are small for any Larmor radius Eq. (D.12) can be simplified to,

$$v_{1_\theta} = -\frac{r}{n}n_0\omega(\frac{q\phi}{T} + \frac{\omega}{\omega^* p}p'X)[1 - (1 - \frac{\omega^*}{\omega})G_0]$$

$$+ \frac{r}{n}n_0\omega\frac{p'}{p}X\ G_1 - n_0(\omega - \omega^*)\frac{r}{n}Y\ G_1$$

$$+ \frac{T}{q}\int_0^{1/B}\frac{d\alpha}{\sqrt{1 - \alpha B}}\alpha B\ \hat{\psi}\cdot\nabla\left\{n_0(1 - \frac{\omega^*}{\omega})\left\langle -\frac{3}{4}\frac{q\phi}{T}z_3\right.\right.$$

$$\left.\left. + \frac{15}{8}X[(1 - \frac{\alpha B}{2})D + \alpha B\frac{\mu_0 p'}{B^2}]\ z_4 + \frac{15}{8}(Y + \frac{\partial X}{\partial\psi})\alpha B\ z_5\right\rangle\right\} \quad .$$

(D.13)

This last expression for v_{1_θ} is also what one obtains if a higher order expansion of f_1 is used to calculate v_{1_θ}, as verified by the author.

Second moments of f_1^0:

$$P_{XX} = m\int d^3v\ f_1^0\ v_X^2 \qquad (D.14)$$

$$= n_0 q[-\phi + \omega\frac{X}{n} - (\omega - \omega^*)\frac{X}{n}G_0]$$

$$+ m\frac{q}{T}(1 - \frac{\omega^*}{\omega})\int d^3v\ f_m\ v_X^2\frac{J_0(a)}{1 - \frac{\langle\omega_D\rangle}{\omega}}$$

$$\times\left\langle[\phi - \omega_D\frac{X}{n}]J_0(a) - v\frac{r}{n}B(Y + \frac{\partial X}{\partial\psi})J_1(a)\right\rangle$$

$$= n_0 T\left\{-\frac{q\phi}{T} - \frac{\omega}{\omega^* p}p'X - (1 - \frac{\omega}{\omega^*})\frac{p'}{p}X\ G_0\right\}$$

$$- 2n_0 T(1 - \frac{\omega^*}{\omega})\int_0^{1/B}d\alpha\ B\sqrt{1 - \alpha B}\left\langle -\frac{3}{4}\frac{q\phi}{T}z_1\right.$$

$$\left. + \frac{15}{8}X[(1 - \frac{\alpha B}{2})D + \alpha B\frac{\mu_0 p'}{B^2}]\ z_6 + \frac{15}{8}(Y + \frac{\partial X}{\partial\psi})\alpha B\ z_7\right\rangle \quad .$$

$$P_{\theta\theta} = m\int d^3v\, f_1^0\, v_\theta^2 = m\int d^3v\, f_1^0\, v_\perp^2 \cos^2\zeta \qquad (D.15)$$

$$= n_0 q\left\{-\phi + \omega\frac{X}{n} - (\omega - \omega^*)\frac{X}{n}G_1\right\}$$

$$+ m\frac{q}{T}(1 - \frac{\omega^*}{\omega})\int d^3v\, f_m \frac{v_\perp^2}{a}\frac{J_1(a)}{1 - \frac{<\omega_D>}{\omega}}$$

$$\times\left\langle[\phi - \omega_D\frac{X}{n}]J_0(a) - v_\perp\frac{r}{n}B(Y + \frac{\partial X}{\partial\psi})J_1(a)\right\rangle$$

$$= n_0 T\left\{-\frac{q\phi}{T} - \frac{\omega}{\omega^*}\frac{p'}{p}X - (1 - \frac{\omega}{\omega^*})\frac{p'}{p}X\,G_1\right\}$$

$$- n_0 T(1 - \frac{\omega^*}{\omega})\int_0^{1/B}\frac{d\alpha\, B}{\sqrt{1 - \alpha B}}\alpha B\left\langle -\frac{3}{4}\frac{q\phi}{T}Z_3\right.$$

$$\left. + \frac{15}{8}X[(1 - \frac{\alpha B}{2})D + \alpha B\frac{\mu_0 p'}{B^2}]Z_4 + \frac{15}{8}(Y + \frac{\partial X}{\partial\psi})\alpha B\,Z_5\right\rangle \ .$$

$$P_{\psi\psi} = m\int d^3v\, f_1^0\, v_\psi^2 = m\int d^3v\, f_1^0\, v_\perp^2 \sin^2\zeta \qquad (D.16)$$

$$= n_0 q\left\{-\phi + \omega\frac{X}{n} - (\omega - \omega^*)\frac{X}{n}(2G_2 + G_1 - 2G_0)\right\}$$

$$+ m\frac{q}{T}(1 - \frac{\omega^*}{\omega})\int d^3v\, f_m\, v_\perp^2\frac{J_0(a) - \frac{1}{a}J_1(a)}{1 - \frac{<\omega_D>}{\omega}}$$

$$\times\left\langle[\phi - \omega_D\frac{X}{n}]J_0(a) - v_\perp\frac{r}{n}B(Y + \frac{\partial X}{\partial\psi})J_1(a)\right\rangle$$

$$= n_0 T\left\{-\frac{q\phi}{T} - \frac{\omega}{\omega^*}\frac{p'}{p}X - (1 - \frac{\omega}{\omega^*})\frac{p'}{p}X\,(2G_2 + G_1 - 2G_0)\right\}$$

$$- n_0 T(1 - \frac{\omega^*}{\omega})\int_0^{1/B}\frac{d\alpha\, B}{\sqrt{1 - \alpha B}}\alpha B\left\langle -\frac{3}{4}\frac{q\phi}{T}(2Z_1 - Z_3)\right.$$

$$+ \frac{15}{8}X[(1 - \frac{\alpha B}{2})D + \alpha B\frac{\mu_0 p'}{B^2}](2Z_6 - Z_4)$$

$$\left. + \frac{15}{8}(Y + \frac{\partial X}{\partial\psi})\alpha B(2Z_7 - Z_5)\right\rangle \ .$$

An expression for $P_{\psi X}$ can be calculated from Eq. (D.10) in the same manner v_{1_X} was calculated. Multiplying Eq. (D.10) by $v_\perp J_1(a)$ and integrating over velocity yields,

$$rB^2\,\hat{X}\cdot\nabla(\frac{P_{\psi X}}{rB^2}) = rB\,n_0 T\frac{p'}{p}a_T^2(1 - \frac{\omega^*}{\omega})\left\{\frac{q\phi}{T}G_1\right.$$

$$- X[\frac{p}{2}(2G_2 + 2G_1 - G_0) + \frac{\mu_0 p'}{B^2}(2G_2 + G_1 - G_0)]$$

$$\left. - 2(Y + \frac{\partial X}{\partial\psi})\,G_1\right\}$$

$$- m\frac{q}{T}\int d^3v\, f_m\, v_\perp J_1(a)\,(\omega - \omega_D)\frac{1}{2}(h'^+ + h'^-) \ . \qquad (D.17)$$

Note that a_I^2 multiplies the other finite Larmor radius terms making this term higher order in finite Larmor radius then the other terms that have been calculated. In the limit $\rho \to 0$ $P_{\psi X}$ goes to zero and is smaller then the other moments of f_1 even for finite Larmor radius. Hence, $P_{\psi X}$ is generally ignored and was included here mainly for completeness.

To calculate the terms $P_{X\theta}$ and $P_{\psi\theta}$ a higher order expansion of f_1 needs to be calculated. Since these moments would then be of order ρ/L_n they will be neglected.

High Frequency Regime, $\omega >> \omega_b$

For frequencies much larger then a typical bounce frequency Eq. (D.2) can be expanded in powers of ω_b/ω directly to obtain expressions for $h^+ + h^-$ and $h^+ - h^-$ needed to find the high frequency moments of f_1. To lowest order in ω_b/ω,

$$\frac{1}{2}(h_0^+ + h_0^-) = \frac{\omega - \omega^*}{\omega - \omega_D}\left\{[\phi - \omega\frac{X}{n}]J_0(a) - v_\perp\frac{r}{n}B(Y + \frac{\partial X}{\partial \psi})J_1(a)\right\} , \quad (D.18)$$

$$\frac{1}{2}(h_0^+ - h_0^-) = -i\frac{\omega - \omega^*}{\omega - \omega_D}|v_\chi|\hat{\chi}\cdot\nabla\left(\frac{\omega_D}{\omega - \omega_D}\frac{X}{n}J_0(a)\right) . \quad (D.20)$$

Eq. (D.20) for $h_0^+ - h_0^-$ is of order $\frac{\omega_b}{\omega}\frac{\omega_D}{\omega}$ smaller then Eq. (D.18) for $h_0^+ + h_0^-$. Since $\omega_b/\omega << 1$ and $\omega_D/\omega << 1$ moments that depend on $h_0^+ - h_0^-$ such as v_{1_χ} and $P_{\psi\chi}$ will be neglected compared to the other moments of f_1^*.

First some preliminary definitions Define the functions Z as follows:

$$n_0 Z_0 = \int d^3v\, f_m \frac{J_0^2(a)}{1 - \frac{\omega_D}{\omega}} , \quad (D.21.0)$$

$$n_0 \frac{T}{m} Z_1 = \int d^3v\, f_m \frac{v_\perp^2}{a}\frac{J_0(a)J_1(a)}{1 - \frac{\omega_D}{\omega}} , \quad (D.21.1)$$

$$2n_0(\frac{T}{m})^2 Z_2 = \int d^3v\, f_m \frac{v_\perp^4}{a^2}\frac{J_1^2(a)}{1 - \frac{\omega_D}{\omega}} , \quad (D.21.2)$$

$$n_0 \frac{T}{m} Z_3 = \int d^3v\, f_m\, v_\chi^2 \frac{J_0^2(a)}{1 - \frac{\omega_D}{\omega}} , \quad (D.21.3)$$

$$n_0 (\frac{T}{m})^2 Z_4 = \int d^3v\, f_m\, v_\chi^2 \frac{v_\perp^2}{a}\frac{J_0(a)J_1(a)}{1 - \frac{\omega_D}{\omega}} , \quad (D.21.4)$$

$$2n_0 \frac{T}{m} Z_5 = \int d^3v\, f_m\, v_\perp^2 \frac{J_0^2(a)}{1 - \frac{\omega_D}{\omega}} , \quad (D.21.5)$$

$$4n_0 (\frac{T}{m})^2 Z_6 = \int d^3v\, f_m \frac{v_\perp^4}{a}\frac{J_0(a)J_1(a)}{1 - \frac{\omega_D}{\omega}} . \quad (D.21.6)$$

In the limit $\rho \to 0$, $Z_0 = Z_1 = Z_2 = Z_3 = Z_4 = Z_5 = Z_6 = 1$.

In the limit $\rho \to \infty$, $Z_0 = Z_1 = Z_2 = Z_3 = Z_4 = Z_5 = Z_6 = 0$. For small ω_D/ω the following expansions for Z_0, Z_1 and Z_2 are sometimes useful.

$$Z_0 = G_0 - \frac{\omega^*}{\omega}\frac{p}{p'}[D\frac{1}{2}(G_0 + G_2) + \frac{\mu_0 p'}{B^2}G_2] , \quad (D.22.0)$$

$$Z_1 = G_1 - \frac{\omega^*}{\omega}\frac{p}{p'}[D\frac{1}{2}(2G_2 + 2G_1 - G_0) + \frac{\mu_0 p'}{B^2}(2G_2 + G_1 - G_0)] , \quad (D.22.1)$$

$$Z_2 = G_1 - \frac{\omega^*}{\omega}\frac{p}{p'}[D\frac{1}{2}(3G_1 + G_0) + \frac{\mu_0 p'}{B^2}(2G_1 + G_0)] . \quad (D.22.3)$$

Zeroth moment of f_1^*:

$$n_1 = n_0\left\{-\frac{q\phi}{T} - \frac{\omega}{\omega^* p'}X + (1 - \frac{\omega^*}{\omega})[(\frac{q\phi}{T} + \frac{\omega}{\omega^* p'}X)Z_0 - (Y + \frac{\partial X}{\partial \psi})Z_1]\right\} . \quad (D.23)$$

First moments of f_1^*:

$$v_{1_\psi} = -\,i\,n_0 T\,\frac{n}{q}\,\frac{1}{rB}\,(1-\frac{\omega^*}{\omega})\left\{(\frac{q\phi}{T}+\frac{\omega}{\omega^*_p}p'X)Z_1 - 2(Y+\frac{\partial X}{\partial\psi})Z_2\right\} \quad . \tag{D.24}$$

Solving for v_{1_θ} from the continuity equation gives,

$$\begin{aligned} v_{1_\theta} &= \frac{r}{n}\,\omega n_0\Big\{-\frac{q\phi}{T}-\frac{\omega}{\omega^*_p}p'X+(1-\frac{\omega^*}{\omega})[(\frac{q\phi}{T}+\frac{\omega}{\omega^*_p}p'X)Z_0 \\ &\quad -(Y+\frac{\partial X}{\partial\psi})Z_1]\Big\} - rn_0\frac{T}{q}\frac{1}{J}\frac{\partial}{\partial\psi}\Big\{J(1-\frac{\omega^*}{\omega})[(\frac{q\phi}{T}+\frac{\omega}{\omega^*_p}p'X)Z_1 \\ &\quad -2(Y+\frac{\partial X}{\partial\psi})Z_2]\Big\} \\ &= \frac{r}{n}\,\omega n_0\Big\{(\frac{q\phi}{T}+\frac{\omega}{\omega^*_p}p'X)[1-G_0+\frac{\omega^*}{\omega}(G_0-G_1)] \\ &\quad -(1-\frac{\omega^*}{\omega})(Y+\frac{\partial X}{\partial\psi})G_1\Big\} \qquad\qquad (D.25) \\ &\quad -rn\,\frac{T}{q}(1-\frac{\omega^*}{\omega})\,\frac{\partial}{\partial\psi}\Big\{(\frac{q\phi}{T}+\frac{\omega}{\omega^*_p}p'X)G_1-2(Y+\frac{\partial X}{\partial\psi})G_1\Big\} \quad . \end{aligned}$$

where for the last expression for v_{1_θ} small ω_D/ω was assumed and the expansions (D.22) where used for Z_0, Z_1 and Z_2 and higher order finite Larmor radius terms (such as $2G_1 - G_0 - G_2$) were neglected.

Second moments of f_1^*:

$$P_{XX} = n_0 T\left\{-\frac{q\phi}{T}-\frac{\omega}{\omega^*_p}p'X+(1-\frac{\omega^*}{\omega})[(\frac{q\phi}{T}+\frac{\omega}{\omega^*_p}p'X)Z_3 - (Y+\frac{\partial X}{\partial\psi})Z_4\right\} \quad . \tag{D.26}$$

$$P_{\theta\theta} = n_0 T\left\{-\frac{q\phi}{T}-\frac{\omega}{\omega^*_p}p'X+(1-\frac{\omega^*}{\omega})[(\frac{q\phi}{T}+\frac{\omega}{\omega^*_p}p'X)Z_1 - 2(Y+\frac{\partial X}{\partial\psi})Z_2]\right\} \quad . \tag{D.27}$$

$$P_{\psi\psi} = n_0 T\left\{-\frac{q\phi}{T}-\frac{\omega}{\omega^*_p}p'X+(1-\frac{\omega^*}{\omega})[(\frac{q\phi}{T}+\frac{\omega}{\omega^*_p}p'X)(2Z_5-Z_1) - 2(Y+\frac{\partial X}{\partial\psi})(2Z_6-Z_2)\right\}. \tag{D.28}$$

APPENDIX E

Equilibrium and Stability Results for the Levitated Octupole

The following data are the results of the equilibrium and stability calculations for the Levitated Octupole. For the stability calculation the equilibrium were self consistent except for β = 18%, 19% and 20% where the β = 17% equilibrium was used and the pressure scaled up. The mode described is the marginally stable mode with the maximum temperature. For a given beta if the temperature is less then value listed then unstable modes can exist in the plasma. For this calculation the ion species was assumed to be protons.

β = 5.0 %
peak pressure = 8.76037×10^{3} nt/m^2
B bridge-separatrix = 0.663584 tesla
L_n bridge region = 1.475×10^{-2} meter
toroidal mode number = 941.867
temperature = 2.00019 eV
marginal frequency = 8.25044×10^{4} sec^{-1}
peak single particle density = 1.36680×10^{22} #/m^3
ion Larmor radius = 2.17761×10^{-4} meters

β = 6.0 %
peak pressure = 1.05535×10^{4} nt/m^2
B bridge-separatrix = 0.664879 tesla
L_n bridge region = 1.469×10^{-2} meter
toroidal mode number = 452.894
temperature = 24.4561 eV

marginal frequency = 4.64651×10^{5} sec^{-1}
peak single particle density = 1.34668×10^{21} #/m^3
ion Larmor radius = 7.59961×10^{-4} meters

β = 7.0 %
peak pressure = 1.23610×10^{4} nt/m^2
B bridge-separatrix = 0.666189 tesla
L_n bridge region = 1.463×10^{-2} meter
toroidal mode number = 339.870
temperature = 77.0162 eV
marginal frequency = 1.03501×10^{6} sec^{-1}
peak single particle density = 5.00872×10^{20} #/m^3
ion Larmor radius = 1.34597×10^{-3} meters

β = 8.0 %
peak pressure = 1.41796×10^{4} nt/m^2
B bridge-separatrix = 0.667432 tesla
L_n bridge region = 1.456×10^{-2} meter
toroidal mode number = 287.814
temperature = 156.004 eV
marginal frequency = 1.67669×10^{6} sec^{-1}
peak single particle density = 2.83650×10^{20} #/m^3
ion Larmor radius = 1.91206×10^{-3} meters

β = 9.0 %
peak pressure = 1.60066×10^{4} nt/m^2
B bridge-separatrix = 0.668572 tesla
L_n bridge region = 1.448×10^{-2} meter
toroidal mode number = 256.231
temperature = 256.176 eV
marginal frequency = 2.33115×10^{6} sec^{-1}
peak single particle density = 1.94991×10^{20} #/m^3
ion Larmor radius = 2.44603×10^{-3} meters

β = 10.0 %

peak pressure = 1.78357×10^4 nt/m^2

B bridge-separatrix = 0.669522 tesla

L_n bridge region = 1.441×10^{-2} meter

toroidal mode number = 236.193

temperature = 372.641 eV

marginal frequency = 2.97807×10^6 sec^{-1}

peak single particle density = 1.49367×10^{20} #/m^3

ion Larmor radius = 2.94592×10^{-3} meters

β = 11.0 %

peak pressure = 1.96658×10^4 nt/m^2

B bridge-separatrix = 0.670316 tesla

L_n bridge region = 1.433×10^{-2} meter

toroidal mode number = 220.672

temperature = 501.772 eV

marginal frequency = 3.59828×10^6 sec^{-1}

peak single particle density = 1.22310×10^{20} #/m^3

ion Larmor radius = 3.41440×10^{-3} meters

β = 12.0 %

peak pressure = 2.14885×10^4 nt/m^2

B bridge-separatrix = 0.670861 tesla

L_n bridge region = 1.425×10^{-2} meter

toroidal mode number = 208.814

temperature = 641.123 eV

marginal frequency = 4.19346×10^6 sec^{-1}

peak single particle density = 1.04597×10^{20} #/m^3

ion Larmor radius = 3.85637×10^{-3} meters

β = 13.0 %

peak pressure = 2.33022×10^4 nt/m^2

B bridge-separatrix = 0.671192 tesla

L_n bridge region = 1.416×10^{-2} meter

toroidal mode number = 202.731

temperature = 780.347 eV

marginal frequency = 4.77373×10^6 sec^{-1}

peak single particle density = 9.31891×10^{19} #/m^3

ion Larmor radius = 4.25243×10^{-3} meters

β = 14.0 %

peak pressure = 2.51003×10^4 nt/m^2

B bridge-separatrix = 0.671267 tesla

L_n bridge region = 1.408×10^{-2} meter

toroidal mode number = 195.576

temperature = 927.015 eV

marginal frequency = 5.30780×10^6 sec^{-1}

peak single particle density = 8.44983×10^{19} #/m^3

ion Larmor radius = 4.63435×10^{-3} meters

β = 15.0 %

peak pressure = 2.68809×10^4 nt/m^2

B bridge-separatrix = 0.671114 tesla

L_n bridge region = 1.399×10^{-2} meter

toroidal mode number = 189.790

temperature = 1.07958×10^3 eV

marginal frequency = 5.84110×10^6 sec^{-1}

peak single particle density = 7.77039×10^{19} #/m^3

ion Larmor radius = 5.00233×10^{-3} meters

β = 16.0 %

peak pressure = 2.86386×10^4 nt/m^2

B bridge-separatrix = 0.670712 tesla

L_n bridge region = 1.391×10^{-2} meter

toroidal mode number = 188.839

temperature = 1.22440×10^3 eV

marginal frequency = 6.37643×10^6 sec^{-1}

peak single particle density = 7.29932×10^{19} #/m^3

ion Larmor radius = 5.33049×10^{-3} meters

β = 17.0 %

peak pressure = 3.05234×10^{4} nt/m^2

B bridge-separatrix = 0.671757 tesla

L_n bridge region = 1.383×10^{-2} meter

toroidal mode number = 184.737

temperature = 1.38717×10^{3} eV

marginal frequency = 6.89988×10^{6} sec^{-1}

peak single particle density = 6.86686×10^{19} #/m^3

ion Larmor radius = 5.66492×10^{-3} meters

β = 18.0 %

peak pressure = 3.23189×10^{4} nt/m^2

B bridge-separatrix = 0.671757 tesla

L_n bridge region = 1.383×10^{-2} meter

toroidal mode number = 180.654

temperature = 1.58814×10^{3} eV

marginal frequency = 7.49170×10^{6} sec^{-1}

peak single particle density = 6.35070×10^{19} #/m^3

ion Larmor radius = 6.06141×10^{-3} meters

β = 19.0 %

peak pressure = 3.41144×10^{4} nt/m^2

B bridge-separatrix = 0.671757 tesla

L_n bridge region = 1.383×10^{-2} meter

toroidal mode number = 177.092

temperature = 1.80170×10^{3} eV

marginal frequency = 8.09777×10^{6} sec^{-1}

peak single particle density = 5.90896×10^{19} #/m^3

ion Larmor radius = 6.45609×10^{-3} meters

β = 20.0 %

peak pressure = 3.59099×10^{4} nt/m^2

B bridge-separatrix = 0.671757 tesla

L_n bridge region = 1.383×10^{-2} meter

toroidal mode number = 173.934

temperature = 2.02604×10^{3} eV

marginal frequency = 8.71032×10^{6} sec^{-1}

peak single particle density = 5.53123×10^{19} #/m^3

ion Larmor radius = 6.84625×10^{-3} meters

APPENDIX F

Multipole Equilibrium and Stability Codes

All computer codes used for the calculations presented in this thesis reside on the National MFE computer system. The codes are optimized to run on the Cray-1 computer. These codes are available upon request from the author, user number 1455. See the file named MULTINFO in user 1455 FILEM area for additional information and status of the codes available. The following codes were used for the calculations presented in this thesis:

OCTEC An MHD equilibrium code that solves the Grad-Shafranov equation, Eq. (2.5), in toroidal geometry. OCTEC uses the pressure profile given in Eq. (2.11). This code allows the user to define up to 20 conducting line segments and 10 rings to model a wide range of multipole devices. OCTEC generates the file EQINST necessary for all the stability codes listed here. This file contains a map of equilibrium quantities as a function of ψ and relative length along field lines.

STABN The first of two codes used to calculate high n MHD modes. STABN solves Eq. (3.16) along field lines over a specified number of flux surfaces and generates all the coefficients

necessary to solve Eq. (3.16) for the ψ variation of the mode.

STABNR The second of two codes used to calculate high n MHD modes. STABNR takes the coefficients generated by STABN and solves Eq. (3.16) for the ψ variation of the mode. It also reconstructs and plots X_0.

STABKO Solves the Kruskal-Oberman stability problem in multipole geometry. This code solves Eq. (3.16) for critical pressure gradient and the mode structure of the $n \to \infty$ mode.

STACK This is the first of two codes used to calculate the finite Larmor radius stabilization of the ballooning mode. It is iterated with the code STACKR. Given ω, n and ρ_i this code solves the $n \to \infty$ equation, Eq. (6.9) along field lines and calculates the quantities a_0, a_1, ... , a_5 for subsequent use in the radial code STACKR.

STACKR The second of two codes used to calcualte the finite Larmor radius effects on the balooning mode. STACKR solves the radial part of the finite Larmor radius problem. This code solves equations Eq. (6.13), Eq. (6.17), Eq. (6.19) and Eq. (6.20). This code is iterated with STACK until a self-consistent solution is reached.

BIBLIOGRAPHY

[1] D. W. Swain, S. C. Bates, C. E. Bush, R. J. Colchin, et al., in Controlled Fusion and Plama Physics (Proc. 9th Europ. Conf. Oxford, 1974), 44.

[2] R. W. Schumacher, M. Fukac, A. Y. Wong, R. G. Suchannek, K. L. Lam, K. Yatsu, Phys. Rev. Lett., 46, 1391 (1981).

[3] D. A. D'Ippolito, E. A. Adler, Y. C. Lee, Phys. Fluids 23, 794 (1980).

[4] J. H. Halle, A. G. Kellman, R. S. Post, S. C. Prager, E. J. Strait, M. C. Zarnstorff, Phys. Rev. Lett. 46, 1394 (1981).

[5] M. W. Phillips, Univ. of Wisconsin-Madison Plasma Physics Rept. DOE/ET/53051-26 (1981), (available on request from: Plasma Physics Group, Dept. of Physics, University of Wisconsin, Madison, WI 53706).

[6] M. N. Rosenbluth and C. L. Langmire, Ann. Phys. 1, 120 (1957).

[7] I. B. Bernstein, E. A Frieman, M. D. Kruskal, R. M. Kulsrud, Proc. Roy. Soc., Ser. A 244, 17 (1958).

[8] J. M. Greene and J. L. Johnson, Plasma Phys. 10, 729 (1968).

[9] T. Ohkawa and D. W. Kerst, Nuovo Cimento 22, 785 (1981).

[10] J. L. Johnson, R. M. Kulsrud, K. E. Weimer, Plasma Phys. 11, 463 (1969).

[11] M. D. Kruskal and C. R. Oberman, Phys. Fluids 1, 275 (1958).

[12] M. N. Rosenbluth and N. Rostoker, Phys. Fluids, 2, 23 (1959).

[13] H. R. Lewis and K. R. Symon, J. Math. Phys. 20, 413 (1979).

[14] M. N. Rosenbluth, N. A. Krall, N. Rostoker, Nucl, Fusion: 1962 Suppl. Part 1, 143 (1962).

[15] P. H. Rutherford and E. A. Frieman, Phys. Fluids 11, 569 (1968).

[16] J. B. Taylor and R. J. Hastie, Plasma Phys. 10, 479 (1968).

[17] P. Rutherford, M. Rosenbluth, W. Horton, E. Frieman, B. Coppi, Pl. Phys.-Contr. Nucl. Fusion Res., Vol. I, 367 (1968).

[18] R. J. Hastie and J. B. Taylor, Plasma Phys. 13, 365 (1971).

[19] C. W. Horton, J. D. Callen, M. N. Rosenbluth, Phys. Fluids 14, 2019 (1971).

[20] M. S. Chu, C. Chu, G. Guest, J. Y. Hsu, T. Ohkawa, Phys. Rev. Lett. 41, 247 (1978).

[21] M. N. Rosenbluth and M. L. Sloan, Phys. Fluids 14, 1725 (1971).

[22] P. C. Liewer and C. S. Liu, Univ. of Maryland-College Park Physics Pub. 78-146 (1978).

[23] J. W. Connor, R. J. Hastie and J. B. Taylor, Proc. R. Soc. Lond. A. 365, 1 (1979).

[24] Y. C. Lee, J. W. Van Dam, J. F. Drake, A. T. Lin, P. L. Pritchett, D. D'Ippolito, P. C. Liewer, C. S. Liu, in Plasma Physics and Controlled Nuclear Fusion (Proc. 7th Int. Conf. Innsbruck, 1978) Vol. 1, IAEA, Vienna, 799 (1979).

[25] J. W. Van Dam, UCLA Ph.D. Thesis, PPG-415 (1979).

[26] T. M. Antonsen and B. Lane, Phys. Fluids 23, 1205 (1980).

[27] E. A. Frieman, G. Rewoldt, W. M. Tang, A. H. Glasser, Phys. Fluids, 23, 1750 (1980).

[28] J. W. Connor, R. J. Hastie and J. B. Taylor, Plasma Phys. 22, 757 (1980).

[29] W. M. Tang, J. W. Connor, R. J. Hastie, Nuc. Fusion 20, 1439 (1980).

[30] M. W. Phillips, Univ. of Wisconsin-Madison Plasma Physics Rept. PLP 808 (1979), (available on request from: Plasma Physics Group, Dept. of Physics, University of Wisconsin, Madison, WI 53706).

[31] K. Lackner, Comm. Phys. Comm. 12, 33 (1976).

[32] J. L. Johnson, H. E. Dalhed, J. M. Greene, R. C. Grimm, et al., Princeton Univ. Plasma Physics Laboratoryy Rept. PPL-1463 (1978).

[33] M. S. Chu, D. Dobrott, T. H. Jensen, T. Tamaro, Phys. Fluids 17, 1183 (1974).

[34] B. Marder and H. Weitzner, Plasma Phys. 12, 435 (1970).

[35] J. D. Callen and R. A. Dory, Phys. Fluids 15, 1523 (1972).

[36] Y. Suzuki, Nucl. Fusion 14, 345 (1974).

[37] R. Spencer, Phys. Fluids 23, 1691 (1980).

[38] M. W. Phillips, Univ. of Wisconsin-Madison Plasma Physics Rept. PLP 765 (1978), (available on request from: Plasma Physics Group, Dept. of Physics, University of Wisconsin, Madison, WI 53706).

[39] D. Dobrott and R. W. Moore, General Atomic Company, San Diego, Report GA-A15864 (1980).

[40] E. A. Adler and Y. C. Lee, Phys. Fluids 24, 1086 (1981).

[41] R. W. Moore and D. Dobrott, General Atomic Company, San Diego, Report GA-A16235 (1981).

[42] G. O. Spies, Phys. Fluids 19, 427 (1976).

[43] T. M. Antonsen, B. Lane, J. J. Ramos, Phys. Fluids 24, 1465 (1981).

[44] T. G. Northrop, "The Adiabatic Motion of Charged Particles," Wiley(Interscience), New York, 1963.

[45] J. W. Connor and R. J. Hastie, Phys. Rev. Lett. 33, 202 (1974).

[46] P. H. Rutherford, Lin Chen, M. N. Rosenbluth, Princeton Univ. Plasma Physics Laboratory Rept. PPL-1418 (1978).